Delft University of Technology

Master Thesis

Sparse Array Antenna Concepts for Spaceborne SAR Applications

Author:
S. Jacobs

Supervisors:
Prof. Dr. A. Yarovoy
Dr. Ir. S. Monni
Dr. Ir. D. Bekers

A thesis submitted in fulfilment of the requirements for the degree of Master of Science

in the

Microwave Sensing, Signals and Systems Group
Department of Microelectronics

October 8, 2019

"Accuracy of observation is the equivalent of accuracy of thinking."

Wallace Stevens

Contents

List of Figures

List of Tables

Chapter 1

Introduction

Observation is the key to knowledge. Therefore, techniques for observation are in rapid evolvement. Today, observation happens at almost all scales, from particle detections in the Large Hadron Collider to the observation of new planets millions of lightyears away. An important field of observation is earth observation, as it provides valuable and accurate information about the health and wealth of our planet. Earth observation plays a key role in the monitoring of pollutant concentrations [1], in the monitoring of the origin and impact [2] of natural disasters such as earthquakes and hurricanes, in the measurement of ocean currents and wind currents [3], in weather forecasting and in the monitoring of the health of the rain forests [4]. A nice overview of earth observation applications can be found in [5].

Earth observation is a large field of research and a myriad of techniques have been employed in the construction of earth observation instruments. Typical examples are various types of radars and lidars, radiometers and instruments that do not employ remote sensing strategies, such as weather balloons. The measurements performed by this last group are contact-based and thus need to be carried out on-site. In this thesis the focus will be on instruments based on spaceborne synthetic aperture radar (SAR).

The remainder of this chapter is organised as follows. In the next section, Section 1.1, the context in which the research has been carried out will be outlined, along with the research objectives. After that, a short introduction on the topic of SAR will be presented in Section 1.2.[1] In the sections to follow the main lines of reasoning will be presented (Section 1.3), as well as a short summary of the novelties and the corresponding results (Section 1.4). Finally the organisation of this thesis will be detailed in Section 1.5.

1.1 Research Context and Objective

The research presented in this thesis is the result of a larger study initiated by the European Space Agency (ESA) and partly carried out at the Nederlandse Organisatie voor Toegepast

[1] A more in-depth review of synthetic aperture radar can be found in Appendix A.

Natuurwetenschappelijk Onderzoek (TNO). ESA is one of the main initiators of studies and follow-up projects in the field of spaceborne earth observation. Considering the maturity of this field, research projects are now dedicated to increasing instrument flexibility and performance and to reducing instrument cost. Less formally speaking, improved instrument flexibility allows the instument to be used for a larger variety of tasks, while improved instrument performance allows the instrument to perform the tasks better.

There are several ways in which these goals can be approached. Increasing the operating frequency can lead to increased instrument performance as well as a reduction of the instrument cost. A higher operating frequency allows for further miniaturization of the instrument and leads to a higher (theoretical) resolution.

Moving from the classical elliptic dish antennas to the more modern phased array antennas leads to improved instrument flexibility and robustness. Phased array antennas have certain advantages over elliptic dish antennas, such as gradual breakdown, more control on the farfield pattern and the possibility to compensate for defective elements. Of course, these advantages come at a cost. Compared to elliptic dish antennas, phased array antennas tend to be complex, large, heavy and thus expensive.

As phased array antennas become more mature, they become increasingly more reconfigurable. This reconfigurability will allow, in time, for fully reprogrammable beamshapes, analysis of multiple beams at once and, since the signals from the individual elements can be recorded, application of offline techniques on the acquired datasets. Clearly, these are appealing properties for an instrument to have. However, the previously mentioned costs need to be kept in check.

The research question of the study initiated by ESA can be stated as follows: Is it possible to design and build a Ka-band SAR using phased array antennas, exploiting sparsity to keep the costs and complexity to a minimum? In this thesis the focus will be on the antenna system, so the research question considered in this thesis can be stated as follows.

Research Question *Is it possible to design a sparse phased array antenna geometry that can be used in a Ka-band spaceborne SAR and is more cost-efficient than a comparable state of the art regular phased array antenna?*

In order to formulate an answer to the research question, the following support questions have been identified.

1. *What are the characteristics of currently operating earth observation instruments?*
2. *What are the most important drivers in the requirement analysis?*
3. *Which design guidelines should be considered?*
4. *What is the range of acceptable sparsity levels?*

1.2 Synthetic Aperture Radar

In the previous section the research context and research objectives have been stated. In this section the basic operation of a SAR will be introduced. To that end, first the Side Looking Aperture Radar (SLAR) will be introduced, because a lot of the properties of a SAR system can be identified already in this less complex system. Then, a simplyfied view of the geometry will be given. At the end of this section, some of the most important parameters that define the basic performance of the SAR will be explained.

It is assumed that the reader is familiar with the basic operating principles of a radar system. If not, [6] and [7] are excellent introductory texts on this subject. In fact, most of the theory that is presented here is derived from these two sources[2].

1.2.1 What is Synthetic Aperture Radar?

Conventional SLAR systems suffer from the fact that their azimuth resolution depends on the width of the platform. In order to illuminate a spot of a given size a certain beamwidth is required. The requirements on this beamwidth tighten if the distance to the platform increases. This in turn leads to unrealistic requirements on the width of the antenna aperture, especially for spaceborne instruments.

As its name implies, a Synthetic Aperture Radar combines several radar measurements from various locations along the track of the platform in order to synthesize a virtual antenna. This virtual antenna can have a much larger azimuthal dimension than the width of the original antenna. Hence, the problem sketched in the previous paragraph can be solved this way.

1.2.2 Basic operation of a SLAR

One of the earliest and most simple forms of airborne radar systems is the Side Looking Aperture Radar (SLAR). The basic configuration of a SLAR system is depicted in two figures. Figure 1.1 depicts the environment from above. The platform, which can be some form of aircraft or a satelite, moves along the track, which is indicated at the top of the figure. The radar images the swath, indicated by the gray area at the bottom of the figure. Notice that at any given time only the slice directly to the side of the platform is being imaged. This is comparable to the estimation the angle of approach of a target in a conventional rotating radar.

The other figure, Figure 1.2, depicts the environment from behind. Notice that, as opposed to the alongtrack dimension, the radar illuminates the whole width of the swath. This is comparable with the estimation of the range of a target in a conventional rotating radar.

[2] Ch. 9 from [6] and Ch. 2 and 9 from [7], to be precise.

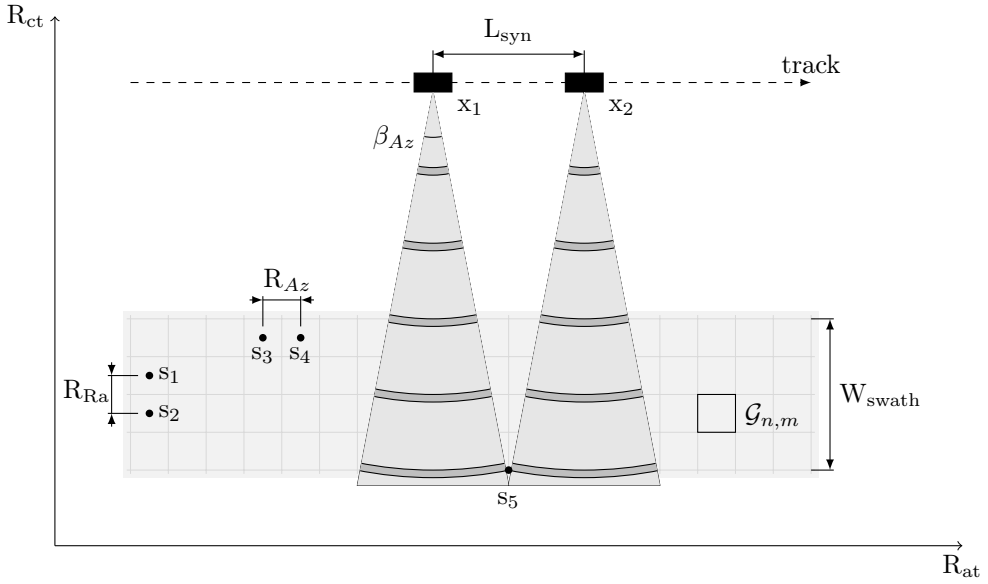

Figure 1.1: S(L)AR Environment (CT-AT)

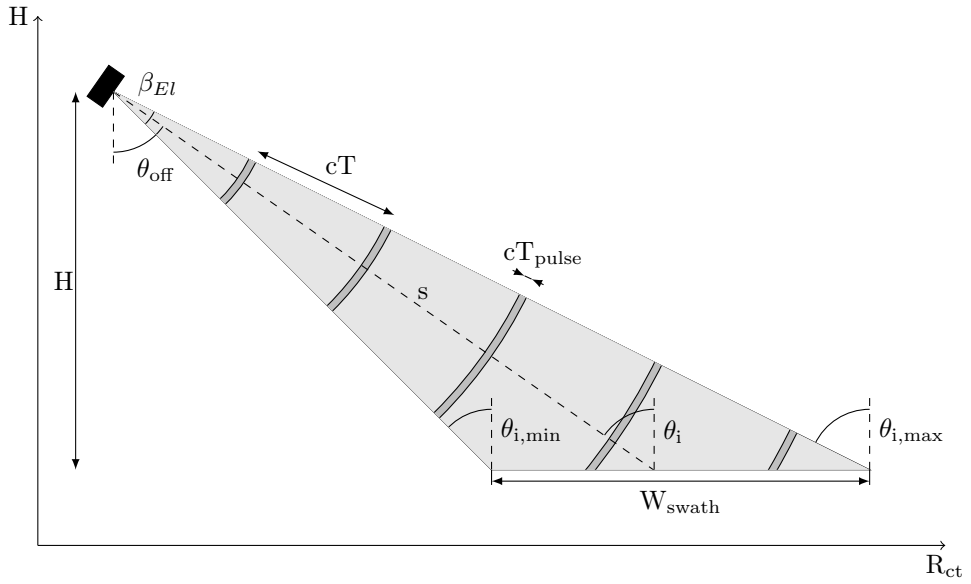

Figure 1.2: S(L)AR Environment (H-CT)

1.2.3 The Synthetic Aperture

In a phased array antenna system, electromagnetic waves incident to the antenna aperture are measured at different positions. These measurements are then coherently combined in such a way that only waves incident from certain directions persist, while waves from all other directions are suppressed. Although this happens concurrently in a regular phased array antenna, this is not necessary. If the measurement data, both amplitude and phase, are somehow stored, then this process of coherent addition can be performed at a later stage. Considering this, it is also possible to use one antenna to do a single reading, move it to the next position and repeat this

process until all measurement data are obtained from all element positions, provided that, of course, the incidence fields remain constant during the measurement sequence. This is the idea behind a SAR.

The imaging of a particular scatterer starts as soon as it enters the radarbeam. Likewise, it ends as soon as it leaves the radarbeam. This is made more clear in figure 1.1: scatterer s_5 enters the radarbeam as soon as the platform passes position x_1 and leaves the radarbeam as soon as the platform passes position x_2. Thus, this part of the track can be thought of as a very large phased array antenna and is therefore called the synthetic aperture.

It should also be noted that, for SAR processing, the radar measurements need to be coherent. That is, along with the amplitude reading, definite phase information needs to be available. Also, the incident fields need to be constant. Under those conditions, the usual phased array antenna processing can be used to synthesize large antenna apertures.

The prime advantage of SAR over SLAR is the fact that the azimuthal resolution, R_{Az} is independent of H. Also, the azimuthal resolution improves as the antenna width decreases.

1.3 Research lines

When spaceborne SAR systems are considered, there is usually a difference in both the scanning requirements and the sidelobe level requirements between the azimuth dimension and the elevation dimension. Because of this, most of the currently operating spaceborne SAR instruments that exploit phased array lattices use subarraying in the azimuthal dimension while maintaining individual element control in the elevation dimension.

The array lattices considered in this research consist of an order of magnitude more radiating elements than the largest array lattice currently employed in a spaceborne sar instrument. Because of this no existing synthesis method can be applied directly. On top of that, it is desirable to produce parts of such a large array lattice using a serial production process. This puts restrictions on how the array lattice may be organised.

Keeping these things in mind, simple generating schemes will be considered in this thesis. Simple schemes scale well with the problem size and are likely to produce array lattices that comply with the industrial feasibility requirements. Besides being simple, the generating schemes will focus on the ensemble behavior of the radiating elements, rather than on the individual radiating elements.

In this thesis two approaches will be considered. The first approach introduces sparsity using two independent methods. One method will introduce sparsity in the azimuth dimension, while the other method will introduce sparsity in the elevation dimension. Note that most currently operating spaceborne SAR instruments employ array lattices that have been generated using this approach. In the second approach it will be attempted to introduce sparsity in the two dimensions simultaneously. Both approaches will be investigated briefly. After that, the most promising approach will be submitted to an in-depth investigation.

1.4 Novelties

Although a miryad of synthesis techniques have been reported in the recent literature for the synthesis of sparse array lattices, no solution seems to be available to the problem that is being investigated in this thesis. As can be seen in Chapter 3, most papers synthesize either only linear phased array antennas or using not more than 2000 elements, almost two orders of magnitude less than what is required for the problem at hand. Also, to the best of the authors knowledge, not a single technique available in the literature synthesizes a phased array antenna that is industrially feasible as defined in Section 2.2.

The synthesis methods described in this thesis differ in these respects from the recent literature. Because they rely on simplicity and focus on the ensemble behavior of the radiating elements they scale well and are easily adapted to other requirements, such as a limited number of building blocks.

One of the most prominent results that has been designed in such a way is the variable-length linear subarrays array lattice concept. This concept uses subarrays of various lengths in a stochastic way to introduce a level of irregularity in the phase center positions.

1.5 Outline of the Thesis

This thesis is organised in 7 chapters. The chapter following this introduction, Chapter 2, will elaborate on the research question as well as on the context in which this research has been carried out. All content presented in this chapter are considered boundary conditions to this research. Thereafter, in Chapter 3, the results of a literature survey will be presented. This chapter uses a lot of the concepts defined in Section 2.3. Several different sparse phased array antenna synthesis strategies will be discussed and compared with each other. At the end of this chapter some conclusions are drawn from the survey, which form the basis for the implementation, which will be detailed in Chapter 4. The implementation embodies the plan and the philosophy behind the chosen approach. Furthermore, the implementation embodies a clear description of the work that has been carried out for this research. The execution of the research plan will be presented in Chapter 5 and in Chapter 6. In Chapter 5 the initial investigation will be presented, while in Chapter 6 the in-depth investigation will be presented. Finally, the last chapter provides a summary, the conclusions, the limitations and some suggestions for further work (Chapter 7).

The next chapter details on the problem context and the problem definition.

Chapter 2

Problem Definition

In the previous chapter the background of this research was sketched. This led to the research question. In this chapter, first the research context will be detailed in Section 2.1. This is the set of boundary conditions that apply to this research and the rationale behind them. After that the research problem will be defined in Section 2.2. This section defines the set of rules within which the research question will be answered. Finally some concluding remarks will be provided in Section 2.4.

The research question was defined in Chapter 1. It was supported by four additional subquestions. For the sake of clarity they have been repeated below.

Research Question *Is it possible to design a sparse phased array antenna geometry that can be used in a Ka-band spaceborne SAR and is more cost-efficient than a comparable state of the art regular phased array antenna?*

1. *What are the characteristics of currently operating earth observation instruments?*
2. *What are the most important drivers in the requirement analysis?*
3. *Which design guidelines should be considered?*
4. *What is the range of acceptable sparsity levels?*

In order to answer the research question, a set of top level requirements need to be identified for the instrument at hand. Then two regular phased array antennas must be designed using state of the art synthesis methods: a transmit antenna and a receive antenna. These antennas will be referred to as the benchmark antennas. The research question can be answered positively if two designs can be synthesized that at least comply with these requirements and outperform the benchmark antennas with respect to cost-efficiency. If no such design can be found, then the answer to the research question should be negative.

2.1 Problem Context

The toplevel requirements for the spaceborne SAR and its antenna system derive directly from the mission requirements as specified by ESA.[1] These requirements in turn derive from two projected applications: the evaluation of a digital elevation map and environmental monitoring.

In order for the instrument to be capable of performing both identified tasks, two SAR modes have to be implemented. The digital elevation map will require a Stripemap mode, while environmental monitoring will require a ScanSAR mode. For the digital elevation map a height resolution of 1 m is required, as well as a spatial resolution of 12 m by 12 m after multilooking. Environmental monitoring misions are usually characterised by a low resulution but a big swath width.

In ScanSAR mode a minimum swath width of 50 km is required. This operative mode drives the beamsteering requirements. In elevation a steering of $\pm 10°$ is required, while in azimuth a steering of $\pm 2°$ is required.

In Stripemap mode a spatial resolution of 12 m by 12 m (after multilooking) must be achieved, as well as a height resolution of 1 m. A spatial resolution of 1 m by 1 m is sufficient to achieve this, which drives the antenna lengths of both benchmark antennas. According to the alongtrack resolution requirement and Equation A.2, both antennas will have an antenna length of 2 m.

The height of both antennas is driven by different aspects. The transmit antenna height is driven by the required swath width, the required scanning range and by the desire to avoid ambiguities. Following the derivation in [8], it follows that the transmit antenna height must be between 0.3 m $< L_{el} <$ 0.6 m. A transmit antenna height of 0.6 m has been selected, which results in an elevation beamwidth of 0.7°. For this antenna height, the minimum pulse repetition frequency must be larger than 7 kHz, which limits the maximum swath width to 8 km.

Based on the required steering range, an element spacing of around 0.8 λ has been used. An estimate for the number of controls then follows to be $N_c = \frac{H}{0.8\lambda} \approx 90$.

The receive antenna height is driven by the desired instrument sensitivity, possibly by the implementation of SCORE. In order to implement SCORE, the receive antenna must have a smaller beamwidth, in the order of 0.25 °. In order to comply with the instrument sensitivity requirement, a receive antenna height of 2.24 m has been selected.[2]

Finally, the following set of properties and operating conditions have been selected for the instrument under consideration such that these are in coherence with the optimal operating conditions for the projected applications. Some of these follow from earlier studies with proprietary documentation and are thus stated without argumentation. The instrument is a sidelooking SAR system mounted on a satellite. The satellite will traverse a track that varies in height between 400 km and 510 km. The antenna is mounted such that its unsteered main beam is centered at 33° from the nadir angle in elevation and looking sideways in azimuth, orthogonal to the

[1] See Section 1.2 and Appendix A for an overview of Synthetic Aperture Radar.

[2] Note that if SCORE will not be used then a wider beamwidth is desired. This does not negate the argument of the instrument sensitivity. The increase in instrument sensitivity while maintaining a wider beamwidth can be achieved. For instance, a solution could be to combine multiple antennas incoherently.

direction of propagation. The access region of the SAR is thus between 23° and 43° in elevation and between -2° and 2° in azimuth. The desired instrument sensitivity is -15 dB.

2.2 Problem Definition

In the previous section the context of the research question was detailed. This question consists of two parts: the first part asks whether or not is is possible to build a sparse phased array antenna system that can be used for Ka-band SAR applications and achieves (at least) similar performance as the benchmark antennas. The second part asks whether or not such a system can be cost-effective. This problem can be formalised as follows:

Formal Problem Definition *Given an aperture size, a desired fill factor, a set of lattice constraints and a set of specifications for the array factor, find a set of radiating element locations and a vector of excitation coefficients such that the resulting array factor is in compliance with the specifications, all lattice constraints have been met and the total cost has been minimized.*

In order to compare the performance of a new design with that of the benchmark antenna system a number of performance measures will be evaluated. The first metric will be the number of transmit modules or receive modules that will be required for the construction of the design. The second metric will be a measure of how well the design guidelines have been followed. The third metric of comparison will be the pattern on the two principal planes in a worst-case steering scenario. The final metric will be a comparison of the two-dimensional array factors for all extreme steering angles.

The first metric is a measure of sparsity (in controls). As discussed in section 1.1, sparsity is both directly and indirectly related to the total monetary cost of the antenna. The second metric is a measure of industrial feasibility, as will be introduced in the following subsection. Again this metric is related to the total monetary cost. The third metric is a measure of performance. For the elevation dimension two masks have been specified. These masks are depicted in the figures 2.1 and 2.2. For the azimuth dimension it is sufficient if the pattern stays below the envelope of the pattern of the benchmark antenna. The fourth metric acts as a final check and should uncover undesired off-principal-plane behavior.

It should be noted that the RX Elevation mask depicted in figure 2.2 depends on the scan angle in elevation. This is because of the region around -33°, where the level of the mask drops to -40 dB. This region blocks strong reflections from the earth and is therefore referred to as the nadir-dip. Since the position of the earth remains constant as the beam is scanned, the nadir-dip must remain at the same position as well.

2.2.1 Design Guidelines

The second metric that will be used to benchmark a given antenna systems performance is related to industrial feasibility. In this subsection three guidelines will be stated that should

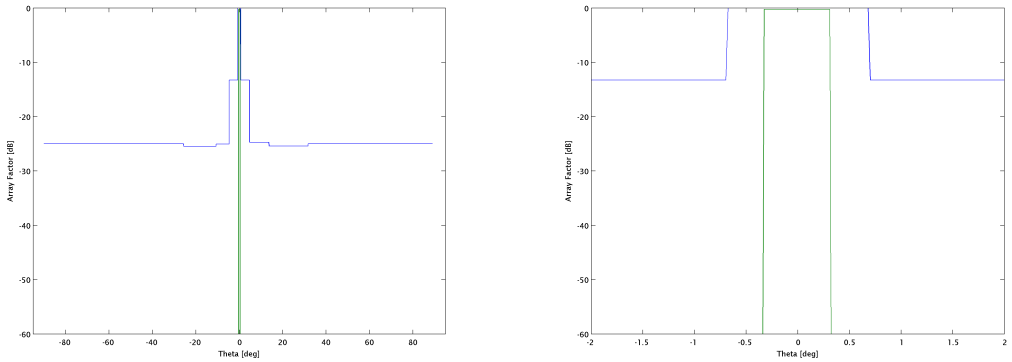

(a) TX elevation mask, no scanning (b) TX elevation mask, no scanning (zoom)

Figure 2.1: TX elevation mask specification for when no scanning has been applied

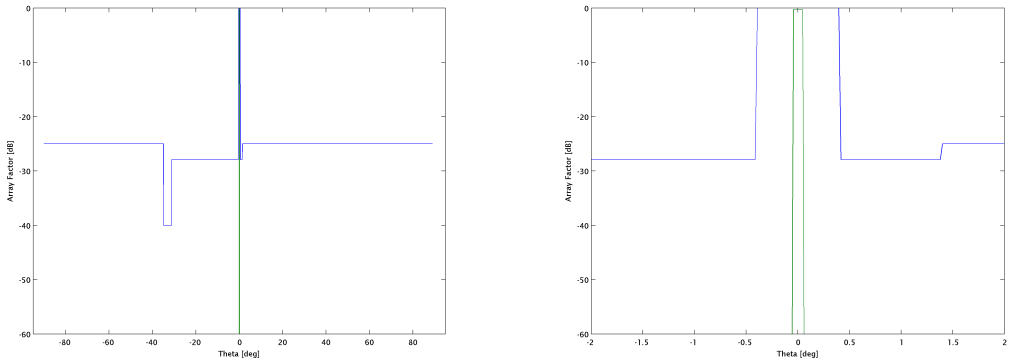

(a) RX elevation mask, no scanning (b) RX elevation mask, no scanning (zoom)

Figure 2.2: RX elevation mask specification for when no scanning has been applied

ensure the industrial feasibility of a given antenna system. They originate from a number of discussions with Thales Alenia Space. Therefore, these are based on their experience (and on scommon sense). They are summarized and discussed below.

1. The electronics should follow a regular grid.
2. Not more than four different building blocks should be used.
3. The antenna aperture should consist of similar tiles.

The first guideline allows for a simple organisation of the electronic modules. This reduces the design time and design cost of the electronics layer. The second guideline is in line with the first. Each building block needs its own frontend. Limiting the number of different building blocks limits the number of different frontends that need to be designed. The final guideline allows for a single production and testing procedure for the tiles, which also suppresses related engineering costs.

2.2.2 Benchmark Antennas

In this subsection the benchmark antennas will be introduced based on the requirement analysis of Section 2.1.

It is common for spaceborne SAR applications that the elevation requirements are much more stringent than the azimuth requirements. Therefore, phased array antennas targeting these type of applications often employ subarraying along the azimuth dimension. The same rationale will be applied for the benchmark antennas.

The interelement spacings are chosen based on the steering requirements. The horizontal spacing of the benchmark antennas is 0.745 λ or 6.25 mm. The vertical spacing is 0.835 λ or 7.00 mm. With these spacings the first grating lobe will remain outside the visible space when the beam is steered to the extreme steering angles.

The basic element from which the benchmark antennas will be constructed is a horizontally oriented ten-element linear subarray. These subarrays will be implemented as slotted waveguides. For the remainder of this thesis, the slots are assumed to be isotropic radiators, unless otherwise indicated. Eight of these subarrays are vertically stacked in a tile. These tiles are then used to fill the entire antenna aperture. For the TX benchmark antenna, 32 of such tiles are placed along the azimuth dimension, while 12 of such tiles are placed along the elevation dimension. Thus, the TX benchmark antenna consists of 96 by 320 radiating elements. For the RX benchmark antenna, again 32 of such tiles are placed along the azimuth dimension, while 40 of such tiles are placed along the elevation dimension. Thus, the RX benchmark antenna consists of 320 by 320 radiating elements. This leads to an antenna width of 2.01 meter for both the TX benchmark antenna and the RX benchmark antenna. Similarly, the height of the TX benchmark antenna is 0.68 meter and the height of the RX benchmark antenna is 2.25 meter.

The design of the RX benchmark antenna is a more challenging problem than the design of the TX benchmark antenna. On one hand this is because the RX benchmark antenna consists of more radiating elements. On the other hand, the radiation patterns are restricted by more stringent specifications, as can be seen in the figures 2.1 and 2.2. For the remainder of this thesis it is assumed that any synthesis method that can find a suitable design for the RX benchmark antenna will be capable of doing the same for the TX benchmark antenna. Therefore the RX benchmark antenna is the only antenna that will be considered. References to the benchmark antenna refer thus to the RX benchmark antenna. An impression of the array lattice of this antenna is given in Figure 2.3.

Without any form of tapering, the antenna depicted in Figure 2.3 does not comply with the elevation mask specifications. In order to do so, the benchmark antennas use a 20 point -28 dB taylor taper in the elevation dimension. The resulting radiation pattern can be found in Figure 2.4, where the extreme steering angles have been applied.

Notice that the lattice of the benchmark antennas is subarrayed and has an interelement spacing larger than $\lambda/2$ in both dimensions. Thus, following the definition of sparsity as introduced in Section 2.3, the benchmark antenna is already a sparse antenna. This should be kept in

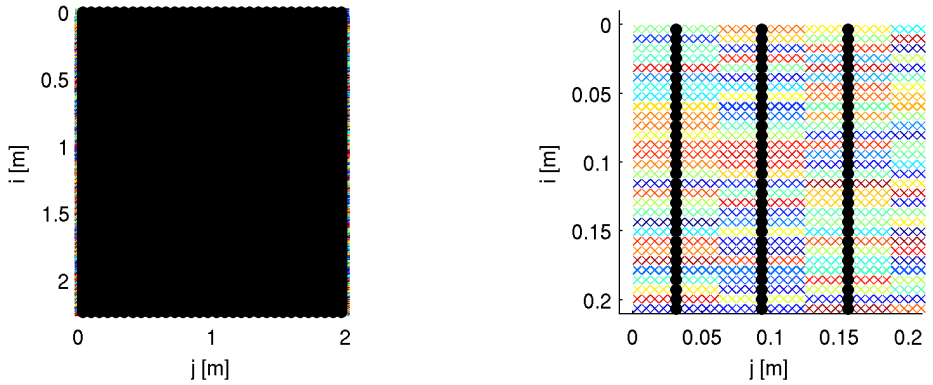

(a) Benchmark Array Lattice

(b) Benchmark Array Lattice (zoom)

Figure 2.3: Impression of the benchmark array lattice. Subfigure 2.3b depicts a zoom of the top-right corner of the lattice.

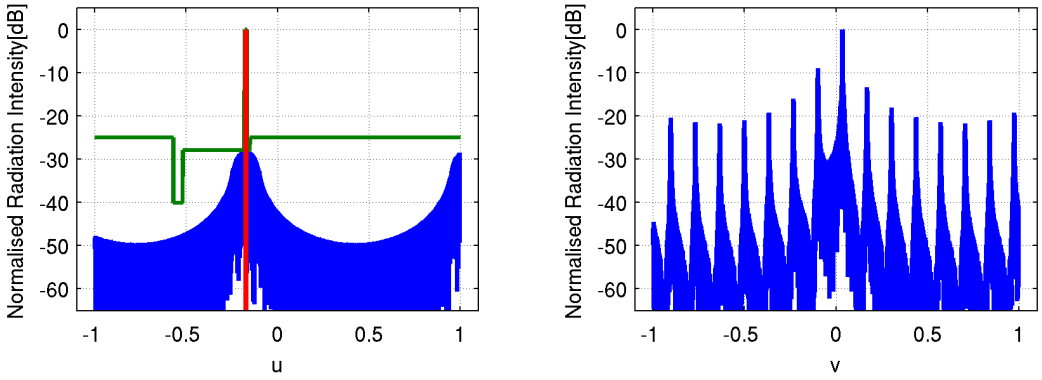

(a) Elevation Cut, -10 deg scan

(b) Azimuth Cut, 2 deg scan

Figure 2.4: Principal plane cuts of the benchmark antenna. Subfigure 2.4a depicts the elevation cut steered to -10 deg, while Subfigure 2.4b depicts the azimuth cut scanned to 2 deg.

mind when comparing the performance of the various synthesis methods with those discussed in Chapter 3.

2.2.3 Levels of Sparsity

So far the advantages of sparsity have been discussed. However, introducing sparsity also limits the instrument sensitivity. For the rx antenna, the instrument sensitivity is proportional to the amount of power that has been intercepted. Similarly the tx antenna, the instrument sensitivity is proportional to the amount of power that has been radiated. These quantities depend directly on the number of radiating elements, and thus on the level of sparsity.

Subarrays can be used to overcome some of these limitations. However, there are limits on what the current state-of-the-art semiconductor devices can deliver when it comes to power amplification. This is mostly a problem for the tx antenna, as the low-noise amplifiers have a

large dynamic range. Therefore, a lot more radiating elements can be combined in rx than in tx before the respective amplifier starts to clip.

The benchmark antenna has been overdimensioned by a factor of 2 dB with respect to the instrument sensitivity. Furthermore, it uses a taylor-taper, which has a taper loss of 3.5 dB. This leads to an absolute minimum acceptable fill-factor of 30 percent w.r.t. the benchmark antenna, under the condition of no taper loss.

2.3 Definitions

Several terms will be used to describe and compare various sparse phased array antenna synthesis techniques. These terms are summarized in Table 2.1. In this table, the terms are listed in the left colom, while their definitions are given at the appropriate place in the right column. Most definitions are related to the performance of phased array antennas, but some are related to the performance of synthesis techniques. This relation is indicated in the third column. Some of these definitions require additional explanations or remarks, which are given below.

Table 2.1: Definitions of performance characteristics

Relation	Term	Definition
Antenna	Aperture shape	The shape of the space in which the radiating elements are contained. The aperture shape can either be linear (−), circular (∘) or rectangular (□).
Antenna	Expected computational effort	An order of magnitude approximation of the time that it takes for the synthesis technique to run on moderate hardware.
Antenna	Fill factor	The number of controls that the synthesized phased array antenna consist of divided by the number of controls that a full regular array of the same size would consist of.
Antenna	Building complexity	An educated guess on the industrial feasibility of the concept.
Antenna	Lattice type	The lattice can either be thinned regular (TR) lattice, a subarrayed (SA) lattice or a completely irregular (CI) lattice.
Antenna	Mask characteristics	The shape of the radiation pattern of the synthesized antenna. This shape can be either pencil beam or shaped beam.
Antenna	Number of elements	The reported number of elements a synthesized sparse phased array antenna consists of.
Antenna	PSLL	The peak sidelobe level, i.e. the maximum value of the highest sidelobe.

Antenna	Sparsity	Sparsity implies a reduction in some variable. For instance, a phased array antenna that is sparse in elements consists of fewer elements than a regular phased array antenna of equal size.
Synthesis	Usefulness	An educated guess on how useful the paper will be for the synthesis problem described in the project proposal.
Synthesis	Equi-amplitude elements	The synthesis procedure requires all elements to have the same amplitude. The beamshape is controlled using phase-tapering only.

The *fill factor* is a direct measure of the amount of sparsity that has been obtained during the synthesis procedure. It is defined as the ratio between the number of elements the sparse phased array antenna consists of and the number of elements a regularly filled phased array antenna of the same size would consists of. Thus, the lower the fill factor the more sparse the phased array antenna is. Several synonyms and related terms are used in the literature. One of these is the reduction factor, which equals one minus the fill factor. The reduction factor thus increases with increasing sparsity.

The *peak sidelobe level (PSLL)* is the largest value of the radiation pattern of the phased array antenna outside the main lobe. It is a typical result that has been reported in almost all papers summarized in this document. Sidelobe behavior is directly related to the radiation pattern requirements, so this property can be used to get an indication whether the sparse phased array antenna will meet these requirements. It should be noted however that the sidelobe level is also strongly dependent on other factors, such as the average inter-element spacing.

Phased array antennas can exhibit two types of *sparsity*: they can be sparse in radiating elements and/or sparse in controls. Sparse in radiating elements means that the phased array antenna consists of fewer individual radiating elements than that a regular phased array antenna of the same size would consist of. Sparsity in elements leads to a lower limit on the total radiated power and to a higher average sidelobe level, which is an elementary drawback, in the sense that it cannot be compensated for afterwards. Sparse in controls means that there are fewer control variables than that the full description of the excitation signals would require. A phased array antenna that is sparse in controls may thus have the same number of radiating elements as a regular phased array antenna, but less excitation signals, for example by combining groups of elements as subarrays. Phased array antennas that are sparse in controls also have to deal with a higher average sidelobe level and possibly with large grating effects, which also are elementary drawbacks.

The *usefulness* of the techniques to synthesize a sparse phased array antenna is again more an educated guess than an obvious or well-defined property. In general, papers are considered useful if the methods presented in those papers can contribute to a solution that meets the requirements as specified in [8, 9]. Such contributions can consist of a promising synthesis technique, but also of interesting ideas applied to general techniques, such as to speed up the convergence of an iterative algorithm or to compute the radiation pattern in an efficient way. Papers that consider

the synthesis of phased array antennas with different properties than those targeted in this paper, for instance linear apertures instead of planar apertures, or with a different number of elements, are considered less useful. Whether a paper is considered useful or not is described for each paper apart in the section "What is possible for us?"

2.4 Concluding Remarks

What should be remarked is that the benchmark antenna is a state-of-the-art sparse phased array antenna system. Therefore, increasing the level of sparsity with respect to this antenna by only a modest amount while maintaining the same cost efficiency would be a major achievement.

The next chapter will provide a discussion of the literature relevant to the problem.

Chapter 3

Literature Survey

The previous chapter detailed on the problem context and the problem definition. In this chapter a discussion of the relevant literature will be given. This chapter starts with a short discussion of the different sparse array lattice types. After that the general structure of an array lattice synthesis method will be described in Section 3.2. This general structure connects the various papers considered in this literature survey. After that, an overview of this literature survey will be given in Table 3.1. In this table the synthesis methods and reported performances will be compared and their relative usefulness will be given. Finally, based on this survey a number of conclusions will be drawn which will inspire the implementation in Chapter 4.

3.1 Introduction

There are several reasons why sparse and possibly irregular array lattices are preferred over filled regular ones. Array lattices that are sparse in elements are lighter, require less transmit- and/or receive modules and cut in the related expenses. Apart from that density tapering techniques can be used to synthesize (not necessary sparse) phased array antennas with equal amplitude elements and arbitrary beam shapes. Array lattices that are sparse in controls also require less transmit and/or receive modules and hence also cut in the related expenses. However, array lattices that are sparse in controls but not in elements do not suffer from the limited total radiated power drawback[1] mentioned in the previous chapter.

Considering the underlying types of sparsity, the resulting phased array antennas exhibit array lattices that are one of three types. They can be thinned regular (TR), completely irregular (CI), or subarrayed (SA). Phased array antennas that consist of thinned regular lattices and completely irregular lattices are usually, but not necessary, sparse in elements, while phased array antennas that consist of subarrayed lattices are usually, but again not necessary, sparse in controls.

[1] Strictly speaking, this is only true if the electronics are capable of handling the resulting power density with sufficient efficiency.

3.2 Synthesis procedure

Most synthesis processes can be divided into three of steps. Usually the process starts with some form of pre-processing. After that the main synthesis step is executed. This is where most of the work is done. Finally some post-processing is done to fine-tune the results.

3.2.1 Preprocessing

This preprocessing step can consist, for instance, of the synthesis of a regular phased array antenna, which is then optimized during consecutive steps [10–16]. Other preprocessing steps are possible as well, for instance the setting of additional design constraints in order to limit the search space [17–19]. This can be necessary to ensure good results and/or to speed up convergence of the consecutive global search algorithm. Almost all methods require some parameters that control the behavior of the algorithms and that are set beforehand by qualitative and/or empirical arguments. In this document, these actions are considered configuration and not preprocessing.

3.2.2 Synthesis

After a possible preprocessing step, the main synthesis step is executed. This step can consist of removing elements of the previously synthesized regular phased array antenna, a process known as thinning [11, 13, 16, 20]. Thinning is one of the easiest ways to obtain sparse phased array antennas and can be applied to very large initial arrays [13]. Also, because of the irregularity that is introduced in the electronics, construction complexity is usually high.

A possible alternative to array thinning is to combine several elements into more directive super-elements. Each group of elements share a single control. This process is known as subarraying [11, 21]. A good overview of the various subarraying techniques is presented in [22, 23], while a more thorough treatment of the material can be found in [20]. Phased array antennas that consist of subarrays are sparse in controls and are often regularly filled. Hence, they do not have the limitations on total radiated power mentioned in Chapter 2. However, because of the regular array lattice they are based on, they exhibit both the grating- and sidelobe behavior of the underlying lattice as well as of the subarray lattice. By using an irregular subarray lattice this effect can be minimized [20]. The application of a phased array antenna aperture tiling based on polyominos is an example of such an effort [21, 23]. Polyomino-shaped subarrays fill up the entire phased array antenna aperture, while the distribution of their phase centers prevent them from developing large grating lobes. A similar approach was followed by [24]. By mirroring and rotating arbitrary subarrays they managed to synthesize a phased array antenna with a reduced sidelobe level, but also to derive analytical expressions for the expected value and variance of the antenna gain.

As was shown in [12], it is also possible to combine TR and SA, yielding a phased array antenna that has thinned subarrays as its elements. The main advantage of this technique is that identical blocks can be constructed for the subarrays. This results in a high level of industrial feasibility.

Another possibility can be to move the elements to completely arbitrary locations [14], or to synthesize new completely arbitrary element locations based on the previously synthesized regular phased array antenna [10, 15]. Phased array antennas with completely irregular element lattices can also be synthesized directly [17–19]. CI array lattices can be advantageous because equiamplitude elements can be used, lower peak sidelobe levels can be achieved, and/or more power can be radiated than a simple amplitude-taper would allow.

There are various ways to synthesize either of the previously mentioned array lattice types. These methods can be divided in four groups: direct methods that are deterministic, direct methods that are stochastic, iterative methods that are deterministic and iterative methods that are stochastic. Direct methods are, generally speaking, more specific than iterative methods and embody a good understanding of the subject that is being optimized. Iterative methods are more general: if iterative methods converge, some form of error criterium is reduced each time the method iterates. Solutions that are obtained with stochastic methods have a high probability to conform with the specifications. On the contrary, deterministic methods will reach at least some local optimum, if it is in the searchspace.

Four examples of direct deterministic methods are presented in [10, 11, 14, 15]. These methods can be based on the cumulative current density distributions of the reference array [10, 15], on the covariance between the element excitations corresponding to various shaped beams [11], and on the limiting behavior of specific functions characteristic for various element constellations [14].

The only two methods that are direct stochastic methods are the random density taper method as described in [13] and the Bayesian Compressive Sensing method as described in [19]. The method in [13] is stochastic because the element locations which are activated are picked according to a probability distribution. Because of the probabilistic nature of the method a number of independent runs must be executed in order to increase the probability of a satisfactory solution. Note that the solutions don't improve with each iteration, so it is no iterative algorithm, but rather a Monte-Carlo-like technique. The method in [19] is stochastic because it actually finds a solution that has the highest probability to optimize the cost function. Note that this is the only method that employs a stochastic cost-function. It might be argued that it is therefore the only true stochastic method discussed in this survey.

Examples of iterative deterministic techniques are members of the gradient-descend family, members of the conjugate gradient family, the topological gradient method as employed in [11], the quasi-newton method as employed in [15] and the iterative fourier transform density taper method as employed in [13].

The final group of methods are the stochastic iterative methods. The most well-known examples of this group are the algorithms that are based on natural processes, such as the evolutionary algorithms and the fractal-based methods. Evolutionary algorithms are widely used nowadays. Examples are the Genetic Algorithms as used in [11, 12, 17, 18], the process of Simulated Annealing as used in [11] and the particle swarm optimization as used in [16]. Fractal-based algorithms are based on self-similarity and have been successfully employed in [17, 18].

3.2.3 Postprocessing

Often the final step of the synthesis procedure consists of some form of local optimization [10, 11, 15]. Phased array antenna synthesis is often done using global search algorithms. Typically, results from global search algorithms are not (locally) optimal, which is why the application of a local search algorithm can still improve the solution. Another reason why postprocessing can be necessary is to verify additional and/or stricter requirements which cannot be incorporated easily into the main synthesis step.

3.3 Summary

In Table 3.1 a detailed comparison of various prominent works in the sparse phased array antenna literature is presented. From this table the main conclusion is that most synthesis problems that are considered in the current literature are not directly comparable to our synthesis problem. To the best of our knowledge there is no technique available that is simultaneously capable of dealing with all aspects mentioned in the remainder of this chapter. Thus the philosophies behind each technique available should be considered and, if useful, followed in order to come up with a new methodology that is capable of doing the synthesis.

Table 3.1: Comparison between various works in the literature. Abbreviations and symbols are explained in Table 2.1. Note that not all concepts listed in this table are both objective and quantifiable. If they are not, a progressbar has been used to indicate that this concept should be seen in relation to other papers. Thus, a progressbar reflects the (possible subjective) judgement of the author rather than some well-defined quantity.

	First author	Aperture shape	Lattice type	Construction complexity	Equiamplitude elements?	Expected comp. effort	Number of Elements	Fill factor	Peak Sidelobe Level	Mask characteristics	Usefulness
[10]	Bucci	–	CI		Yes		301		-25 dB	Pencil	
[11]	Caille	○	TR, SA		Yes		280-400		-25 dB	Shaped	
[12]	Haupt	–□	TR, SA		No		792		-23 dB	Pencil	
[13]	Keizer	○□	TR		No		144-136172		-50 dB	Pencil	
[24]	Kerby	○□	SA, CI		No		1440	N.A.	-20 dB	Shaped	
[14]	Kumar	– ○ □	CI		No		49	N.A.	-17 dB	Pencil	
[15]	Luison	–	CI		Yes		36		-17 dB	Shaped	
[21]	Mailloux	□	SA		No		432		-25 dB	Pencil	
[17]	Petko	–	TR, SA, CI		Yes		256		-19 dB	Pencil	
[18]	Petko	–	TR, SA, CI		Yes		1948		-20 dB	Pencil	
[25]	Pierro	□	SA		No		529	N.A.	-20 dB	Pencil	
[19]	Viani	–□	TR, SA, CI		No		1024		-30 dB	Shaped	
[16]	Wang	–□	TR		Yes		108		-26 dB	Pencil	

3.4 Conclusions

Based on Table 3.1 a number of conclusions can be drawn. These conclusions are listed in this section.

3.4.1 Number of radiating elements

For our synthesis problem a benchmark SAR system [26] is considered that uses two antennas. The transmit phased array antenna consists of 30720 radiating elements connected to 3072 controls and the receive phased array antenna consists of 122880 radiating elements connected to 12288 controls. The only paper that reports a successful synthesis of a layout with a comparable number of radiating elements is [13]. However, these layouts are based on thinning regular layouts, which has implications for both the sensitivity and the industrial feasibility of the system. Whether this will be prohibitive or not needs to be further investigated.

3.4.2 Sidelobe level and beam shape

Based on the SNR and industrial feasibility requirements, phased array antennas that are sparse in controls seem the most promising for our project. However, works in the literature that focus on sparse phased array antennas composed of equal subarrays [12, 17, 18, 21, 24] almost all focus on relatively high sidelobe levels. On top of that, multiple beams or different beam shapes are not considered. Although this does makes the problem challenging, a couple of positive things should be noted as well. Although the sidelobe levels are not comparable, the average sidelobe level depends heavily on the number of radiating elements used in the array. On top of that, the background for the required sidelobe levels reported in [26] is not very clear. This means that they might be relaxed when the total SAR performance is considered.

3.4.3 Fill factor

The benchmark system discussed earlier in this section consists of slotted waveguides, where each waveguide consists of 10 slots. This means that the reference solution already has a fill factor of 10%, well below the fill factors reported in Table 3.1. The only paper that approaches this figure is [21], which exploits L-octominos to achieve a fill factor of 12.5%. What kind of performance can be achieved by using higher order polyominos is subject of further research.

3.4.4 Aperture shape

Various reported synthesis techniques are either specifically tuned to linear or circular apertures or have only been tested for such apertures. This severely limits the span of useful techniques for our project.

3.4.5 Synthesis strategy

Based on these conclusions, the most viable strategy for our synthesis problem seems to be as follows:

1. With respect to the lattice choice, the focus should be placed on subarray techniques because of the sensitivity and industrial feasibility requirements.
2. Due to the problem size the choice for iterative optimization procedures would not be logical. Instead, a forward Monte-Carlo-like synthesis technique is more promising, where a relatively small number of designs are generated that have a high a-priori probability to comply with the specifications, as has been done in [13]. From these designs the best is then selected. Such an approach is not limited to subarrayed lattices, but can be extended to thinned regular lattices (which has in fact been done by [13]) and completely irregular lattices. Note that this can also be done in an hierarchical way, which allows for faster array factor computations [17, 18].
3. Finally, a local optimization step can be added to make sure all requirements are met.

The next chapter provides an overview of the work that has been carried out in this thesis. In particular the approach and the philosophy will be discussed.

Chapter 4

Implementation

The previous chapter presented a survey of the literature relevant to this research. It concluded that no method exists that can solve the problem defined in section 2.2 directly. In order to construct such a method existing methods need to be adapted. This chapter will discuss the chosen approach.

In this chapter the implementation will be detailed. In section 4.1 the research plan will be discussed, followed in section 4.2 by the philosophy behind it. Section 4.3 discusses some important details modelling details. This chapter concludes with a full investigation of the benchmark array lattice in section 4.4. This section also introduces how array lattice concepts are presented in the remainder of this thesis. Finally section 4.5 will provide some concluding remarks.

4.1 Research Plan

There are two general approaches to the problem defined in Chapter 2. The first approach would be to apply two different one-dimensional synthesis techniques for the azimuth and elevation dimensions. This is the approach that has been used in the design of the benchmark antenna. The other approach would be to use a two-dimensional synthesis technique directly in both dimensions.

Based on this the research plan has been formulated as follows. As a first step both approaches will be explored briefly. The first approach is widely used and it is therefore likely to at least achieve acceptable results. The second approach is relatively unexplored. Therefore it is not clear up front what kind of results can be expected. These observations do especially hold true when the design guidelines are considered. Based on the results of this initial investigation one of the two approaches will be chosen for a more in-depth investigation.

4.1.1 Initial Investigation

For the initial investigation of the first approach 3 variations on the benchmark array lattice will be considered. These variations will only affect the azimuth dimension, the elevation dimension will not be changed. The first variation will be the concept of variable-length linear arrays, the second variation will be the application of staggering to the benchmark antenna and the third variation will be the application of staggering to the variable-length linear arrays.

For the initial investigation of the second approach an attempt will be made to extend the work presented in [21]. In this work polyomino-shaped subarrays are used to fill the antenna aperture. The initial investigation will focus on obtaining complete fillings for polyominoes of order 4, 8 and 16. Finally the array factors of these complete tilings will be investigated.

4.1.2 In-depth Investigation

Should the first approach be chosen after the initial investigation, the in-depth investigation will focus on the following details. For the azimuth dimension, first the effect of different subarray lengths will be investigated. After that an attempt will be made to increase the compliance with the design guidelines as discussed in section 2.2. This will be done by randomly thinning linear subarrays of length 20. This will reduce the amount of irregularity in phase center locations, but it will also allow, to some extend, the use of tiles. Hence it is a tradeoff between grating effects and compliance with the design guidelines.

For the elevation dimension the concept of density tapering [27] will be investigated. In particular the rationale behind the approach of [15] will be followed. In order to allow for beam scanning, two approaches will be considered.

Should the second approach be chosen after the initial investigation, the focus will be on the construction of a global optimization method. This method should combine the larger building blocks defined in the initial investigation such that the array factor is compliant with the mask specification. One might consider, for instance, groups of polyomino-shaped subarrays as genes of a genetic algorithm. This is similar to what has been done in [17, 18], trading fractals for other types of subarrays.

4.2 Philosophy

The philosophy behind the research plan builds on two observations. The first observation is that the benchmark antenna has in the order of 100000 radiating elements. This is at least an order of magnitude larger than comparable array lattice concepts discussed in Chapter 3. The second observation is that most of the methods discussed in Chapter 3 depend heavily on (global and nonlinear) optimization techniques. Such methods are computationally heavy and do not

scale linearly with the problem size.[1] As a result, it prevents these methods from reaching a solution for the problem at hand within an acceptable timeframe.

With the problem size in mind, the constructed method should use a simple scheme to fill the antenna aperture. Simple methods have a number of additional advantages besides scalability. The design guidelines, for instance, demand simple designs. Also, simple schemes are more easily adapted to the problem at hand. Examples of such schemes will be presented in Chapter 5 and in Chapter 6.

Besides being simple, the method should aim to exploit ensemble behavior rather than trying to place radiating elements on an inidividial basis. The number of radiating elements is large, so ensemble behavior will likely dominate the individual radiating element contributions.

4.3 Modelling details

In this thesis multiple array lattice characteristics will be presented. This section details on the computation and the presentation of these characteristcs. First the general representation of an array lattice will be discussed. After that a couple of words will be spend on the computation of the autocorrelation function (ACF). Finally, in the third subsection the computation of the (normalized) radiation pattern will be briefly discussed.

4.3.1 Array Lattice Model

In the remainder of this thesis various array lattice concepts and their corresponding (normalized) radiation patterns will be presented. This subsection details on how these array lattices have been modelled and how their corresponding (normalized) radiation patterns have been computed.

4.3.1.1 Geometry

All array lattices that have been considered in this thesis are separable. This means that the radiating elements are organised in equal rows and columns. The spacing between these rows and columns may still be arbitrary. This assumption allows the illumination coefficients to be stored in a matrix of the same dimensions as the grid containing the radiating elements. This matrix will be referred to as I, the matrix of illumination coefficients.

Apart from the matrix of illumination coefficients the dimension specifications are stored. These contain either a vector of coordinates of the rows (r_i) and columns (r_j) or, in the case of a regularly spaced dimension, information about the difference between two consecutive rows (d_i) or columns (d_j). The origin is considered at the top-left corner of the antenna. From the origin, the i-axis is oriented vertically downward, while the j-axis is oriented horizontally to the right.

[1] In fact, according to [28] in [10], the computational complexity of these kind of problems grows exponentially with the number of unknowns. Hence they are classified as NP-Hard problems, which is a worst case scenario.

4.3.1.2 Subarrays

Subarrays are supported by means of a subarray matrix (S), a vector of subarray coefficients (I_s), a vector of taper coefficients (I_t) and a vector of phase center coordinates (r_{PC}). The subarray matrix is a matrix that relates the subarray coefficients and the taper coefficients to the illumination coefficients by means of a matrix-vector product. This is summarized in Equation 4.1. In this equation, $\cdot$ is the elementwise multiplication operator. The phase center coordinates are computed from the (geometric) mean of the element coordinates weighted by the corresponding values in the subarray matrix.

$$I = S(I_s \cdot I_t) \tag{4.1}$$

4.3.2 Beam steering

Beamsteering has been implemented at subarray level. Note that single element control can be obtained by setting S to the identity matrix. The illumination coefficients will be computed according to Equation 4.2. In this equation $u = \cos\theta \sin\phi$ and $v = \sin\theta \sin\phi$.

$$I = S(e^{-ik(ur_{PC_i} + vr_{PC_j})} \cdot I_t) \tag{4.2}$$

4.3.3 Autocorrelation

In the next two chapters the irregularity in phase center positions has been used to predict grating effects. The autocorrelation function can be used to quantify this irregularity. A high value of the autocorrelation function implies that there are a lot of coefficients that add up constructively, thus forming a grating lobe. The autocorrelation function is also directly related to the squared-magnitude of the radiation pattern via the Wiener-Khinchine theorem.

The autocorrelation has been implemented as follows. First all phase centers were projected onto a line using a standard orthogonal projection. The line is modelled using a highly oversampled grid of 2^{21} samples. Since this projection is done in the digital domain, mismatches between sample positions and the gridpoints making up the line must be accounted for. This is done using small-banded gaussian kernels. For each phase center a gaussian kernel was generated. This kernel has a mean equal to the projected phase center location and a variance such that its support is small. From this line the autocorrelation is computed using the Wiener-Khinchine theorem: $ACF(x) = \mathcal{F}^{-1}|\mathcal{F}\{x\}|^2$.

It should be noted that unit illumination has been assumed for all analyses that make use of the autocorrelation function. Also subarray patterns have been omitted. Only the irregularity in phase center positions has been assessed.

4.3.4 Radiation Pattern

From the illumination coefficients the radiation pattern can be computed according to equation 4.3. If one or more dimensions are regular fast fourier transform (FFT) techniques are used in computation of the radiation pattern. This leads to a great speedup but at the cost of some inaccuracy.

$$U(u,v) = 20 \cdot \log 10 \left(\sum_{i,j} I(i,j) \cdot e^{ik(ur_i + vr_j)} \right) \tag{4.3}$$

4.4 Taylor-Tapered Benchmark Antenna

The taylor-tapered benchmark array lattice concept represents the current state-of-the-art of Ka-band spaceborne SAR antennas and will therefore be used to benchmark all other array lattice concepts discussed in this thesis. This section reviews this array lattice concept. This review serves as template for the discussions of the various other antenna concepts considered throughout this thesis. Therefore its structure will be explained briefly.

The discussions of the various antenna concepts all obey the same structure, although components may be omitted if they are duplicate or in some way not applicable for a given antenna concept. First the rationale behind the antenna concept will be discussed. After that the method from which the array lattice has been generated will be provided, followed by a visual impression of the lattice. After that the principal plane cuts will be presented and discussed. The height of the first grating lobe in the azimuth cut will be mentioned explicitly. After that the full two-dimensional radiation patterns will be depicted and discussed. Finally the radiation pattern will be evaluated based on the rationale. If randomness has been exploited in the generation of the array lattice also the reproducibility of the results will be evaluated.

4.4.1 Rationale

The rationale behind the design of the benchmark array lattice has been sketched in Section 2.2. The resulting array lattice uses horizontally oriented ten element subarrays as a basic building block. The horizontal interelement spacing was 0.745 λ or 6.25 mm, while the vertical interelement spacing is 0.835 λ or 7.00 mm. For an array lattice of 320 by 320 elements this leads to an antenna width of 2.01 meter and an antenna height of 2.25 meter.

4.4.2 Array Lattice

The array lattice of the benchmark antenna has been repeated in Figure 4.1a. A zoom of the top-left corner of the antenna can be found in Figure 4.1b. The subarrays can be identified in this last figure. The lines of black dots illustrate the regularity in the phase center locations.

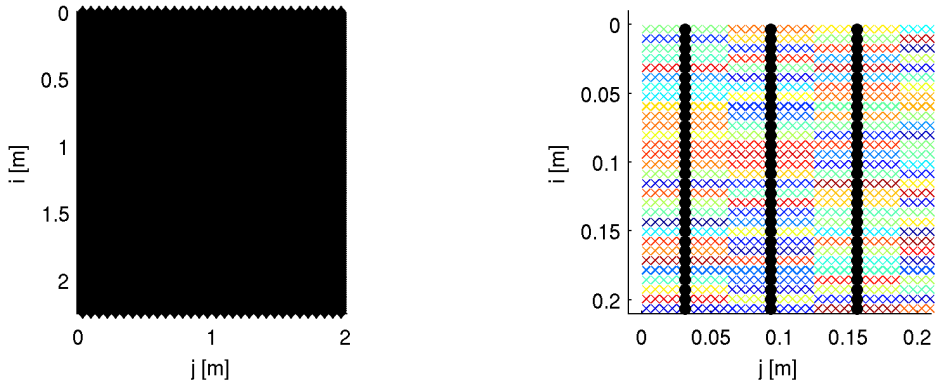

(a) Benchmark Array Lattice

(b) Benchmark Array Lattice (zoom)

Figure 4.1: Impression of the benchmark array lattice. Subfigure 4.1b depicts a zoom of the top-right corner of the lattice.

4.4.3 Principal Plane Cuts

The elevation cut of the benchmark array lattice is depicted in Figure 4.2. This figure illustrates the chosen spacing: the grating lobe on the right almost enters the visible space. The effect of the taylor taper is also visible, especially around the main beam. The azimuth cut is depicted in Figure 4.3. This figure shows a large number of suppressed grating lobes, which contradicts with the rationale. They can be explained as follows: the radiating element grid can be written as the convolution between the ten element grid of a subarray and the grid of the phase center locations. Due to the fourier relation between the grids and the radiation patterns, convolution in the array lattice domain leads to multiplication in the radiation pattern domain. Thus, the azimuth cut shows the normalised radiation pattern of a grid with a spacing of 7.45 λ filtered by the normalised radiation pattern of a subarray. The first grating lobe is at -9 dB.

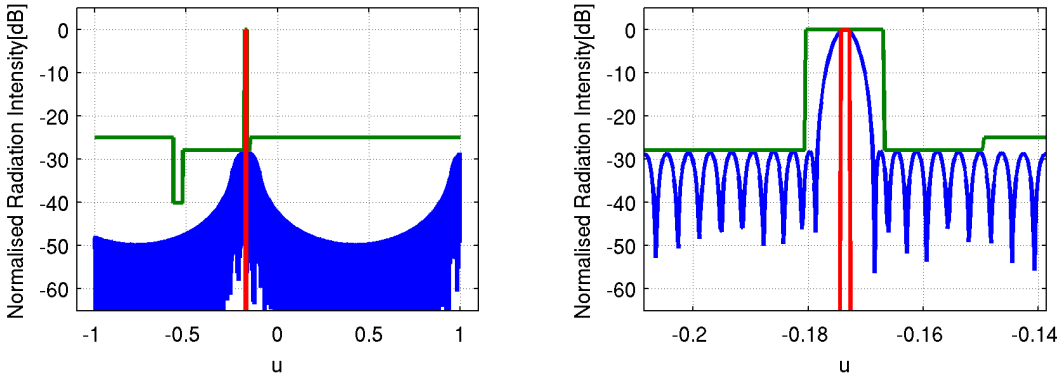

(a) Elevation Cut, 10 deg scan

(b) Elevation Cut, 10 deg scan (zoom)

Figure 4.2: Elevation cut and corresponding zoom for the benchmark array lattice

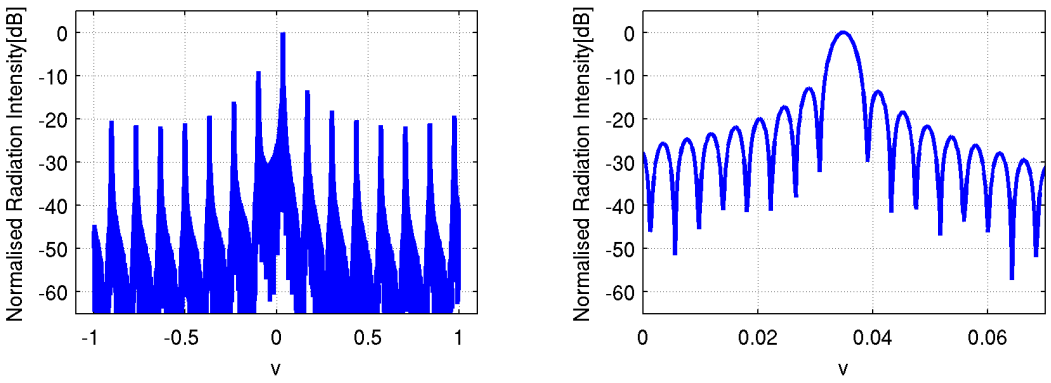

(a) Azimuth Cut, 2 deg scan

(b) Azimuth Cut, 2 deg scan (zoom)

Figure 4.3: Azimuth cut and corresponding zoom for the benchmark array lattice

4.4.4 Two-dimensional Radiation Patterns

The two-dimensional radiation pattern of the benchmark array lattice has been depicted in Figure 4.4. In this figure the beam has been scanned to (10,2) deg. While the principal plane cuts serve as a first impression of the behavior of the array lattice, the two-dimensional radiation pattern provides more insight. This figure shows that the principal plane cuts naturally extend to other regions as well. This is due to the separability of the array lattice when subarraying has been applied.

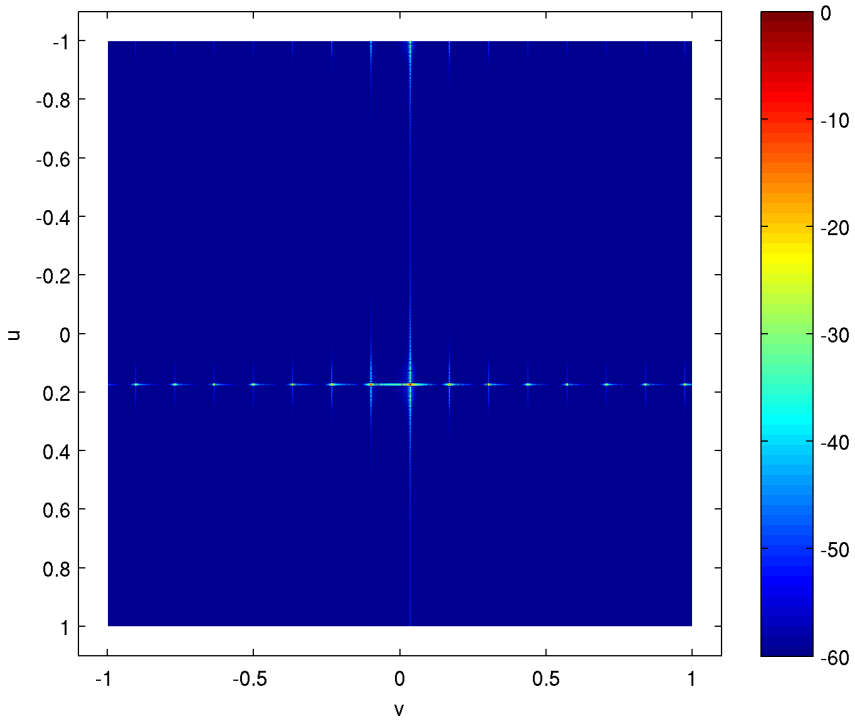

Figure 4.4: Two-dimensional normalised radiation pattern of the benchmark array lattice. The main beam of the array lattice concepts has been scanned to (10,2) deg.

4.5 Conclusion

This chapter started with a discussion about the chosen approach. The plan that will be followed consists of two phases: the initial investigation and the in-depth investigation. During the initial investigation the azimuth dimension and the elevation dimension will first be treated independently. After that a full two-dimensional approach will be investigated. The most promising of these two approaches will be explored more vigorously in the in-depth investigation.

The philosophy behind the research plan builds on two observations. The first is that the benchmark antenna has in the order of 100000 radiating elements. The second is that most methods described in the literature scale exponentially with the number of elements. From this perspective, the constructed method should use a simple scheme to fill the entire array face. Besides that, it should aim to achieve a certain distribution of radiating elements, rather that trying to place radiating elements on an individual basis. Following this phylosophy a number of antenna concepts have been analyzed.

In section 4.3 the most important modelling details were provided. These details are a necessity for anyone who seeks to reproduce the results presented in this thesis. Most noteworthy, in the computation of the array factor only first order effects have been considered.

Finally, section 4.4 discussed the details of the benchmark array lattice. In this section the graphics used to present an antenna concept were introduced. Also all antenna concepts that will be presented in the following chapters will be discussed using the same structure.

The next chapter will present the initial investigation.

Chapter 5

Initial Investigation

In the previous chapter the implementation was discussed, which consisted of the research plan, the research philosophy, the implementation details and a discussion of the benchmark antenna. In this chapter the initial investigation will be presented. According to Section 4.1, the initial investigation considers two possible approaches. The first approach uses different synthesis techniques for the azimuth and the elevation dimensions, while the second approach considers both dimensions simultaneously.

In the discussion of the first approach three array lattice concepts will be evaluated. These concepts are all variations derived from the benchmark antenna. That is, they share the same number and organisation of radiating elements and the same interelement spacing. The first array lattice concept will be the variable-length linear arrays array lattice concept. This concept will be presented in Section 5.1. Designs that belong to this family of array lattice concepts differ from the benchmark antenna in their subarray organisation. The second array lattice concept will be the staggered benchmark array lattice concept. This concept introduces a random integer offset for each row in the array lattice. The third array lattice concept will apply staggering to the first array lattice concept. It is therefore named the staggered variable-length linear arrays array lattice concept. Both the second and the third array lattice concept will be presented in Section 5.2

For the initial investigation of the second approach a synthesis method based on polyominoes will be evaluated. This fully two-dimensional synthesis method allows for some irregularity in the phase center positions using only a limited number of subarrays. Their presentation in Section 5.3 starts with the investigation of subarrays that consist of four radiating elements. The generation of array lattices using polyominoes is far from trivial and some of the computational issues will be discussed. After that an attempt will be made to extend this method to subarrays that embody more radiating elements. Although no such method could be implemented in time, the approach will be discussed.

At the end of this chapter the use of the autocorrelation function will be discussed as a potential building block for a more rigorous synthesis technique. This function has the appealing property

that it relates a description of the array lattice to the magnitude of the power spectrum, a property known as the Wiener-Khinchine theorem.

5.1 Variable-length Linear Arrays Array Lattice Concept

The first variation of the benchmark antenna is the variable-length linear arrays array lattice concept. This concept improves sparsity in controls with respect to the benchmark antenna by using larger linear arrays. This will lead to grating effects due to the larger average spacing between the phase centers of the subarrays. These grating effects need to be reduced by introducing irregularity in the phase center positions. In order to achieve this subarrays of four different lengths will be used.

5.1.1 Generation of the Array Lattice

Array lattices for the variable-length linear arrays array lattice concept are generated using the following scheme. In the first step, all possible rows from which the antenna aperture can be constructed will be computed. Then, for each row in the antenna aperture, a random row will be selected. After 320 rows the entire antenna aperture has been filled.

The problem of finding all different rows can be translated in a linear algebra problem: given a set of 4 lengths, find all integer linear combinations of these lengths that add up to the number of columns in the row. Thus, if $\{a, b, c, d\}$ is the set of lengths and nJ is the number of columns in a row, then the problem is to find all integers $\{a', b', c', d'\}$ such that $a'a + b'b + c'c + d'd = nJ$.

This problem has been solved using a brute-force solution. The pseudo code for the algorithm has been listed in Listing 5.1. A row is represented using the four integers a', b', c', d'. Once a random row has been selected, the next step is to expand this representation into a string consisting of a' a's, b' b's, c' c's and d' d's. Thus, if $\{a', b', c', d'\} = \{1, 2, 3, 4\}$, this string would look like abbcccdddd. The row is then formed by taking a random permutation of this string. Finally, each letter is replaced by a subarray of the length corresponding to the letter.

```
1  solutions = []
2  for aInd := 1 to ⌈nJ/a⌉
3    for bInd := 1 to ⌈nJ/b⌉
4      for cInd := 1 to ⌈nJ/c⌉
5        for dInd := 1 to ⌈nJ/d⌉
6          if a*aInd + b*bInd + c*cInd + d*dInd == nJ
7            solutions.append(aInd bInd cInd dInd]);
```

Listing 5.1: Compute all possible lines

5.1.2 Discussion of the Array Lattice

As with the benchmark array lattice discussed in Section 4.4 a typical array lattice that belongs to the variable-length linear arrays array lattice concept is depicted in Figure 5.1. For the generation

of this array lattice subarrays of lengths $\{13, 15, 17, 19\}$ have been used. When compared to the array lattice of the benchmark antenna, it can be observed that most of the regularity of the phase centers has been destroyed. In particular in the center of the array the phase centers follow a random pattern. At the left and right boundaries the linear structure is still present, so some grating effects are expected.

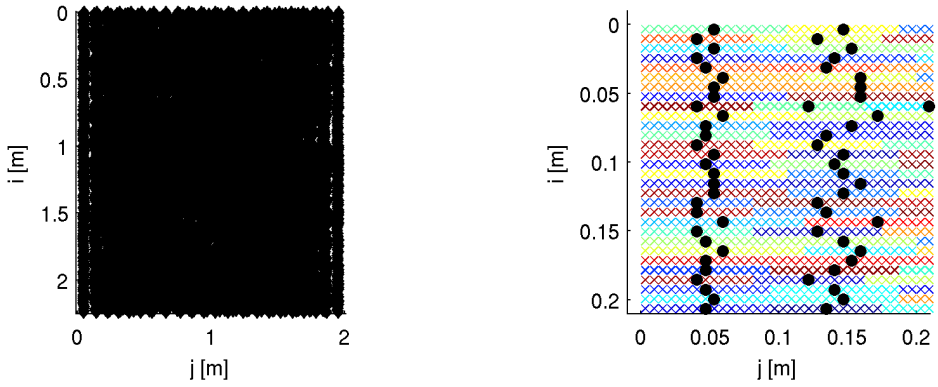

(a) Array Lattice

(b) Array Lattice (zoom)

Figure 5.1: Linear Arrays Antenna - Array Lattice

Considering the design guidelines as stated in Section 2.2, the following can be observed. Because of the introduced irregularity the phase centers do no longer follow a regular grid. Therefore, the electronics grid has also become irregular, so the first design guideline has been violated. Only four different subarrays have been used for this antenna concept, so the second design guideline has been honored. The final guideline demands that tiles can be identified. It could be argued that rows could be considered tiles. However, the number of subarrays is not the same for each row and also the phase center positions differ, so this is not trivial. Therefore the third guideline will not be considered violated nor honored.

5.1.3 Principal Plane Cuts

The elevation cut of the variable-length linear arrays antenna equals that of the benchmark antenna and was depicted in Figure 4.2. The azimuth cut is depicted in Figure 5.2. Compared to the azimuth cut of the benchmark antenna (see Figure 4.3), a suppression of grating lobes can be observed. This is the result of the irregularity introduced by using variable-length linear arrays. The first grating lobe is below -13 dB, 4 dB below the first grating lobe of the benchmark antenna, while the average subarray length has been increased from 10 to 16.

5.1.4 Two-dimensional Radiation Patterns

The two-dimensional radiation pattern of an array lattice that belongs to the variable-length linear arrays array lattice concept has been depicted in Figure 5.3. In this figure the beam has been scanned to (10,2) deg.

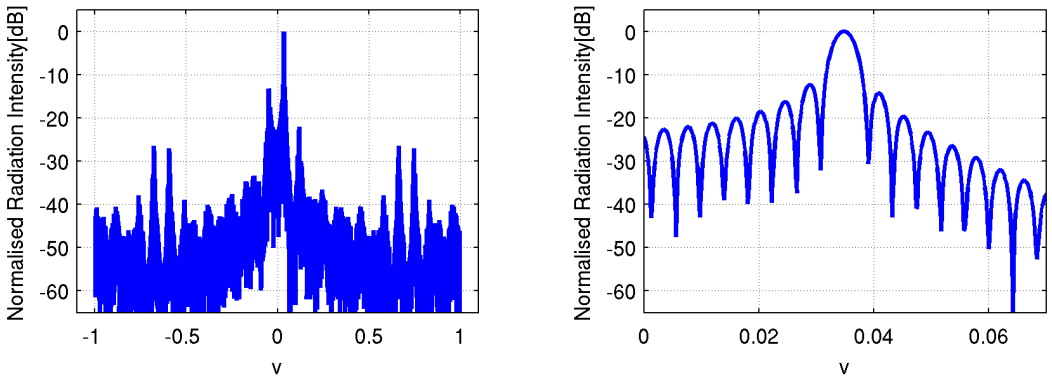

(a) Azimuth, 2 deg scan

(b) Azimuth, 2 deg scan (zoom)

Figure 5.2: Linear Arrays Antenna - Azimuth Cut

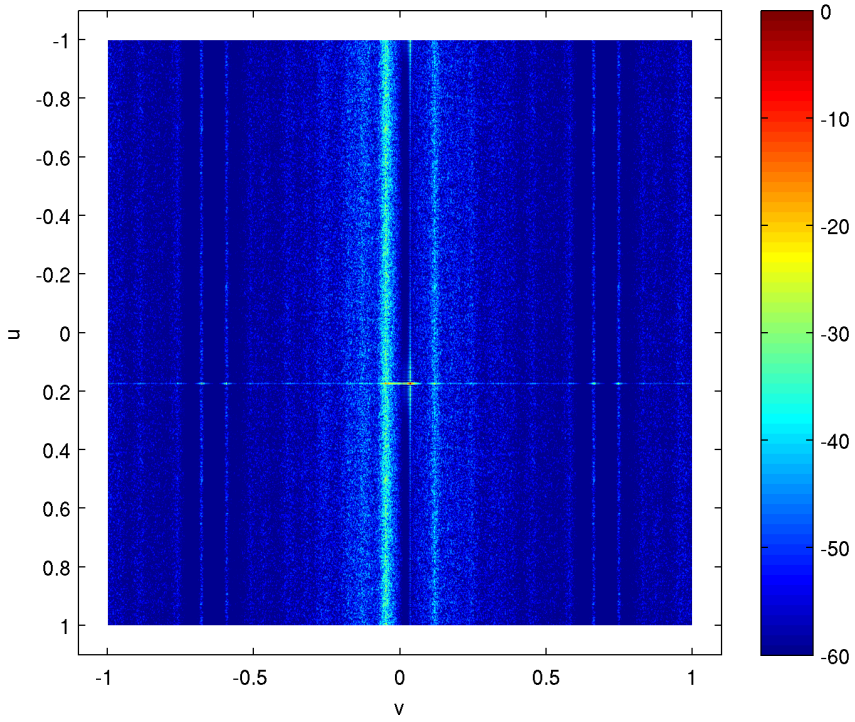

Figure 5.3: Two-dimensional normalised radiation patterns of the variable-length linear arrays array lattice concept. The main beam of the array lattice concepts has been scanned to (10,2) deg.

From Figure 5.3 it can be seen that the subarrays affect indeed only the azimuth dimension. This is indicated by the vertical lines in the figure: the radiation pattern is almost independent of u. It was expected that the taylor taper would affect these lines, as it did in the two-dimensional radiation pattern for the benchmark antenna. (See Figure 4.4). Why this is not the case remains an open question.

5.1.5 Variability between Designs

The principal plane cuts discussed in the previous subsection are referred to as the principal plane cuts that correspond to the variable-length linear arrays array lattice concept. However, the algorithm that generates these array lattices is non-deterministic. Therefore it should be investigated to what extend the principal plane cuts presentend in this section are indeed characteristic for the variable-length linear arrays array lattice concept.

In order to investigate this 200 different array lattices have been generated. For each lattice three different scan angles were investigated: (-10,2), (0,2) and (10,2). Their radiation pattern has been computed on a 8192 by 8192 grid, which has been downsampled to a resolution of 1024 by 1024 using a max filter. For each coordinate the variance has been estimated using the standard non-biased variance estimator (5.1), where μ equals the sample average (5.2).

$$\mathrm{VAR(U)} = \frac{1}{\mathrm{N}-1}\sum_{i=1}^{\mathrm{N}}[U_i - \mu]^2 \tag{5.1}$$

$$\mu\mathrm{(U)} = \frac{1}{\mathrm{N}}\sum_{i=1}^{\mathrm{N}}U_i \tag{5.2}$$

The resulting variance has been depicted in Figure 5.4. This figure shows that the variance in radiation pattern between different array lattices that belong to the family of variable-length linear arrays has a maximum value of -75 dB. Therefore the azimuth cut depicted in Figure 5.2 are indeed representative for members of the variable-length linear arrays array lattice concept.

5.2 Staggering

The second and third variation of the benchmark array lattice apply the concept of staggering to the benchmark array lattice and to the variable-length linear arrays array lattice concept. Staggering does not improve sparsity but aims to suppress grating lobes. In order to achieve this additional irregularity will be introduced in the phase center positions of the array lattice.

5.2.1 Generation of the Array Lattices

Staggered array lattices are obtained from regular array lattices as follows. First either a benchmark array lattice or an array lattice that belongs to the variable-length linear arrays array

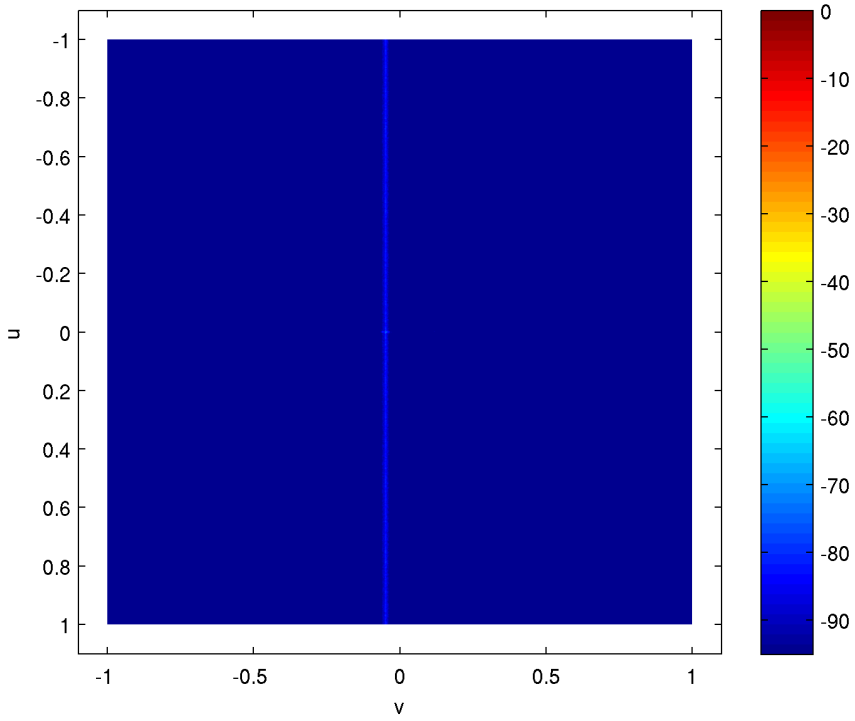

Figure 5.4: Variability in radiation patterns between designs - Linear Arrays

lattice concept will be generated. For each row in this array lattice a random integer n_{st} in the range of acceptable stagger values is chosen. If the selected stagger value is N, then the range of acceptable stagger values is $[0 \ldots \mathrm{N}-1]$. After that all radiating elements in that row are shifted n_{st} times the interelement spacing to the right.[1]

5.2.2 Discussion of the Array Lattices

Zooms of the array lattices of the staggered benchmark array lattice concept are depicted in Figure 5.5. For these array lattices stagger values of respectively 5 and 10 have been used.

A stagger value of 5 leads to a banded structure in the phase center positions. Three of these bands can be recognised in figure 5.5a. In contrast, a stagger value of 10 leads to a uniform distribution of the phase center positions. This has been depicted in Figure 5.5b. Therefore, it is expected that a stagger value of 10 will achieve a better grating lobe suppression.

For the staggered linear arrays similar observations hold, so those array lattices have been omitted here. Because of the larger average subarray length a stagger value of 10 is not enough to achieve a uniform distribution of the phase centers. It is therefore expected that the effect of the chosen different stagger values is less apparent for array lattices that belong to the staggered variable-length linear arrays array lattice concept than it is for array lattices that belong to the staggered benchmark array lattice concept.

[1] Note that the process of staggering results in a small increase of the antenna width. This effect is in the order of 3 percent and negligible for the considered purposes.

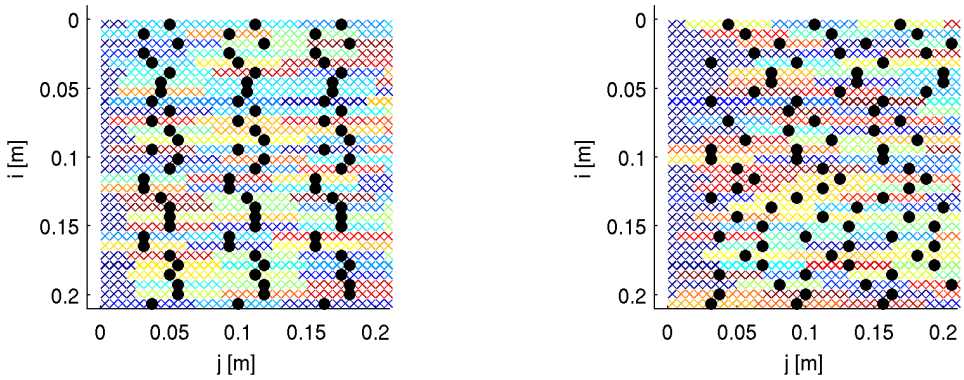

(a) Array Lattice (zoom, 5)

(b) Array Lattice (zoom, 10)

Figure 5.5: Staggered Benchmark Array Lattice Concept - Array Lattice

Considering the design guidelines, for the staggered benchmark array lattices, the following can be observed. Generally speaking, because of the introduced irregularity the phase center positions do no longer follow a regular grid. However, the phase centers of each row do follow a regular grid, and thus the electronics for each row remain regular. Therefore, the first design guideline cannot be considered violated nor honored. Since the same building block has been used as for the benchmark array lattice, the second design guideline has been honored. The final guideline demands that tiles can be identified. It could be argued that rows could be considered tiles. This is reasonable because all rows are the same. Therefore the third guideline has been honored.

For the staggered variable-length linear arrays array lattice concept the same applies as for its unstaggered counterpart. The introduced irregularity in the phase center positions forces the electronics grid to become irregular. Therefore the first design guideline has been violated. Only 4 different subarrays have been used for this array lattice concept, so the second design guideline has been honored. The final guideline demands that tiles can be identified. It could be argued that rows could be considered tiles. However, the number of subarrays is not the same for each row and also the phase center positions differ, so this is not trivial. Therefore the third guideline cannot be considered violated nor honored.

5.2.3 Principal Plane Cuts

The elevation cut of the staggered benchmark array lattice concept and the elevation cut of the staggered variable-length linear arrays array lattice concept equals the elevation cut of the benchmark antenna depicted in Figure 4.2.

From the azimuth cuts of the staggered benchmark array lattice concepts first the concept with the stagger value of 5 will be investigated. This azimuth cut is depicted in Figure 5.8a. It shows that the grating lobes present in the azimuth cut of the benchmark antenna have indeed been suppressed. The first grating lobe is at -12 dB, 3 dB below the first grating lobe of the benchmark antenna. When a stagger value of 10 is considered this changes drastically. As can

be seen in Figure 5.8b, the first grating lobe drops to a level of -36 dB and similar behavior can be seen for the other large grating lobes. The area close to the main lobe is not affected by staggering at all.The average subarray length has remained the same as the subarray length of the benchmark antenna.

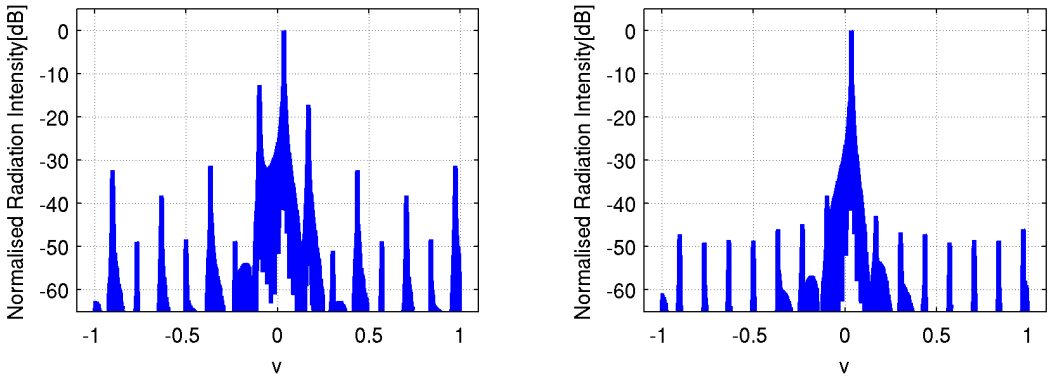

(a) Staggered Benchmark Array Lattice Concept (5)

(b) Staggered Benchmark Array Lattice Concept (10)

Figure 5.6: Staggered Benchmark Array Lattice Concept - Azimuth Cut

From the azimuth cuts of the variable-length linear arrays array lattice concepts first the array lattice concept with the stagger value of 5 will be investigated. This plot is depicted in Figure 5.8c. It shows that the first grating lobe is at -15 dB, 6 dB below the first grating lobe of the benchmark antenna. When a stagger value of 10 is considered this changes, as can be seen in Figure 5.8d. The first grating lobe drops to a level of -21 dB. The other grating lobes are reduced as well, but not as drastically as for the staggered benchmark array lattice concept. Again, the area close to the main lobe is not affected by staggering at all. The average subarray length has increased from 10 to 16.

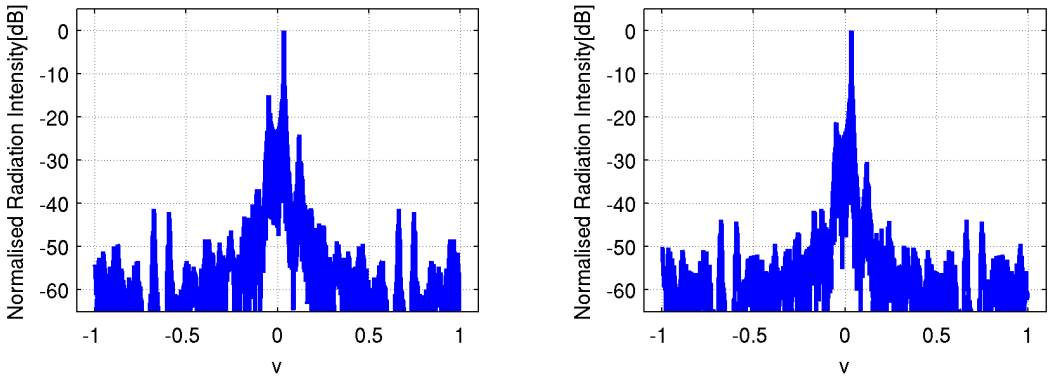

(a) Linear Arrays Array Lattice Concept (5)

(b) Linear Arrays Array Lattice Concept (10)

Figure 5.7: Linear Arrays Array Lattice Concept - Azimuth Cut

5.2.4 Two-dimensional Radiation Patterns

The two-dimensional radiation patterns that belong to the staggered array lattice concepts have been depicted in Figure 5.8. Again, the beams in all subfigures in this figure have been scanned to (10,2) deg.

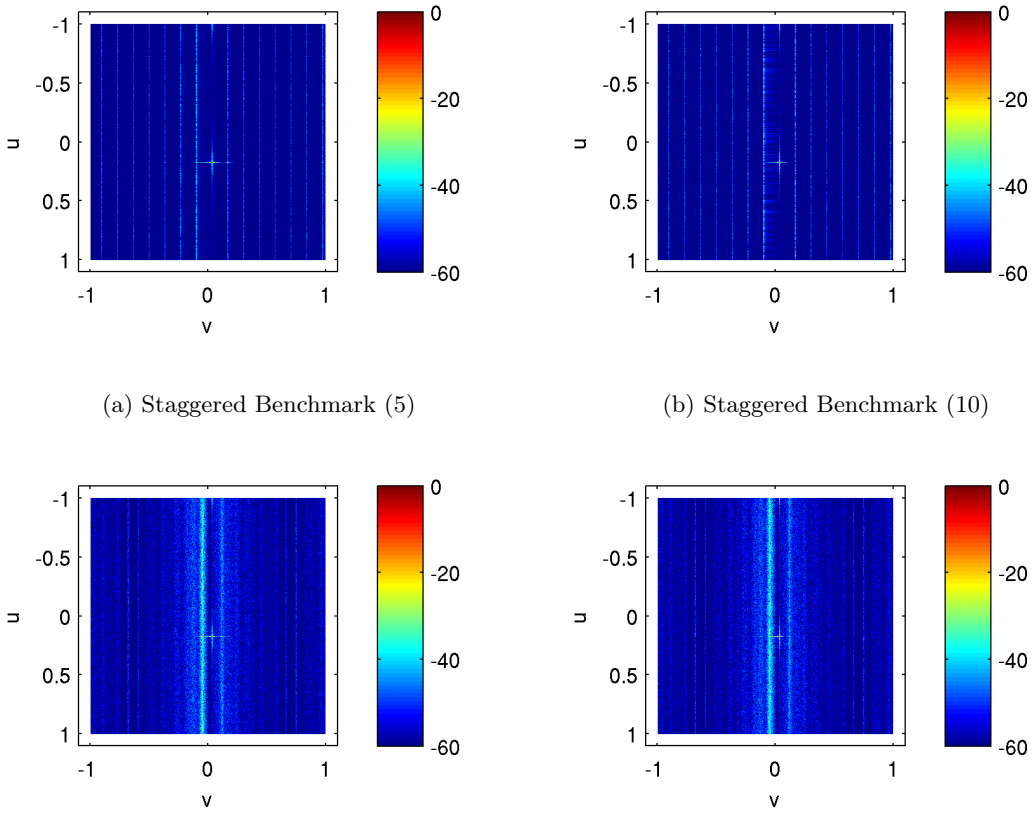

(a) Staggered Benchmark (5)

(b) Staggered Benchmark (10)

(c) Staggered Linear Arrays (5)

(d) Staggered Linear Arrays (10)

Figure 5.8: Two-dimensional normalised radiation patterns of the staggered benchmark array lattice concepts and of the staggered variable-length linear arrays array lattice concepts for the stagger values 5 and 10. The main beam of the array lattice concepts has been scanned to (10,2) deg.

Figure 5.8 is very similar to Figure 4.4 and Figure 5.3 and shows nothing unexpected. The absence of influence of the taylor taper is again observed for all subfigures in this figure.

5.2.5 Variability between Designs

Staggering does not change the variability between designs. An analysis of the variance in the radiation patterns of the staggered array lattice concepts shows similar results as the analysis carried out in the previous section. In particular for the staggered variable-length linear arrays array lattice concept the maximum variance is -72.5 dB.

5.3 Array Lattices based on Polyominoes

In Section 5.1 and in Section 5.2 three different array lattice concepts have been considered. These concepts were all variations on the benchmark antenna. The polyomino array lattice concept differs from these concepts in the sense that it employs a full two-dimensional approach.

The polyomino concept investigated here builds on the work described in [21]. In this paper polyominoes are defined as concatenations of squares like the blocks in the famous tetris game. Each polyomino has a certain order, which is the number of squares that make up the polyomino. There are often various polyominoes that have the same order. For example, tetris uses different tetrominoes in its puzzles, which are polyominoes of order four.

Polyominoes can also be used to cover an array lattice. In [21] it was argued that only a small number of polyominoes can be sufficient to cover the entire array lattice. Besides that it was claimed that it is possible to introduce the required amount of irregularity in the phase center positions to suppress grating lobes. However, the challenge is to generate a cover with the desired level of sparsity, irregularity and industrial feasibility. Besides the general requirements it should be possible to apply an evolutionary optimization algorithm at a later stage. To that end operations like mutation, selection, crossover and inheritance must be defined in a meaningful way.

In order to assess whether the claims made in [21] are still valid for the problem defined in Section 2.2 the 4L polyominoes array lattice concept uses L-shaped tetrominoes for its subarrays. The use of tetrominos will not result in a fill factor that is favorable with respect to the benchmark antenna. To that end polyominoes of at least order 10 need to be used. For the design of the feed network it is desirable that the number of radiating elements in a subarray is a power of two. Hence, polyominoes of order 16 need to be considered at a later time, should the 4L polyominoes array lattice concepts show promising results.

5.3.1 Generation of the Array Lattice

Although polyominoes have been used in [21] to completely tile relatively small apertures, little or no details are provided on how these tilings were obtained. Theory exists that enables one to completely tile a plane using copies of a single polyomino, called a prototile. Of particular interest are Conway's criterion and the translation criterion [29], which give the necessary and sufficient conditions under which a single polyomino can complete tile an infinite plane in $\mathcal{R}^2$. The related problem of telling whether a finite set of polyominoes is capable of completely tiling such a plane is proven to be algorithmically undecidable [30]. Others suggest the use of an evolutionary algorithm [31] for this task. This evolutionary algorithm would encode the a sequence of polyominoes and their orientation as its genes. From these genes a tiling is obtained by wrapping the polyominoes in a spiral-like fashion around the first polyomino. Note that an evolutionary method constructed in this way is not likely to obtain a complete tiling.

One of the most compelling arguments to use polyomino-shaped subarrays is the property that they introduce irregularity in the phase-center positions. Therefore a method based on repetiting

a unit cell that consists of a small number of polyominoes is undesirable. An alternative method could start with a small set of "well-chosen" polyominoes and use an exhaustive search technique such as DLX [32] to find a complete tiling. Unfortunately the complexity of these search strategies increases exponentially in time. This means that there is a certain plane size for which these algorithms fail to obtain a solution within a reasonable timeframe. This plane size is much smaller than the size of the array lattice, which renders this method unusable. Finally, using an evolutionary algorithm the way it was done in [31] is not an option either. This is mainly because it has the same exponential increase in computational complexity as an exhaustive search method [10].[2] Apart from that the application of an evolutionary algorithm in this sense is questionable, because small variations in the polyominoes close to the origin have an impact on the placement of all polyominoes further away from the origin. That way, a small change in the genome leads to a completely different layout, which contradicts with the rationale behind evolutionary algorithms.

Considering the observations earlier in this section, the following method is proposed for the generation of array lattices that consist of 4L polyomino subarrays. First all possible covers for a 12 by 10 rectangle will be computed using an exhaustive search method. Then, from this pool of solutions random tiles will be used to cover the entire array lattice.[3]

The problem of finding all possible covers for the 12 by 10 rectangle is known as the exact cover problem. For this kind of problem several solution methods exist. One of them is Knuth's Algorithm X with dancing links optimization [32], known as DLX. Let A be the set of all possible shapes. Then this algorithm tries to find all subsets of A such that the entire area is exactly covered, which means that there are no gaps between the shapes and that no shapes overlap.

Algorithm X is an exhaustive, recursive depth-first-search algorithm that employs a search heuristic to speed up the process. It can be summarized as follows. First a gridpoint is selected that contains the smallest amount of possible covering shapes. One of these shapes is selected and placed onto the grid. After that all shapes that overlap with the just-placed shape are temporarily removed from the set. This process is recursively iterated until either an exact cover is found or until a gridpoint has been found for which no overlapping shape exist. If an exact cover is found it will be stored. In the next step the method returns to the previous level, restores all shapes that have been temporarily removed from A and tries another shape until all combinations have been tried.

Once all exact covers have been found they can be used as building blocks to exactly cover the entire array lattice. This will be done by drawing random samples from the set of all possible building blocks. These random blocks are then placed next to each other until the entire array lattice is exactly covered.

[2] For this claim the authors of [10] refer to [28]. More recent research indicate that under certain conditions linear increase in computational complexity can be achieved. [33]

[3] This is different from using a unit cell to tile the entire aperture, since each tile is different.

5.3.2 Discussion of the Array Lattice

Zooms of the array lattices are depicted in Figure 5.9. The 12 by 10 blocks can be seen in Figure 5.9a. Figure 5.9b is less clear, it is difficult to visually assess the irregularity in the phase center positions. However, because of the way the array lattice has been generated, it is known that a level of regularity is present. Therefore some grating effects are also expected in the principal plane cuts.

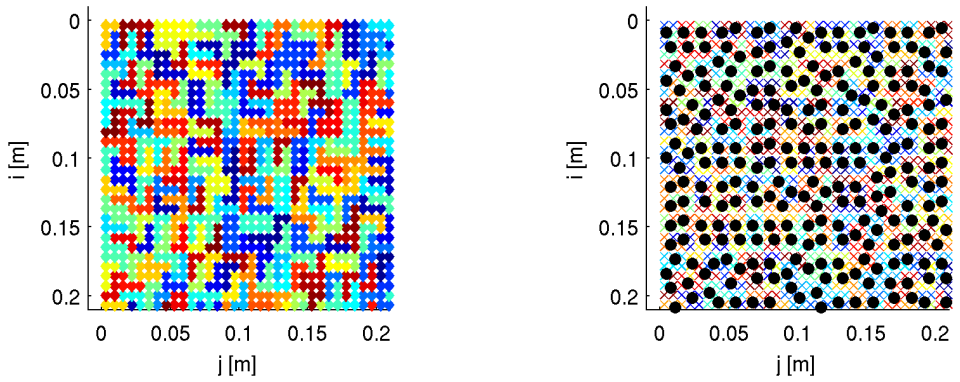

(a) b (b) a

Figure 5.9: 4L Polyominoes - Array Lattice

Although the method by which the array lattice is generated imposes a level of regularity it has a number of advantages. These advantages relate to the desirables mentioned at the beginning of this section. The first advantage is the organisation of the array lattice in tiles. Although the tiles are not the same, they do have the same size, number of radiating elements and the same number and type of subarrays. The second advantage is that the implementation of an evolutionary optimization algorithm is really straight forward. Each tile can be represented as an integer index in the table of all possible tiles. Therefore, each array lattice can be represented as a constant-length vector of integers. Hence, the implementation of mutation, crossover and inheritance becomes trivial. Mutation can be implemented by changing the value of a given integer into a random (but allowed) integer. Crossover can be implemented by swapping two integers that have the same index in the two vectors. Finally inheritance can be implemented by chosing for each index an integer from one of the parent vectors.

Considering the design guidelines the following can be observed. Generally speaking, because of the introduced irregularity the phase center positions do no longer follow a regular grid. Therefore, the first design guideline is considered violated. Since only four building blocks have been used the second design guideline has been honored. The final guideline demands that tiles can be identified. An obvious choice would be to identify the sets of 12 by 10 gridpoints as tiles. Although these sets of subarrays are not identical, they share the same number of subarrays. The irregularity in the electronics has already been penalized, so the third guideline is considered honored.

5.3.3 Principal Plane Cuts

The elevation cut of the 4L polyominoes array lattice concept has been depicted in Figure 5.10a. This figure shows poor performance. A lot of grating lobes violate the mask specifications and the sidelobes next to the main beam do not decay fast enough. The highest grating lobe is at -14 dB. The grating lobes result from the regularity introduced by the tile-based approach.

The corresponding azimuth cut is depicted in Figure 5.10b. This figure shows better performance than the benchmark antenna. This makes sense, since the subarrays of the benchmark antenna have a much larger width, which leads to smaller quantization errors at the boundaries of the subarrays. The highest grating lobe is at -29 dB. Note that the positions of the grating lobes in Figure 5.10b correspond to the positions of the grating lobes of the benchmark antenna in Figure 4.3. Since the tiles have the same width as the subarrays of the benchmark antenna, it can be concluded that the tiles are responsible for the grating lobes in the azimuth cut.

Note that due to the subarray organisation of the array lattice no large difference between the azimuth cut and the elevation cut is to be expected. The observed difference relates to the difference in scan angle and to the difference in interelement spacing.

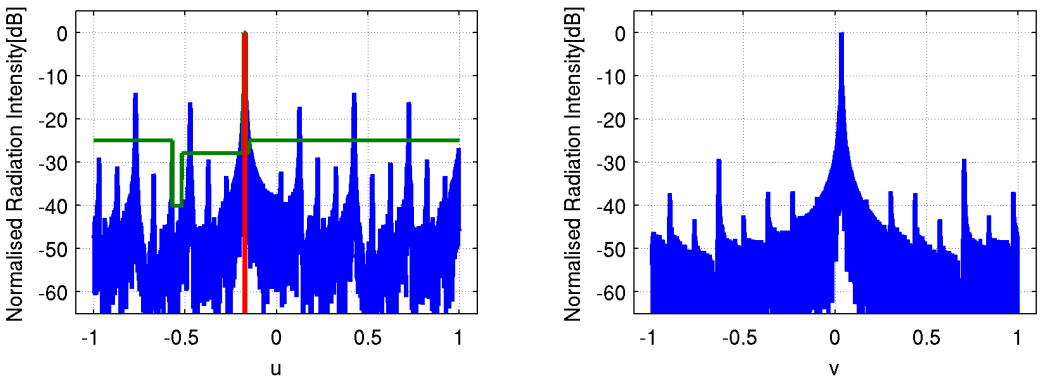

(a) Elevation Cut - 10 deg scan

(b) Azimuth Cut - 2 deg scan

Figure 5.10: 4L Polyominoes - Principal Plane Cuts

5.3.4 Two-dimensional Radiation Pattern

The two-dimensional normalised radiation pattern that belongs to the 4L polyominoes array lattice concept has been depicted in Figure 5.11. This figure shows that the grating lobes observed in Figure 5.10 are not limited to the principal plane cuts. Although not displayed here, this is also the case when the beam is scanned in one of the two principal planes. This is due to the two-dimensional subarrays. These subarrays lead to quantization errors in two dimensions, even if the applied phase taper is independent of one of the two dimensions.

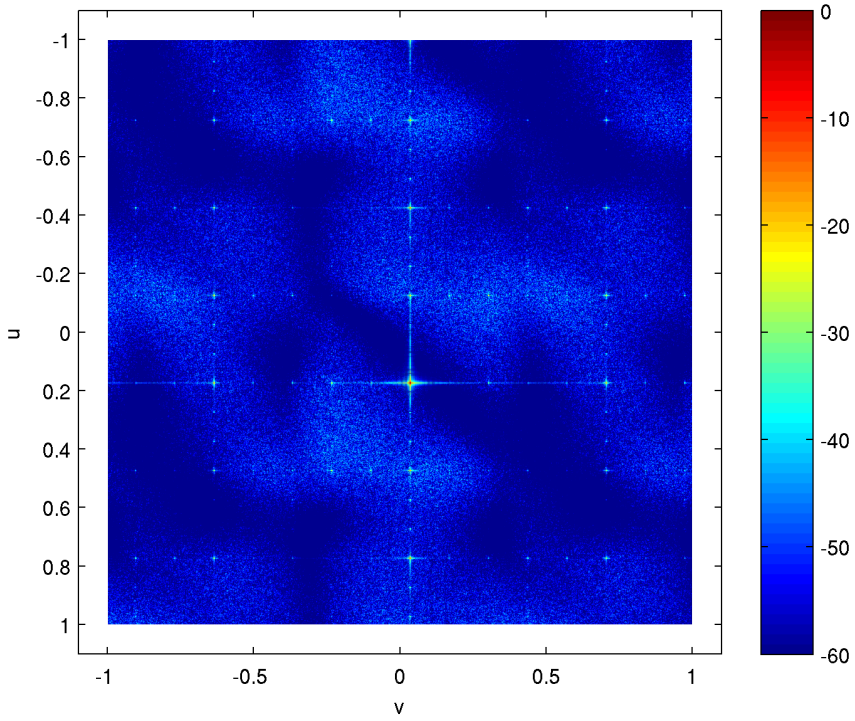

Figure 5.11: 4L Polyominoes - Two-dimensional radiation pattern - (10,2) deg scan

5.3.5 Variability between Designs

Also for the 4L polyominoes a variability analysis has been carried out. The variance between the 200 different designs is -130 dB. Such a low variance indicates that the radiation pattern is largely independent of the selection of tiles. This, combined with the grating lobes shown in Figure 5.10, is a bad foreboding for further optimization steps. It means that any selection of tiles has a very high probability to share the elevation cut and the azimuth cut of Figure 5.10. Therefore it seems unlikely that an optimization routine employed in an additional step will be able to compensate for the grating lobes shown in Figure 5.10.

5.3.6 Array Lattice Concepts based on Octominoes

A logical next step in this investigation would be to consider higher order polyominoes. To that end polyominoes of order eight would have been used. Unfortunately no suitable array lattice generation method could be implemented in time. This in combination with the poor results achieved by the 4L polyominoes array lattice concept led to the choice to disband the full two-dimensional approach in Chapter 6.

Polyominoes of order eight pose a bigger challenge than polyominoes of order four. All difficulties mentioned earlier in this section still hold: no unit cell based approach is desirable, exhaustive search methods are not feasible and methods based on evolutionary algorithms are not feasible and very likely not able to obtain a complete tiling. The tile-based approach described earlier

in this section can also not be used, because it would lead to similar performance, which would be unacceptable.

A possible solution to this problem is inspired by jigsaw-puzzles. To this end DLX was modified such that it obtained all solutions that obeyed two rules. The first rule is that all essential gridpoints should be covered. The second rule is that no shapes are allowed to overlap on anywhere, independent of whether the gridpoints are considered essential or not.

For the construction of a complete tiling, square cells have been defined that consist of 64 grid points. These cells have a square core of 16 grid points, which are considered essential. The core is surrounded by a band of non-essential gridpoints of width two. These cells can now be connected just like the pieces of a jigsaw puzzle. In this way an exact cover can be obtained.

The step to place the tiles onto the grid of 320 by 320 gridpoints proved too difficult to carry out within an acceptable timeframe. The devised approach was to first compute all possible neighbours for each cell. This can and has been efficiently done. The tiling process was implemented using a recursive depth-first search algorithm. This is problematic because each jigsaw-puzzle piece depends at the time of placement on at least two neighbours. Thus, the placement dependency graph is no longer a tree and tree-search algorithms are not suitable.

5.4 Irregularity Analysis based on the Autocorrelation Function

In the previous sections of this chapter the concept of irregularity has been mentioned a number of times. Irregularity was used to estimate the expected grating lobe performance. In this section an attempt will be made to quantify this concept using the autocorrelation function (ACF). This function has been introduced in Section 4.3. It plays a key role in signal processing theory, where it is used to characterize random variables.[35]

The ACF of some signal $I(x)$ as function of some shift τ has been defined in Equation 5.3 as the correlation between I and a shifted version of itself. A more practical implementation of the ACF is given in Equation 5.4. The constant a is chosen such that $I(x) = 0$ for all $|x| > a$. Note that because of this, as τ increases, the intersection of $I(x + \tau)$ and $\overline{I(x)}$ that is nonzero becomes smaller.

In the case that I is used to model the phase center positions of an array lattice, it can be written as a sum of shifted delta distributions. The shifts are found by considering the horizontal coordinates of the phase center positions.[4] Only if the shift τ is chosen such that at least two delta distributions coincide will this result to a nonzero contribution to $R(\tau)$. Thus, in that case, $R(\tau)$ is expected to look like a sum of shifted delta distributions as well.

[4]Note that this is equivalent to projecting the phase center positions onto the horizontal axis.

$$R(\tau) = \frac{E\left[\left(I(x)-\mu\right)\left(I(x+\tau)-\mu\right)\right]}{\sigma^2} \tag{5.3}$$

$$= \int_{-a-\tau}^{a+\tau} I(x+\tau)\overline{I(x)}dx \tag{5.4}$$

The ACF will be evaluated in the horizontal dimension on the phase center positions only. That is, the autocorrelation function has been computed for an array that has radiating elements on the phase center positions of the array under investigation. Furthermore, these radiating elements are assumed to have unit excitations, so no beam scanning or tapering has been applied.

Full-scale plots of the ACF of the benchmark array lattice concept, the variable-length linear arrays array lattice concept and the staggered variations of these array lattice concepts can be found in Figure 5.12. These plots look similar. There are some differences between them, but not enough to justify the differences in the azimuth cuts of these array lattice concepts.

The triangular shapes that make up these six plots can be explained as follows. Each array lattice concept has a constant average phase center density $PH(x)$. That is, every large enough interval $[x, x+\tau]$ contains on average the same number of phase centers. Because the phase center density is uniform, the correlation is proportional to the intersection of $I(x)$ and $I(x-\tau)$. This intersection decreases linearly as the magnitude of the lag $|\tau|$ increases, which explains the triangular shapes.

This large-scale behavior is of little use if the objective is to quantify the irregularity present in the phase center positions. Therefore only lags in the order of the subarray length will be considered. The results for the benchmark array lattice concept are depicted in Figure 5.13b. This figure depicts the azimuth cut side by side with the corresponding zoom of the ACF. Similar figures have been generated for the variable-length linear arrays array lattice concept (Figure 5.14b), for the staggered benchmark array lattice concepts (Figure 5.15) and for the staggered variable-length linear arrays array lattice concepts (Figure 5.16).

From the zooms of these six ACF plots two extreme cases can be identified. These are the benchmark array lattice concept and the staggered benchmark array lattice concept, where a stagger value of ten has been used. The first case shows, in comparison to the other azimuth cuts, high grating lobes. The ACF is very localized: all the energy is concentrated around $\tau = nd_{ph}$, where d_{ph} is the average distance between phase center positions.

This behavior is completely reversed in the second case. Here, the grating lobes are suppressed with respect to the other azimuth cuts. The ACF is very non-localized: all the energy is evenly spread amongst all allowed phase center positions.

These figures show that the ACF can indeed be used to quantify the irregularity in the phase center positions of an array lattice. In fact, the more the energy in the ACF is distributed amongst the allowed phase center positions, the lower the grating lobes will be. The opposite is also true: the more the energy is clustered round the points nd_{ph}, the higher the grating lobes will be. Hence the ACF can predict the grating lobe performance, even without first computing the radiation pattern.

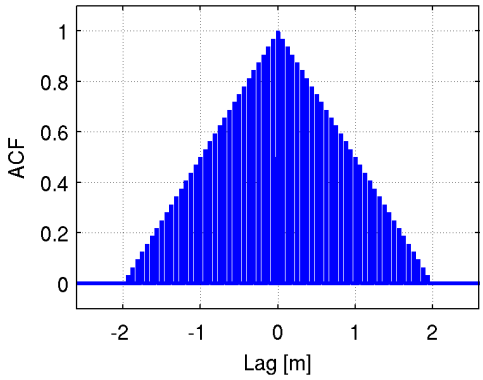

(a) Benchmark Array Lattice

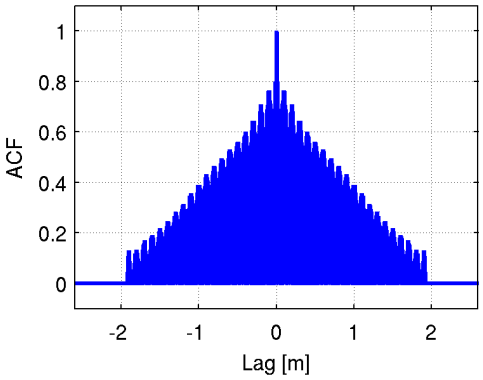

(b) Linear Arrays Array Lattice

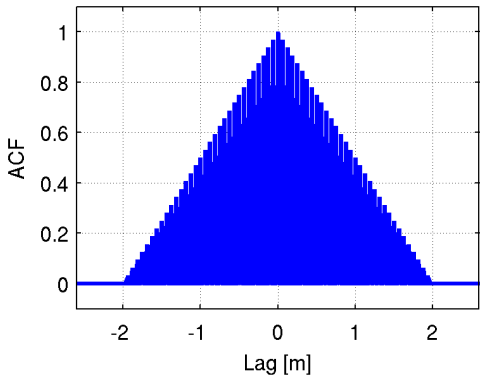

(c) Staggered Benchmark Array Lattice (5)

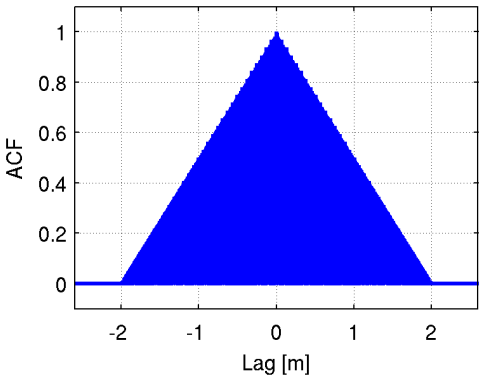

(d) Staggered Benchmark Array Lattice (10)

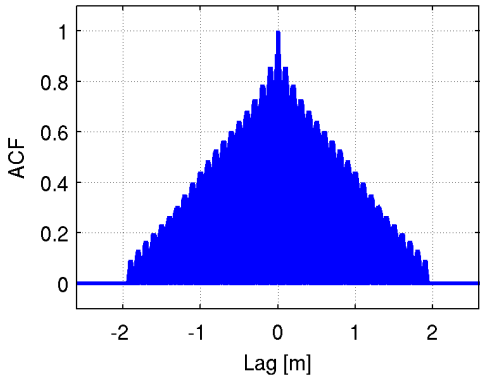

(e) Staggered Linear Arrays Array Lattice (5)

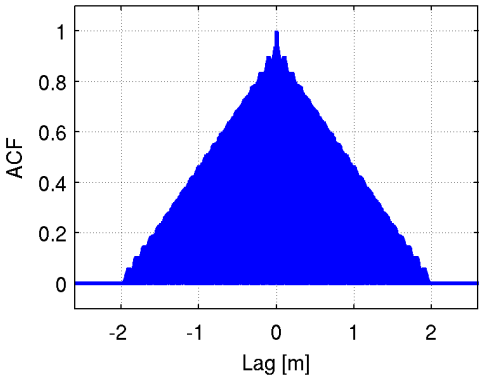

(f) Staggered Linear Arrays Array Lattice (10)

Figure 5.12: Autocorrelation Analysis of the First Approach

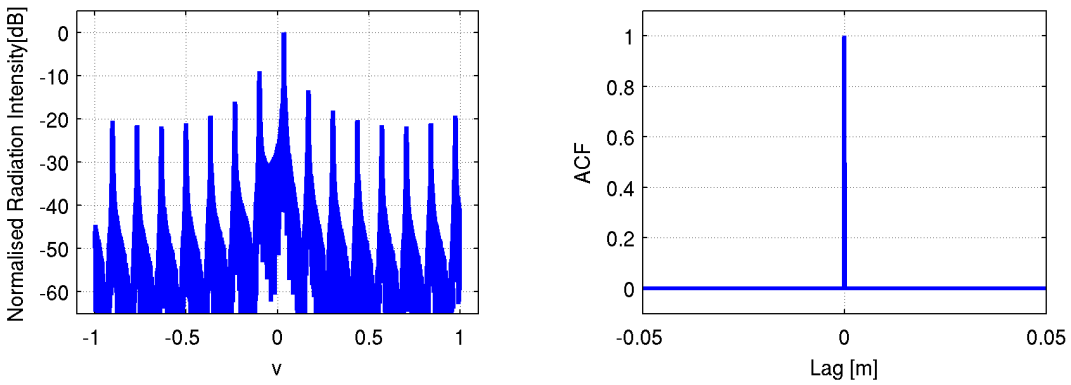

(a) Azimuth Cut, 2 deg scan (b) Autocorrelation Function (zoom)

Figure 5.13: Autocorrelation Analysis of the Benchmark Array Lattice

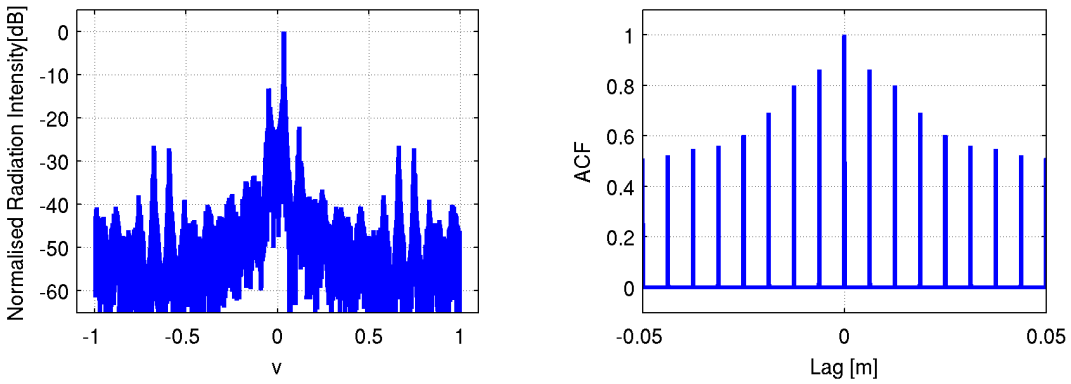

(a) Azimuth Cut, 2 deg scan (b) Autocorrelation Function (zoom)

Figure 5.14: Autocorrelation Analysis of the Linear Arrays Array Lattice

5.5 Conclusion

In this chapter two different approaches were investigated. Based on the principal plane cuts, the two-dimensional radiation patterns, the obtained level of sparsity, the evaluation of the design guidelines presented in Section 2.2 and on the difficulty with which array lattices can be generated, the array lattice concepts that belong to the first approach are definitely superior. Hence, this approach will be submitted to an in-depth investigation in Chapter 6.

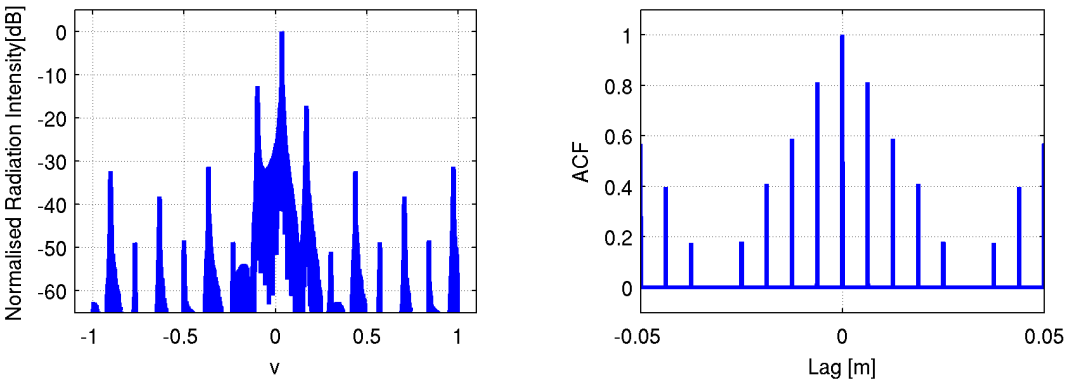

(a) Azimuth Cut, 2 deg scan

(b) Autocorrelation Function (zoom)

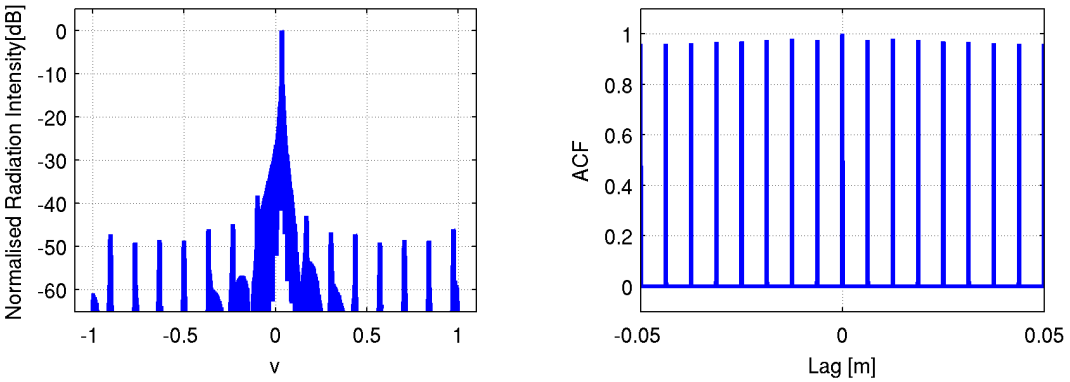

(c) Azimuth Cut, 2 deg scan

(d) Autocorrelation Function (zoom)

Figure 5.15: Autocorrelation Analysis of the Staggered Benchmark Array Lattice

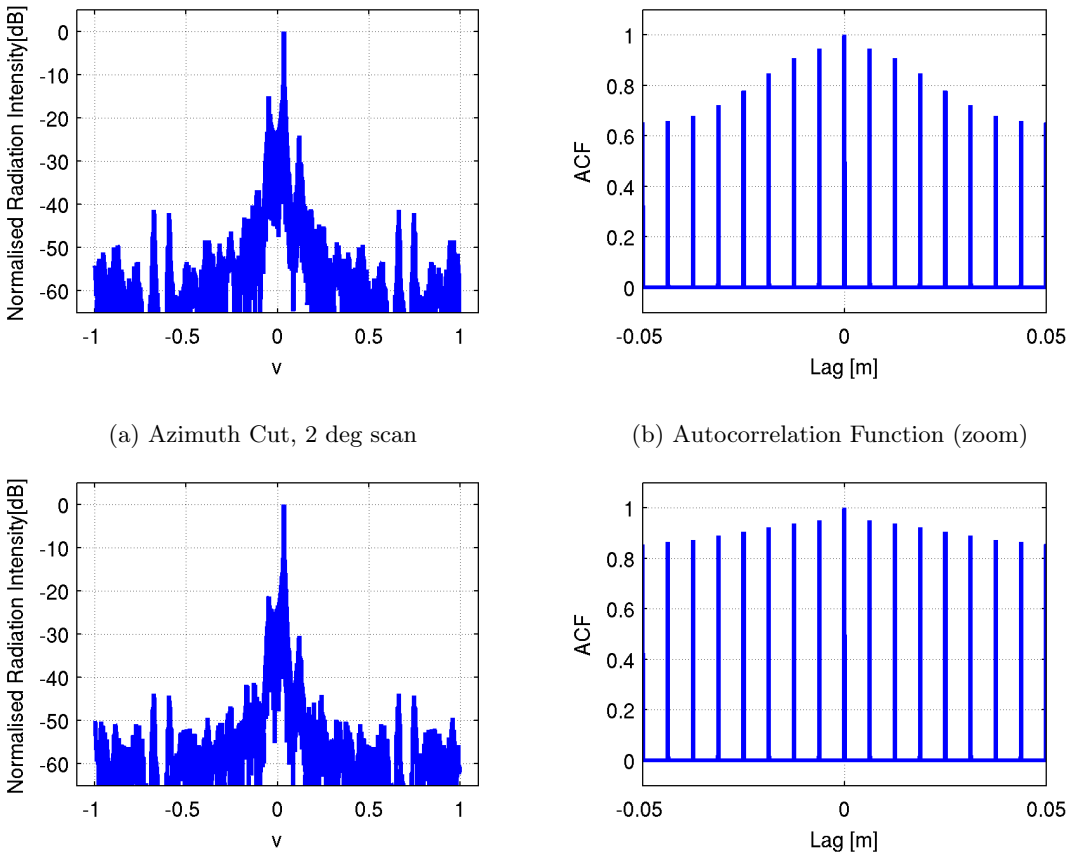

(a) Azimuth Cut, 2 deg scan

(b) Autocorrelation Function (zoom)

(c) Azimuth Cut, 2 deg scan

(d) Autocorrelation Function (zoom)

Figure 5.16: Autocorrelation Analysis of the Staggered Linear Arrays Array Lattice

Chapter 6

In-depth Investigation

The previous chapter discussed the initial investigation. In this part two approaches were considered. The first approach applied two different one-dimensional synthesis techniques to the problem defined in Section 2.2. In contrast, the second approach utilized a single two-dimensional synthesis technique for this purpose. In Section 5.5 it was concluded that the most promising approach is the first one. Therefore this chapter submits the concepts that follow this approach to a more in-depth investigation.

The in-depth investigation will be structured as follows. First the variable-length linear arrays will be further investigated in Section 6.1. This will result in a synthesis method for the azimuth dimension. After that a synthesis method based on density tapering will be proposed for the elevation dimension. This method will be detailed in section 6.2. Finally two designs will be recommended in Section 6.3.

6.1 Linear Arrays Antenna

An initial investigation of the concept of variable-length linear subarrays has already been presented in Section 5.1. This investigation will be continued here. First the effect of various sets of linear subarray lengths will be considered. After that an attempt will be made to reduce the amount of irregularity. Following their rationale, this irregularity is necessary in order to compensate for the increased grating effects that come with large subarrays. However, it contradicts with the requirements related to industrial feasibility.

6.1.1 Influence of Line Lengths

It was noted in section 5.1 that there is not much variance in the radiation patterns of various variable-length linear arrays antennas. These antennas have all been generated from the same set of linear subarray lengths. The azimuth cuts depend almost only on the set of linear subarray lengths from which the variable-length linear arrays antennas have been generated. This subsection investigates that dependence.

In total 16 sets of linear subarray lengths will be investigated. These sets are labeled from A to P and are listed in Table 6.1. Remember that the length of a linear subarray is expressed in radiating elements. If a linear subarray has length 12, then it consists of 12 consecutive radiating elements.

There are two reasons for chosing these sets of linear subarray lengths. The first reason is that the chosen subarrays should introduce as much irregularity in the phase center positions as possible. Based on the theory of combinatorics it is expected that this can be achieved by using prime numbers as subarray lengths. Slightly more general it is expected that the use subarray lengths that have a small number of divisors result in a high level of irregularity. The other reason is that it is desirable to keep the difference in length between subarrays in a set small. This avoids issues with power handling. Considering this, it is expected that the sets A, C, G, I and M show the best performance with respect to grating lobe suppression.

Table 6.1: Linear Array Lengths

Set	Lengths			
A	5	7	9	11
B	6	8	10	12
C	7	9	11	13
D	8	10	12	14
E	9	11	13	15
F	10	12	14	16
G	11	13	15	17
H	12	14	16	18
I	13	15	17	19
J	14	16	18	20
K	15	17	19	21
L	16	18	20	22
M	17	19	21	23
N	18	20	22	24
O	19	21	23	25
P	20	22	24	26

During the discussion of the variable-length linear arrays antennas in the initial investigation the variance in the normalised radiation patterns was depicted in Figure 5.4. Based on this only one antenna per set of linear subarray lengths will be considered. Considering a single design per set of linear subarray lengths is not statistically significant, but reproducibility has been experimentally verified. Based on these results the following trends can be discerned. These trends are supported by the azimuth cuts depicted in Figure 6.1.

Main beam The area close to the main beam remains unaffected by the difference in linear subarray lengths. In particular, for all array lattices, the first sidelobe next to the main beam is between -12 dB and -13 dB. Note that the same observation was made for the concept of staggering.

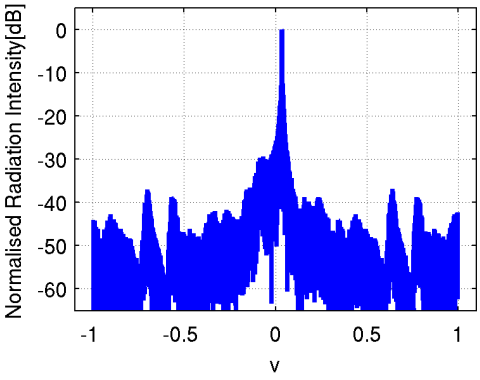

(a) Azimuth cut, 2 deg scan: $[7, 9, 11, 13]$

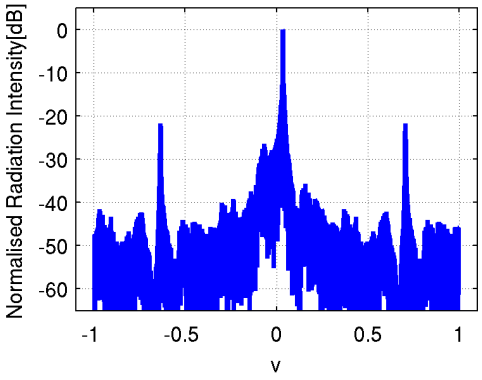

(b) Azimuth cut, 2 deg scan: $[8, 10, 12, 14]$

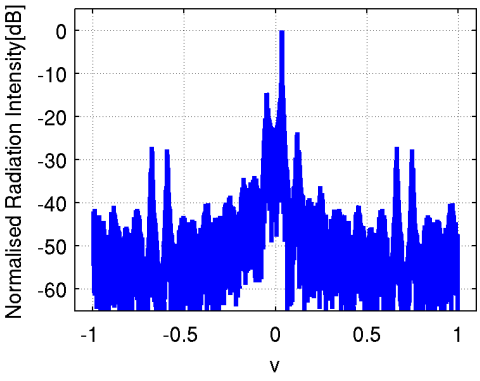

(c) Azimuth cut, 2 deg scan: $[13, 15, 17, 19]$

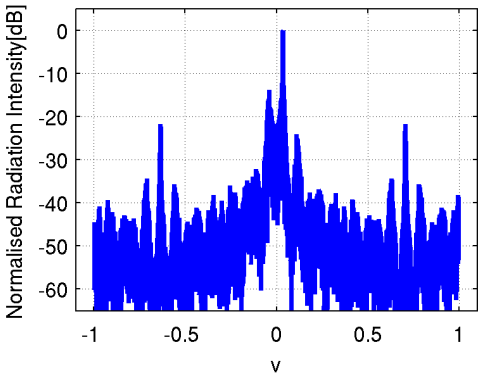

(d) Azimuth cut, 2 deg scan: $[14, 16, 18, 20]$

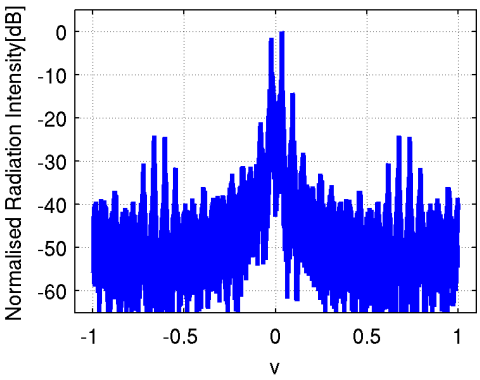

(e) Azimuth cut, 2 deg scan: $[19, 21, 23, 25]$

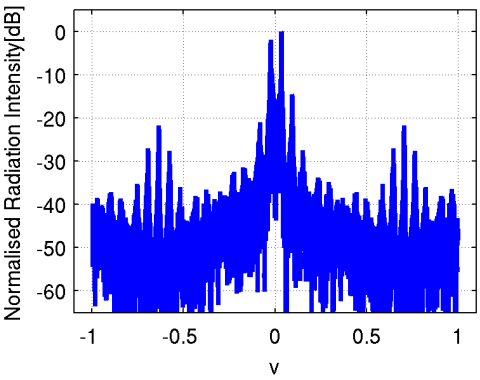

(f) Azimuth cut, 2 deg scan: $[20, 22, 24, 26]$

Figure 6.1: Investigation of the effect of different sets of subarray lengths on the azimuth cuts of the variable-length linear subarrays array lattices

Envelope The envelopes of the different azimuth cuts are similar. This can be seen in the increase in level of the first grating lobe as well as in the behaviour in the regions $v \in [-0.8, -0.45]$ and $v \in [0.55, 0.9]$. The envelope is best observed in the figures 6.1e and 6.1f.

First Grating Lobe The first grating lobe moves towards the main beam and its level increases as the average distance between the phase center positions increases.[1] Starting from the set labeled K the level of this first grating lobe becomes higher than the first grating lobe of the benchmark antenna. For the two sets with the largest linear subarrays, the first grating lobe becomes even as high as the main lobe.

Distance between Grating Lobes The distance between grating lobes decreases as the average distance between the phase center positions increases. This is related to the scaling property of the fourier transform and explains the observed displacement and increase in level of the first grating lobe. It also explains the difference in level of the grating effects around $v = -0.63$ and $v = 0.7$.

Even versus Odd Significantly lower grating lobes are observed when the linear subarray lengths are odd. This is because of the alignment of the grating lobes and the envelope. In the case of the even subarray lengths the grating lobes around $v = -0.64$ and $v = -0.7$ align with the maxima of the envelope.

In short one should remark upon the following notions. Other effects dominate the grating lobe behavior than was expected in the hypothesis. The third observation effectively discards all sets from K to P. From the perspective of sparsity the array lattices that result from the sets I or J are preferable. The array lattice that belongs to the set I performs best when the level of the grating lobes other than the first grating lobe are concerned. The array lattice that belongs to the set J performs best when the level of sparsity and the level of the first grating lobe are concerned. Therefore, the array lattice that belongs to the set J is the most favorable of the investigated array lattices.

6.1.2 Random Tiles

If one compares the azimuth cuts of the benchmark antenna (Figure 4.3) and a variable-length linear arrays antenna (Figure 5.2), the following can be seen. A variable-length linear arrays antenna outperforms the benchmark antenna with quite some margin. Therefore, two array lattice concepts are proposed that seek to trade regularity, and thus industrial feasibility, against increased grating effects.

The first array lattice concept is the concept of randomly placed linear arrays. This lattice concept uses tiles of linear subarrays that consist of 20 radiating elements. From these linear arrays 4 radiating elements will be removed from the ends. This way a single linear array

[1] Interestingly, there is an exception to this rule. The level of the first grating lobe tends to be lower for array lattices that use an even number of radiating elements in their subarrays. This behavior is yet to be understood.

consisting of 16 consecutive radiating elements remains placed in the tile. The second concept is a variation on the first and is called the concept of randomly thinned linear arrays. Instead of removing four radiating elements from the ends, four radiating elements will be removed at random. This allows for more possible phase center positions.

The advantages of both concepts are clear: subarrays consisting of a fixed number of elements are placed in squares on the array lattice, which is great from a construction point of view. On top of that, for the first concept only a single feed network needs to be designed. Then only four interconnects need to be designed in order to connect the feed network to the corresponding electronics grid. However, for both array lattice concepts the phase center positions follow a bandlike structure. These bandlike structures indicate a lot of regularity and therefore severe grating effects will be expected.

For each proposed method only a single design will be presented. Therefore the notions on statistical significancy apply here as well. Again, reproducibility has been experimentally verified. The results are discussed using the same methodology that has been used to discuss the other array lattice concepts.

Discussion of the Array Lattices An array lattice of both concepts has been depicted in Figure 6.2. The bands discussed earlier in this paragraph can be observed. The band structure of the phase centers of both array lattice concepts is remarkably similar. It should however be noted that the phase centers of the first array lattice concept are uniformly distributed, while the distribution of the phase centers of the second concept can be modeled using a normal distribution.

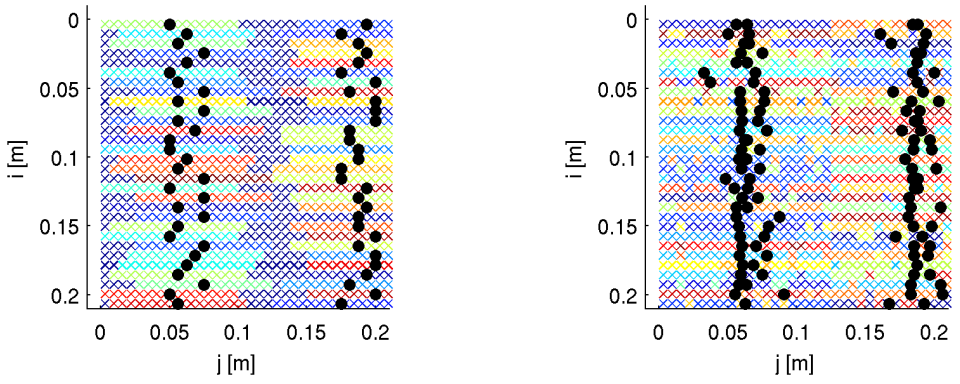

(a) Randomly Placed Subarrays

(b) Randomly Thinned Subarrays

Figure 6.2: Random Tiled Array Lattices

As mentioned earlier it is at least for the first concept possible to arrange the electronics in a regular grid. Besides that not more than 4 building blocks have been used and the antenna aperture consists of similar tiles. Therefore the array lattice of the first array lattice concept is in agreement with the design guidelines proposed in Section 2.2. The second array lattice concept agrees only with the similar tiles requirement.

Discussion of the Azimuth Cuts The elevation cuts of both concepts are the same as the elevation cut of the benchmark antenna depicted in Figure 4.2. The azimuth cuts can be observed in Figure 6.3. In both cases, at two degrees of scanning the first grating lobe has the same hight as the main lobe, which is unacceptable.

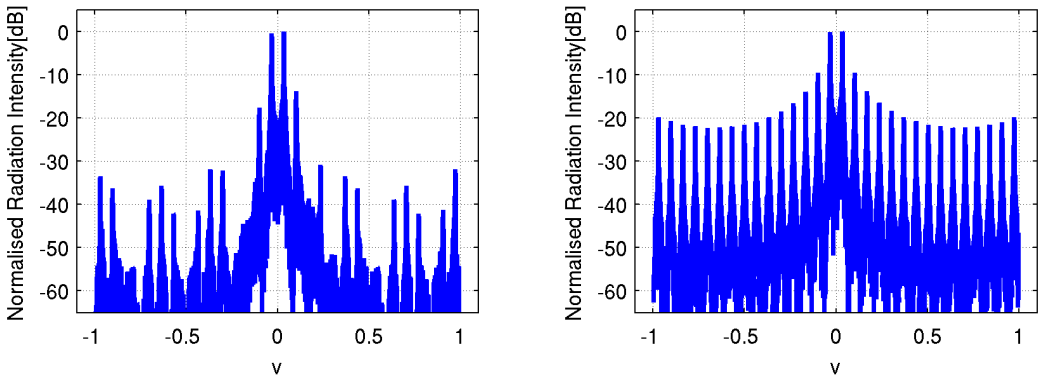

(a) Randomly Placed Subarrays

(b) Randomly Thinned Subarrays

Figure 6.3: Random Tiled Array Lattices - Azimuth Cuts, 2 deg scan

In short one could say that the irregularity introduced by the variable-length linear arrays is necessary. The cut in performance that comes with the proposed random tile methods is a price too high to pay.

6.1.3 Linear Arrays Antennas: Concluding Remarks

In summary, in the in-depth investigation of the variable-length linear array antennas two things were considered. First the effect of linear subarray lengths was investigated. From this investigation it followed that the sets I and J of linear subarray lengths yield the best performance. After that two new concepts were introduced, which sought to reduce irregularity at the cost of a performance penalty. However no acceptable level of performance could be obtained using either one of these two concepts.

Based on the results of these investigations it should be concluded that irregularity is necessary to obtain the same performance as the benchmark antenna. It is possible to reduce the irregularity by choosing a different set of linear subarray lenghts. However this reduction is very modest. Finally it should be concluded that under the restrictions of this project tiles and sufficient performance are mutually exclusive.

6.2 Density Tapering

In the first part of the in-depth investigation the concept of variable length linear arrays has been investigated. This concept obtained sufficient performance in the azimuth dimension. Until now a taylor taper was used to make sure that the elevation cut remained below the mask

specifications. However, a taylor taper has a taper loss in the order of 3.5 dB. Density tapering is a technique that seeks to reduce the fill factor and the taper loss at the cost of a completely irregular lattice while maintaining sufficient performance.

This section is organised as follows. First an implementation of density tapering as presented in [15] will be investigated. After that a number of variations will be proposed and investigated. Finally the resulting density taper will be applied to the benchmark lattice concepts and to the variable-length linear subarray lattice concepts.

The method presented in [15] involves a three-step procedure. The first two steps synthesize a density taper and a set of phase tapers. The third step consists of a local optimization routine. This third step is necessary in order to make sure that all masks are satisfied. Besides that this step allows for the incorporation of other requirements that cannot be easily incorporated in the density tapering procedure.

The beauty of this method is that it simultaneously finds the element positions as well as a set of phase tapers. Each radiation pattern that corresponds to a particular phase taper satisfies a prescribed mask. The downside of this method is that it is overly complex and does not obtain a suitable solution to the problem considered in this project within an acceptable timeframe. In particular the third step takes a very long time to complete. In [15] a runtime of over 10 hours has been reported for a much smaller problem. In this problem less than 64 radiating elements have been used. The radiation patterns were constrained by two mask specifications. The method presented further down this section is inspired by this work, but uses simpler methods in the first and the third step.

6.2.1 The Three-Step Method

The density tapering method presented in [15] was inspired by [10], which in turn uses the work described in [27]. According to these works, density tapering uses N uniformly excited radiating elements placed in a completely irregular lattice in order to emulate the behavior of a chosen continuous current source distribution. In particular, radiating elements will be densely spaced in areas where the level of the continuous current source is high.

In order to find the positions of the radiating elements, first some ideal continuous current source distribution needs to be considered. Based on this the cumulative continuous current source distribution is defined in Equation 6.1. In this equation, I_c is the cumulative continuous source distribution and i_c is the continuous source distribution. The constant a is chosen such that the continuous source distribution is zero outside the domain $[-a, a]$.

$$I_c(x) = \int_{-a}^{x} i_c(\psi) d\psi \tag{6.1}$$

The first step is to obtain a suitable reference source distribution. To this end he authors of [15] rely on the work presented in [34]. This method uses an iterative scheme to find a suitable reference source distribution. This method has two appealing features. The first is that it can

find solutions for several masks simultaneously. Apart from that the method can guarantee convergence because each iteration consists of two projections.

The next step is to find the radiating element positions from the obtained reference source distribution. To this end the interval $[-a, a]$ will be divided in N subintervals. These subintervals are connected by N+1 boundary points denoted as $\hat{x}_0, \hat{x}_1, \ldots, \hat{x}_{\mathrm{N}}$. Furthermore, the subintervals are chosen such that $\int_{\hat{x}_{n-1}}^{\hat{x}_n} i_c(\psi)d\psi = I_c(\hat{x}_n) - I_c(\hat{x}_{n-1}) = \frac{1}{\mathrm{N}}$. Thus each subinterval contains an equal "portion" of the reference source distribution. Finally, the positions of the radiating elements are chosen as the medians of i_c in each interval. As has been shown in [27], this is equivalent to the minimization over a weighted distance (in L^2) between the desired elevation cut and the synthesized elevation cut.

The result of the density taper technique does not comply with the mask specifications. This is especially true further away from the main beam. Furthermore there may be other requirements in place that were violated in step 2. In order to achieve compliance, [15] proposes to employ a quasi-newton optimization routine as a final step. This routine uses the result of the density tapering routine as its initial solution. This optimization routine simultaneously optimizes the n element locations and the dn phase coefficients using the costfunction shown in Equation 6.2. In this discussion n is the targeted amount of radiating elements and d is the number of prescribed masks and N is the number of points on which the array factor has been evaluated.

$$Penalty = \sum_{i=1}^{\mathrm{d}} \sum_{j=1}^{\mathrm{N}} \left[max(AF(u_j) - M_{upper,i}(u_j), 0) + 10min(M_{lower,i}(u_j) - AF(u_j), 0) \right] \quad (6.2)$$

6.2.2 Alternatives for Step 1 and Step 3

Each step in the three-step method serves a certain purpose. However the methods chosen are not necessarily the only way to achieve these purposes. This subsection discusses possible alternatives to the steps chosen by the authors of [15].

6.2.2.1 Reference Source Distribution

In order to come up with a suitable reference source distribution a number of approaches can be taken. In [10] it has been proposed to use a known taper function as reference, such as the taylor taper that has been used in the benchmark antenna. This allows to prescribe a pencil beam pattern with a certain sidelobe level. In order to synthesize a reference source distribution for arbitrary masks, [13] relies on the iterative fft method and [15] relies on the iterative projection method as presented in [34].

The method proposed in [10] does not really obtain a reference source distribution. Instead it uses known taper functions to this end and is therefore the most simple method of the three, but it is also the least flexible method. The iterative fourier transform method is simple but demands that the reference source distribution is sampled at a samplerate of $\lambda/2$. On top of that,

only a single mask can be synthesized for at once and convergence has not been guaranteed. The iterative projection method is more complex but works for arbitrary sampling of the reference source distribution because it does not explicitly depend on the fourier transform. Also multiple beams can be optimized for simultaneously and convergence can be guaranteed.

6.2.2.2 The Density Taper Method

The second step does not allow much variation on the concept level. Therefore there are no alternatives and the method presented in [27] will be used without modification.

6.2.2.3 Final Local Refinement

The three-step method needs a final step in order to make sure that the resulting density taper is in compliance with the specifications. These specifications are not necessarily limited to mask specifications. For instance, there might also be specifications for the minimum interelement spacing. A local quasi-newton optimization routine allows for easy incorporation of such requirements.

There are several local optimization schemes that can be applied in the third step. On top of that, there are several ways in which such a method can be applied. As mentioned, in [15] all specifications are optimized for in a single run using a quasi-newton optimization scheme. However, for the problem at hand such an approach is not computationally feasible. Different optimization schemes are not expected to make an orders-of-magnitude difference. Therefore the remainder of the discussion will focus on different ways to apply the quasi-newton method.

In order to make the third step computationally feasible for the problem at hand, the step is split in two parts, step three and step four. In the third step the quasi-newton method is applied to an enhanced mask without scanning. The enhancement makes sure that the fourth step converges faster. In the fourth step the beam scanning will be implemented. This can be done in two ways. The first way is to use subsequent quasi-newton optimization routines to synthesize phase tapers for discrete scan angles. Alternatively, the density taper can be synthesized such that no mask violations occur as linear beam scanning is applied.

Both implementations of beam scanning have their advantages and their drawbacks. The first method has the advantage that the required mask in step three is less stringent. This has a minor positive effect on the convergence rate and possibly also on the level of sparsity that can be achieved. This method has also a number of drawbacks. The most obvious one is that it is not possible to scan to angles for which no phase taper has been synthesized. Furthermore, the synthesis of each phase taper requires a complete run of a quasi-newton routine, which is computationally expensive but not infeasible.

The second method has the advantage that all scan angles are supported. Furthermore the computation of a phase taper in the fourth step is computationally cheap. The third step however requires a more stringent mask that extends the usual range of u.

6.2.3 The proposed method

The previous subsection discussed several alternatives for the steps in the three-step method presented in [15]. In this section a new method will be presented that is based on a tradeoff of these alternatives. It consists of four steps, where the third step of the three-step method is divided as discussed in the previous subsection. This method has been implemented and the obtained results will be presented when appropriate.

6.2.3.1 Step 1: Iterative FFT Method

In order to apply the density tapering method described in [27] first a reference source distribution is required. This reference source is obtained using the iterative fourier transform method mentioned in [13]. This method is preferred over the iterative projection method described in [34] because of its simplicity. It is also preferred over the method of using the taylor-distribution of the benchmark antenna proposed in [10] because of its flexibility.

The iterative fourier transform method has been summarized in listing 6.1. This method assumes a $\lambda/2$-spaced linear array lattice. The length of this lattice is 2.25 m, which results in 534 radiating elements. Initially, ArrayIllum contains the excitation coefficients of these radiating elements. From that illumination the initial radiation pattern will be computed in 8192 points. The initial radiation pattern will then be stored in ArrayFactor, after which the method starts to iterate.

The first step of each iteration is to apply sanitization to the array factor. This means that first the array factor will be normalised. After that all points whose absolute values violate the mask specification are replaced by the corresponding points at the mask specification. The phase of these points is not altered. After that the corresponding array illumination will be computed. This illumination will in turn also be sanitised, meaning that it will be truncated to 534 samples and normalised. Finally the array factor will be recomputed and then the next iteration begins. Because of the very short runtime no explicit stopping criterium has been used. The method keeps iterating until numIterations have occured.

```
1  ArrayFactor = ifftshift(ifft(ArrayIllum,8192));
2  for iteration := 1 to numIterations
3    ArrayFactor = ArrayFactorSanitization(ArrayFactor);
4    ArrayIllum = fft(fftshift(ArrayFactor),8192);
5    ArrayIllum = ArrayIllumSanitization(ArrayIllum);
6    ArrayFactor = ifftshift(ifft(ArrayIllum),8192);
7  end
```

Listing 6.1: Iterative Fourier Transform Method

The resulting reference source distribution and the corresponding radiation pattern are depicted in Figure 6.4. It should be noted that the normalised magnitude depicted in the upper part of Figure 6.4a is relatively smooth. This is a desired property, which results in a better approximation of the radiation pattern at the end of step two.[2]

[2]It could also be noted that the nadir-dip is wider than the nadir-dip presented in section 2.2. This is related to either of the two beam scanning methods presented in the fourth step. Its discussion will therefore be delayed until the discussion of this step.

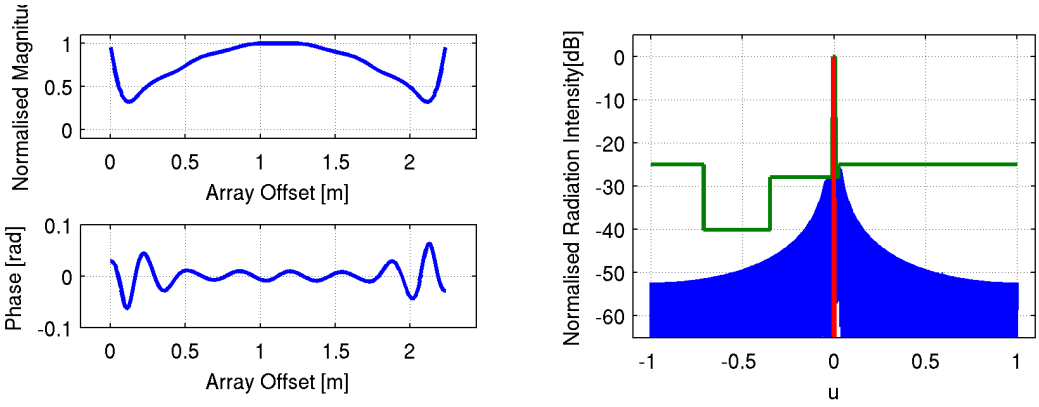

(a) Reference Source Distribution

(b) Radiation Pattern

Figure 6.4: Results of the first step of the proposed density tapering method

6.2.3.2 Step 2: Density Tapering

The second step is to apply the density tapering method described in [27]. To this end 4 values of N are chosen: 320, 288, 256 and 224. These values correspond to reductions in number of radiating elements with respect to the benchmark antenna. The benchmark antenna has 320 rows, so N=320 corresponds to a fill factor of 100 percent. Similarly, N=288 corresponds to a fill factor of 90 percent, N=256 corresponds to 80 percent and N=224 corresponds to 70 percent. Note that these fill factors are expressed with respect to the fill factor of the benchmark antenna. This differs from the definition of the fill factor stated in Section 2.3.

Once the values of N have been chosen the next step is to compute the cumulative distribution function of the reference source. Using this function the boundary points $\hat{x}_n$ can be found by normalizing the cumulative distribution function and selecting the points $I_c(\hat{x}_n) = {}^{n}/_{N}$, $n = 0, \ldots, N$. After that the barycenters of regions between two consecutive boundary points are taken as the positions of the radiating elements.

In order to compute the cumulative distribution function the integral in Equation 6.1 needs to be evaluated. To that end the distribution function of the reference source will be interpolated to a much higher samplerate. For this purpose piece-wise cubic interpolation has been used. After the interpolation step the reference source distribution function is sampled at 8192 points. The next step is to compute the normalized cumulative distribution function by computing the cumulative sum of the interpolated reference source distribution and normalizing it. Finally the positions of the radiating elements can be obtained from the normalized cumulative distribution.

Based on the reference source distribution depicted in figure 6.4a, the four values of N and this method four density tapers have been generated. The density tapers and the corresponding radiation patterns are presented in Figure 6.5 (for N = 320), Figure 6.6 (for N = 288), Figure 6.7 (for N = 256) and in Figure 6.8 (for N = 224). Finally the distance between two consecutive elements has depicted in Figure 6.9. This last figure shows that there is at least a separation of a half lambda between consecutive elements. Notice that the shapes in Figure 6.9 resemble the magnitude of the reference source distribution depicted in the upper part of Figure 6.4a.

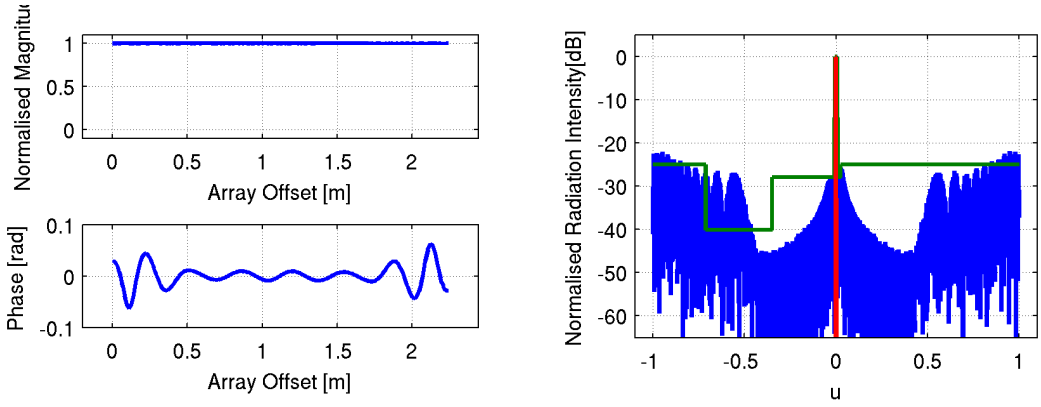

(a) Reference Source Distribution (b) Radiation Pattern

Figure 6.5: Results of the second step of the proposed density tapering method with N = 320

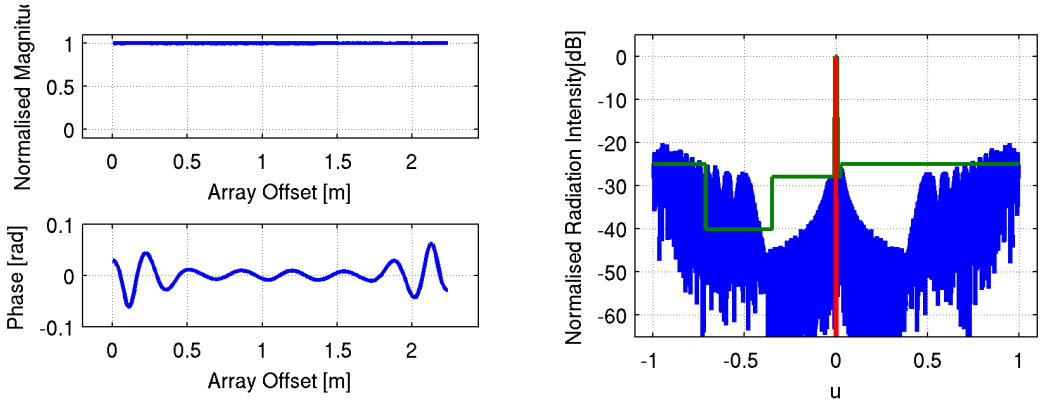

(a) Reference Source Distribution (b) Radiation Pattern

Figure 6.6: Results of the second step of the proposed density tapering method with N = 288

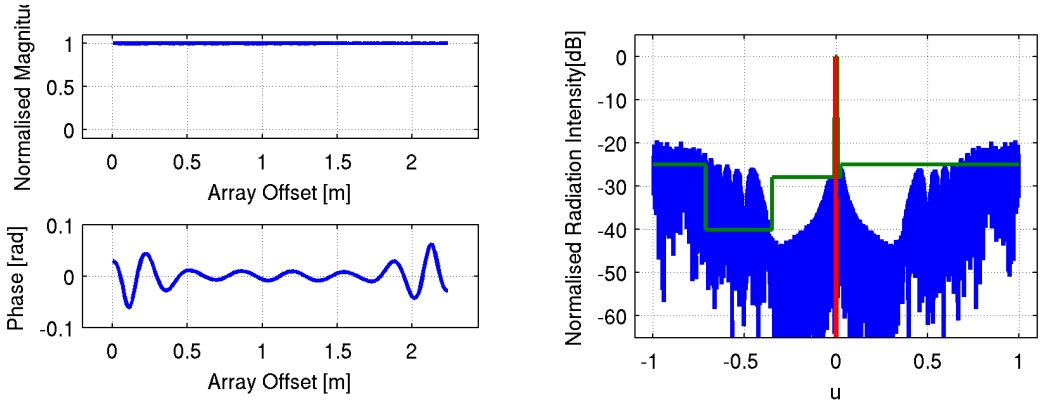

(a) Reference Source Distribution (b) Radiation Pattern

Figure 6.7: Results of the second step of the proposed density tapering method with N = 256

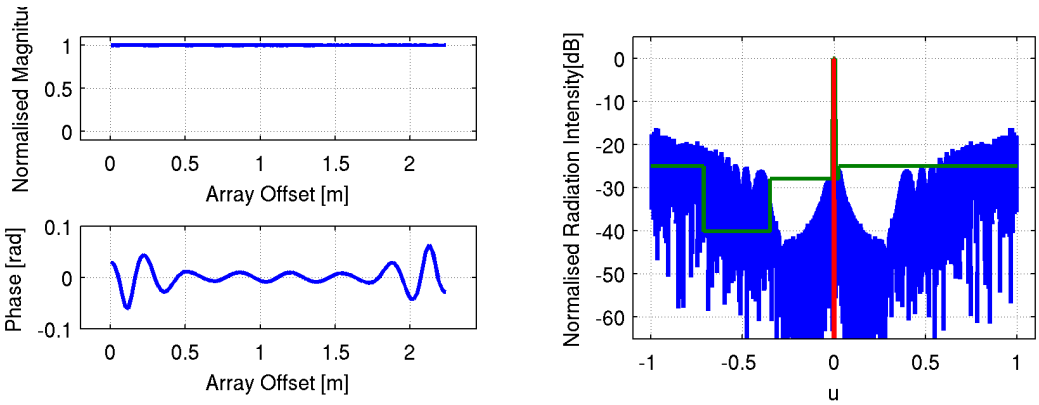

(a) Reference Source Distribution

(b) Radiation Pattern

Figure 6.8: Results of the second step of the proposed density tapering method with N = 224

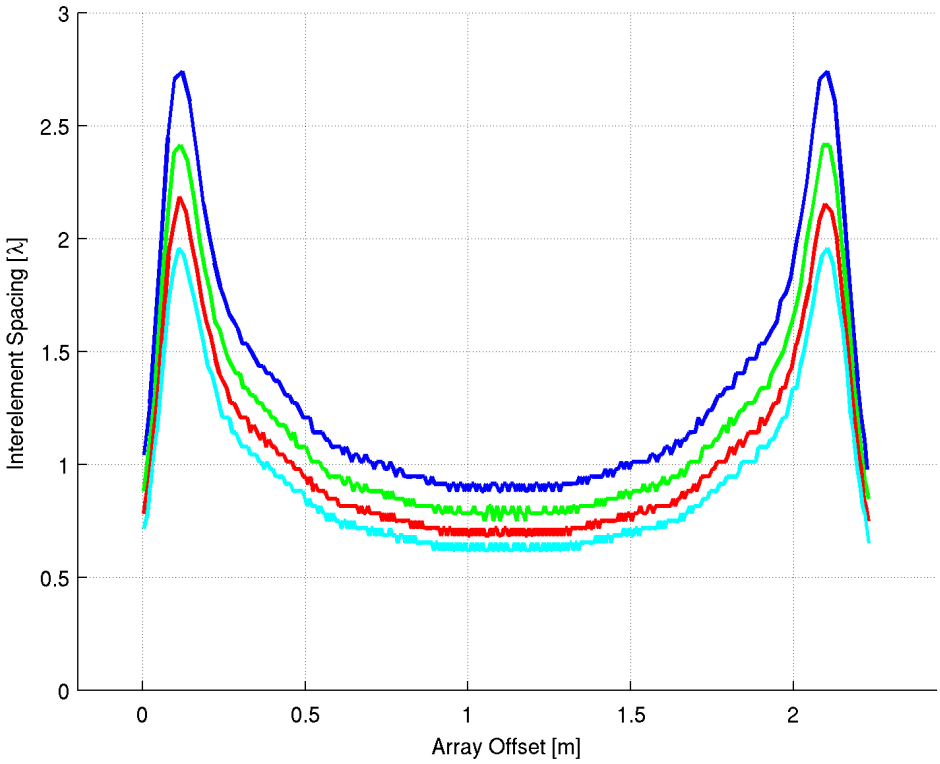

Figure 6.9: Distance to the next radiating element as a function of the position of the target radiating element.

6.2.3.3 Step 3: Optimization of the Broadside Mask

In the previous subsection two alternative methods for the third step have been discussed. These methods have been implemented and will be investigated in the remainder of this subsection. In both cases a the radiating element positions and the phase coefficients will be synthesized first. These tapers satisfy the mask specifications when no scanning is applied. Finally the implementation of beam scanning will be discussed.

The first method optimizes the radiating element positions and the phase coefficients simultaneously for a mask without scanning. This mask has been modified with respect to the mask specification given in Section 2.2. The modification is such that, for each required scan angle, the area near the nadir dip is already in compliance with the mask specifications. The new mask is more stringent and has a negative inpact on the convergence rate. However it results in a speed up of the convergence of subsequent optimization routines that are required in step four. Apart from that the quasi-newton method has been applied in the most straight-forward way, with the cost function depicted in Equation 6.2.

The convergence of the optimization methods has been depicted in Figure 6.10. This figure displays a clear relation between the fill factor and the convergence rate. For the case where N is 320 convergence is achieved within 50 iterations. In contrast, for the case where N is 224 convergence is not achieved at all.

The phase tapers have been depicted in Figure 6.10b, while the interelement spacings and the corresponding radiation patterns are depicted in Figure 6.11 (for N = 320), Figure 6.12 (for N = 288), Figure 6.13 (for N = 256) and Figure 6.14 (for N = 224). The phase tapers seem to be unchanged when compared to the lower parts of Figure 6.5a, Figure 6.6a, Figure 6.7a and Figure 6.8a. The opposite is true radiating element positions. Therefore it can be concluded that the optimization method uses primarily the radiating element positions to achieve compliance with the mask specifications.

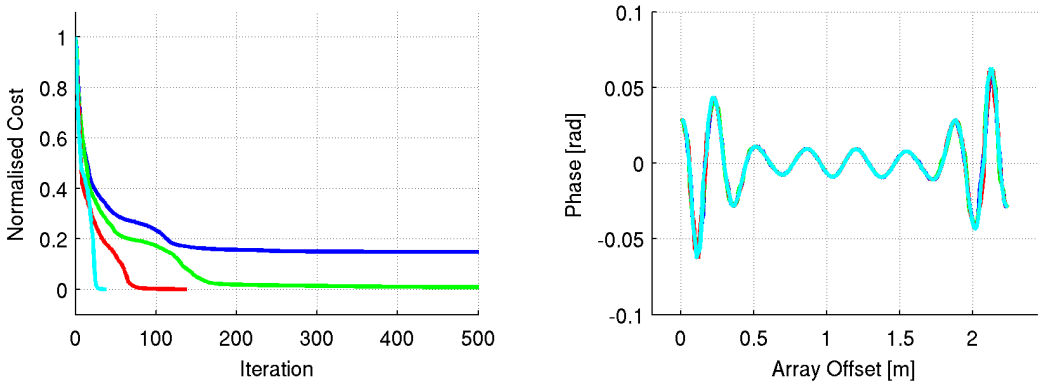

(a) Convergence

(b) Phase Tapers

Figure 6.10: Results of the third step of the proposed density tapering method: Convergence Behavior and Phase Tapers

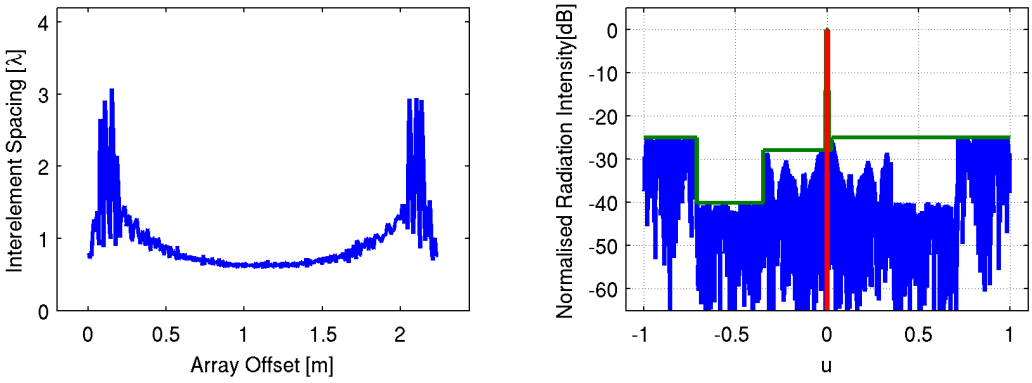

(a) Interelement Spacing (b) Radiation Pattern

Figure 6.11: Results of the third step of the proposed density tapering method with N = 320

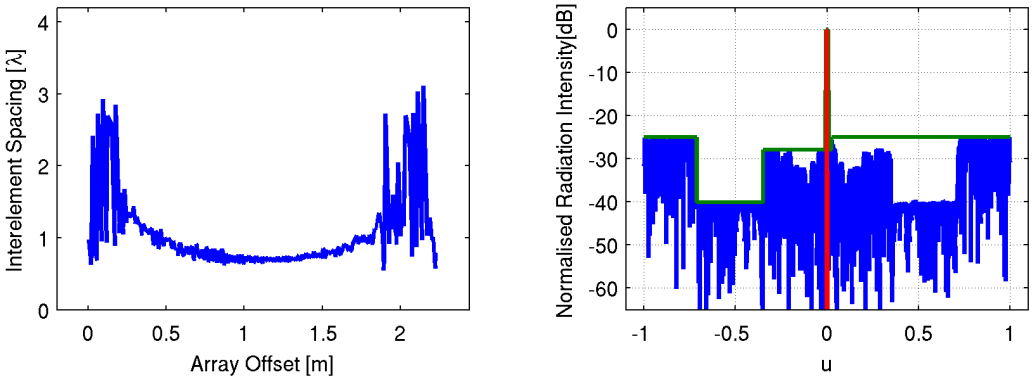

(a) Interelement Spacing (b) Radiation Pattern

Figure 6.12: Results of the third step of the proposed density tapering method with N = 288

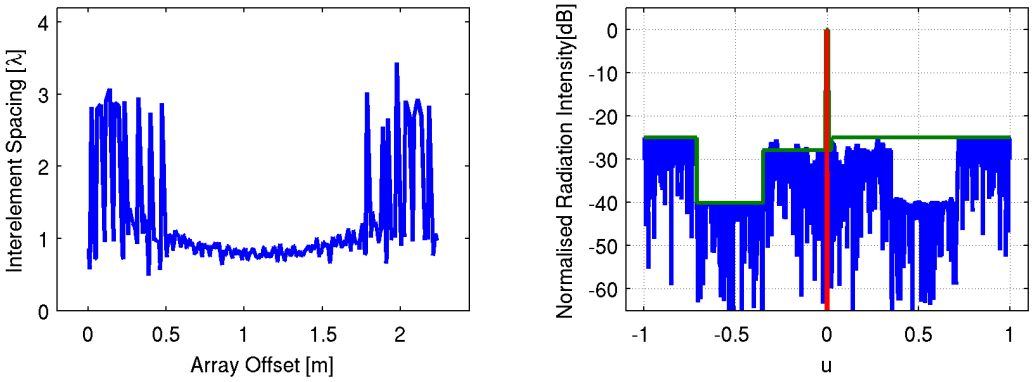

(a) Interelement Spacing (b) Radiation Pattern

Figure 6.13: Results of the third step of the proposed density tapering method with N = 256

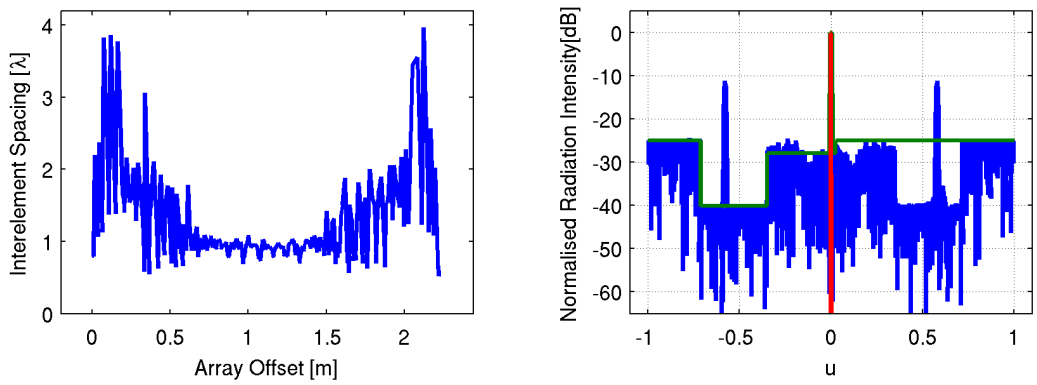

(a) Interelement Spacing

(b) Radiation Pattern

Figure 6.14: Results of the third step of the proposed density tapering method with N = 224

The reason why linear beam scanning cannot be applied is that it causes part of the invisible space[3] to be shifted into the visible space. The second method uses a mask specification that extends in the invisible space. This way no mask violations occur when linear beam scanning is applied. In summary, the difference between the first and the second method in step 3 is that the first method minimizes Equation 6.2 on the domain u = $[-1, 1]$, while the second method minimizes Equation 6.2 on the domain u = $[-1.25, 1.25]$.

For the second method only the case of N = 288 will be considered. This is due to two observations. On one hand some level of sparsity is desired, which is not provided by the case of N = 320. On the other hand the case of N = 256 elements does not converge. This is in contrast with the first method, where the case of N = 256 did converge. However, for the first method, it will be shown in step four that this case fails to converge as soon as beam scanning is implemented.

The convergence of the second method and the corresponding radiation pattern have been depicted in Figure 6.15. When Figure 6.15a is compared to the case with the same fillfactor (the red line in Figure 6.10), it can be seen that the extension of the domain results in a lower convergence rate. Furthermore, notice that the radiation pattern in Figure 6.15b has been depicted on the domain u = $[-2, 2]$. This is done in order to illustrate the effect of minimizing the cost function over a different domain. Finally, for the sake of comparison, the interelement spacing and the radiation pattern on the regular u-domain have been depicted in Figure 6.16.

6.2.3.4 Step 4: Beam Scanning

In step three a density taper and a corresponding phase taper have been obtained for the broadside case. Beam scanning has not yet been considered, although some preparations have been made. Two methods were considered in this step. The first method used a mask specification with a widened nadir-dip with respect to the mask specifications presented in Section 2.2. The

[3]The visible space is defined as the region in which $\sqrt{u^2 + v^2} \leq 1$. The region outside the visible space is called the invisible space.

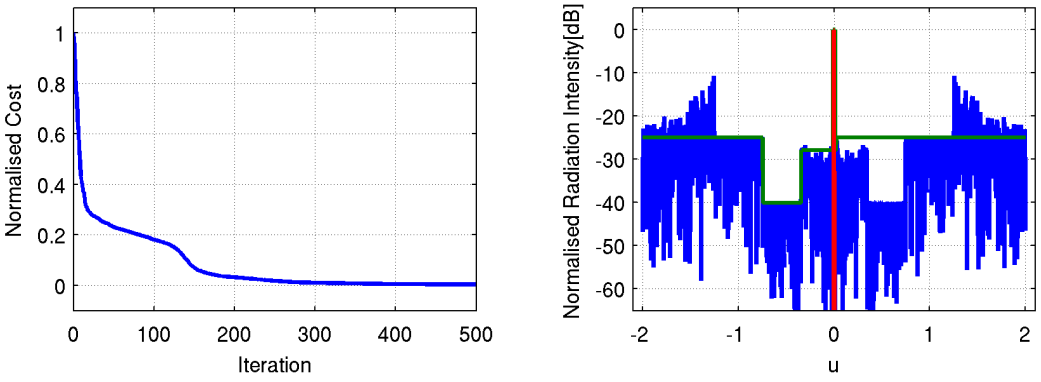

(a) Convergence (b) Radiation Pattern

Figure 6.15: Results of the third step of the proposed density tapering method using a larger domain for u: Convergence Behavior and Wide Radiation Pattern

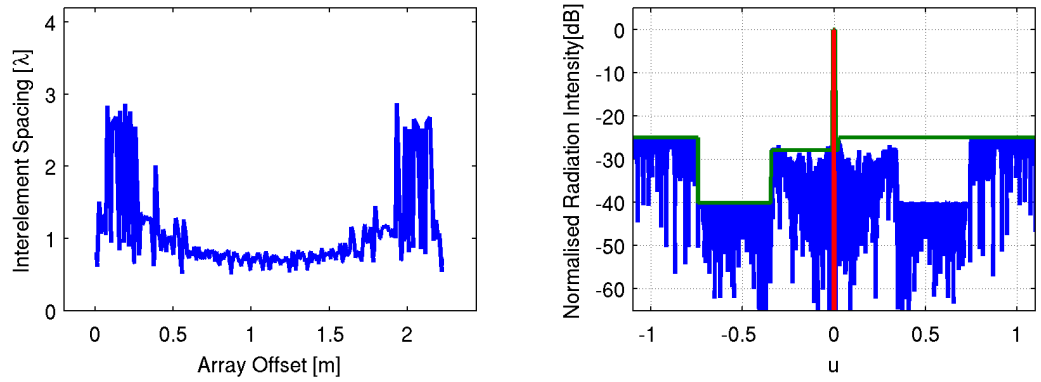

(a) Interelement Spacing (b) Radiation Pattern

Figure 6.16: Results of the third step of the proposed density tapering method using a larger domain for u: Interelement Spacing and Radiation Pattern

second method used in addition to the widened nadir-dip an extension of the mask specification into the invisible space. This method minimizes Equation 6.2 on the domain $u = [-1.25, 1.25]$.

In Section 2.2 a scanrange of $[-10°, 10°]$ was specified. One possible way to implement this is to specify a sufficient number of masks, one for each discrete scan angle. According to Section 1.1 90 discrete scan angles are required. However, for the sake of analysis only 21 scan angles have been considered here. These scan angles together cover the entire scan range. Another possible implementation of beam scanning is to synthesize the density taper in such a way that no mask violations occur as linear beam scanning is applied. This approach has been taken in the second method.

The synthesis of each phase taper requires an additional minimization of Equation 6.2 over the phase coefficients. Hence after step four one set of radiating element positions and 21 phase tapers will be obtained. Beam scanning is then implemented by switching from one set of phase taper coefficients to a different set of phase taper coefficients.

The convergence curves of step four have been depicted in Figure 6.17. In this figure three groups of curves have been plot. The green curves belong to the case where N = 256, the red curves belong to the case where N = 288 and the cyan curves belong to the case where N = 320. The phase tapers and a selected number of normalised radiation patterns that correspond to these cases have been depicted in Figure 6.18 (N = 320), Figure 6.19 (N = 288) and Figure 6.20 (N = 256). The normalised radiation patterns correspond to the cases of 0, ±2 and ± 10 degree of scanning.

For the case of N = 320 convergence has been achieved within 75 iterations. The corresponding radiation patterns support this as no mask violations are observed. In particular for small scan angles the widened nadir-dip is still distinguishable. This indicates that there is some headroom and that higher levels of sparsity or more stringent mask specifications can be achieved. For the more sparse case of N = 288 not all minimization routines obtain full converge. In particular for larger scan angles such as depicted in Figure 6.19f small mask violations can be observed. These mask violations are small and considered acceptable. However, this also indicates that the sparsity limit has been reached. Indeed, for the case of N = 256 most minimization routines do not converge at all. This can also be seen in their radiation patterns: even for a modest scan angle mask violations of the order of 10 dB can be observed. These mask violations are considered unacceptable.

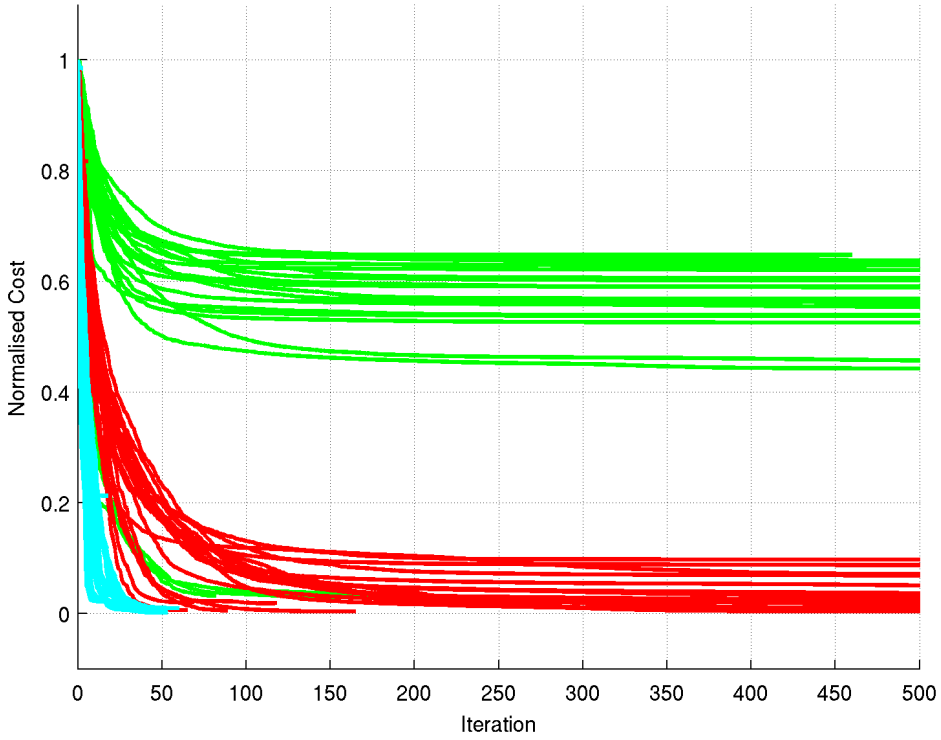

Figure 6.17: Results of the fourth step of the proposed density tapering method: Convergence

For the second method beam scanning is done by applying a linear phase taper to the excitation coefficients. This results in a translation of radiation pattern depicted in Figure 6.15b. In step

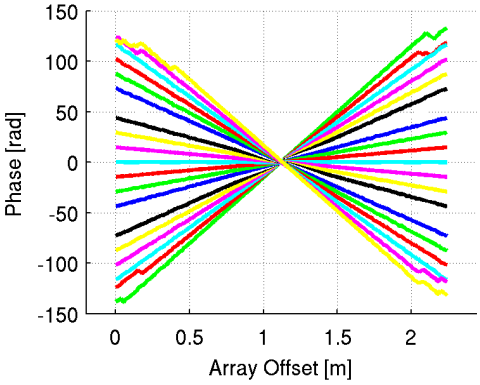

(a) Phase Distributions

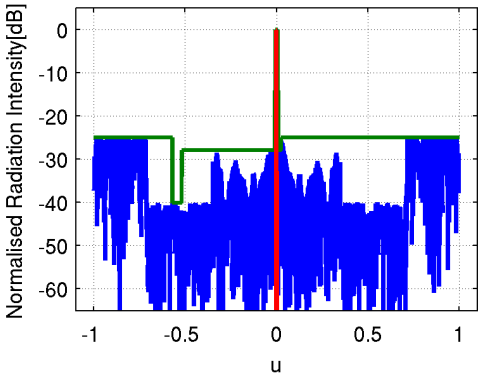

(b) 0 deg scan

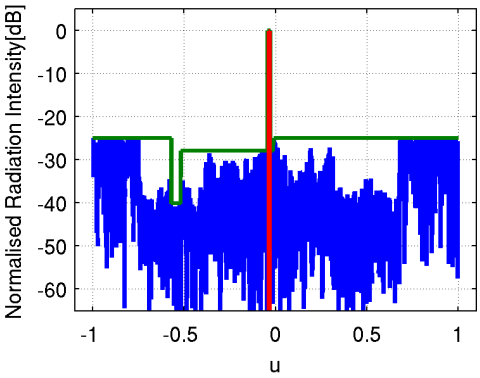

(c) -2 deg scan

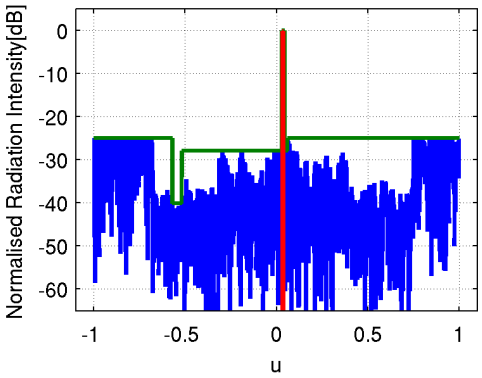

(d) 2 deg scan

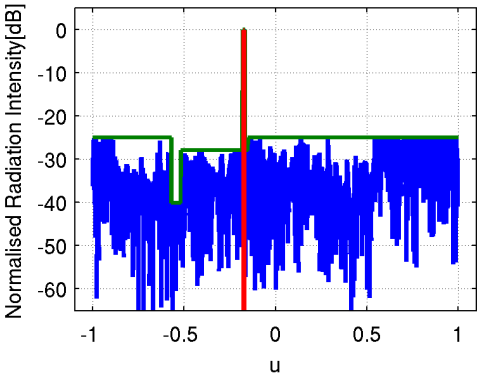

(e) -10 deg scan

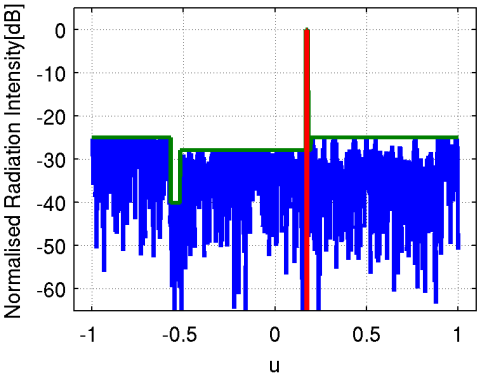

(f) 10 deg scan

Figure 6.18: Results of the fourth step of the proposed density tapering method with N = 320: Phase tapers and some characteristic scan angles

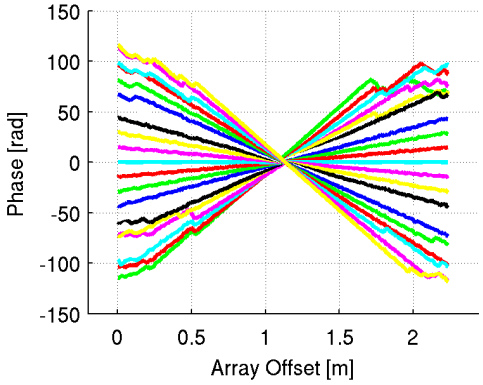

(a) Phase Distributions

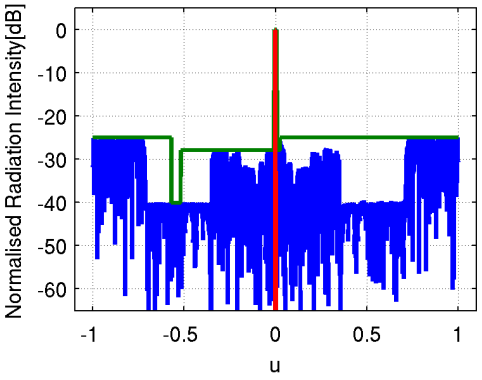

(b) 0 deg scan

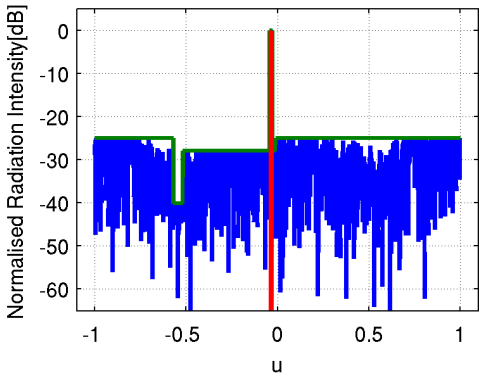

(c) -2 deg scan

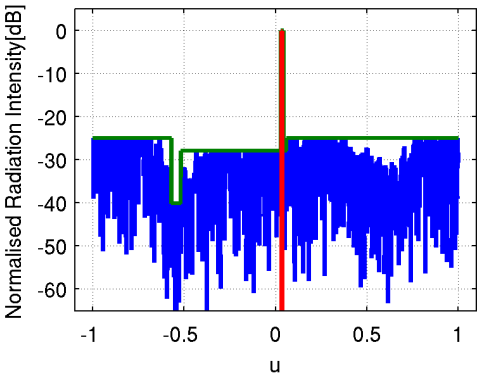

(d) 2 deg scan

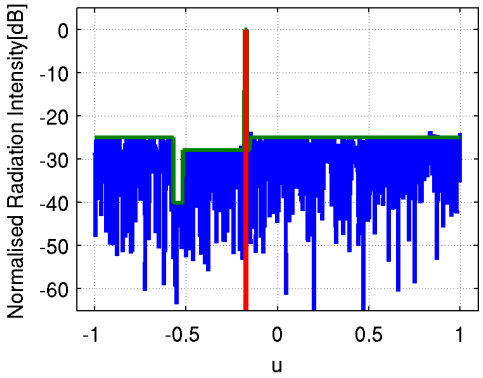

(e) -10 deg scan

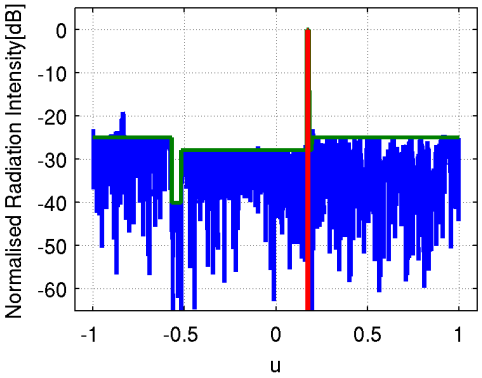

(f) 10 deg scan

Figure 6.19: Results of the fourth step of the proposed density tapering method with N = 288: Phase tapers and some characteristic scan angles

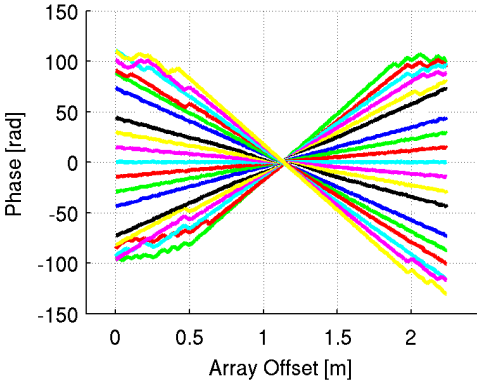

(a) Phase Distributions

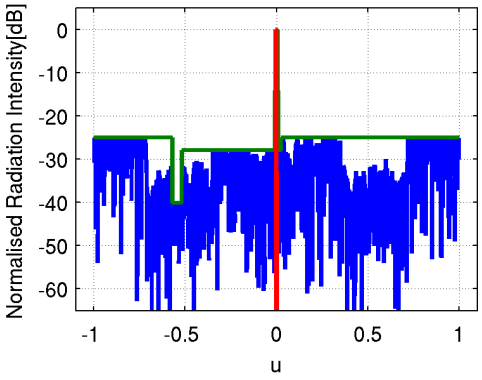

(b) 0 deg scan

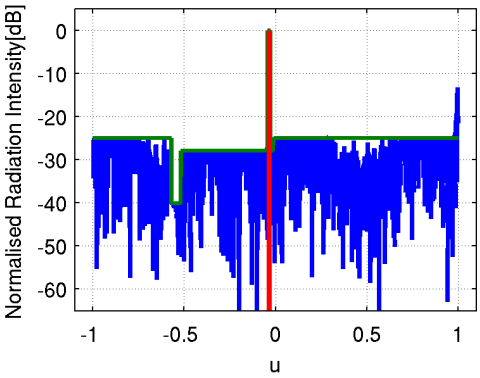

(c) -2 deg scan

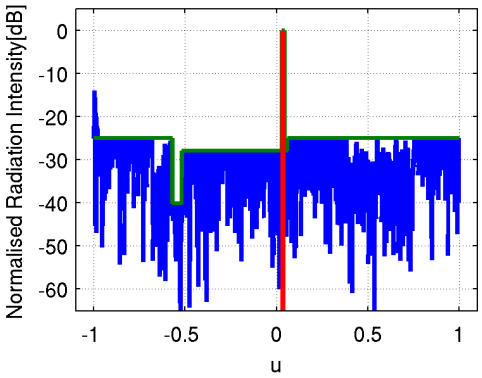

(d) 2 deg scan

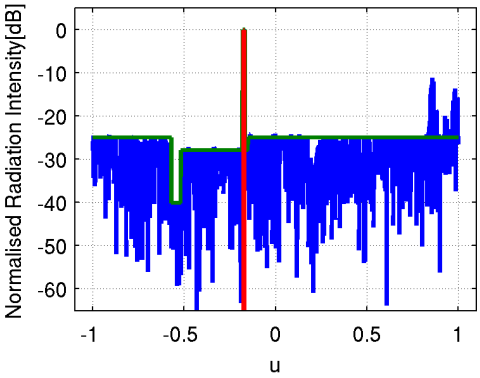

(e) -10 deg scan

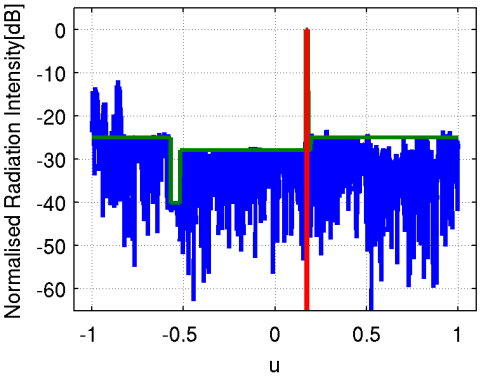

(f) 10 deg

Figure 6.20: Results of the fourth step of the proposed density tapering method with N = 256: Phase tapers and some characteristic scan angles

three it was pointed out that this pattern was constructed in such a way that this type of scanning can be applied without violating the mask specifications. Hence, arbitrary scan angles can be obtained with a minimum amount of effort.

This notion is supported by Figure 6.21, in which the phase tapers as well as the normalised radiation patterns for the scan angles 0, ±2 and ± 10 degree have been depicted. In particular Figure 6.21e and Figure 6.21f illustrate the compliance with the mask specifications.

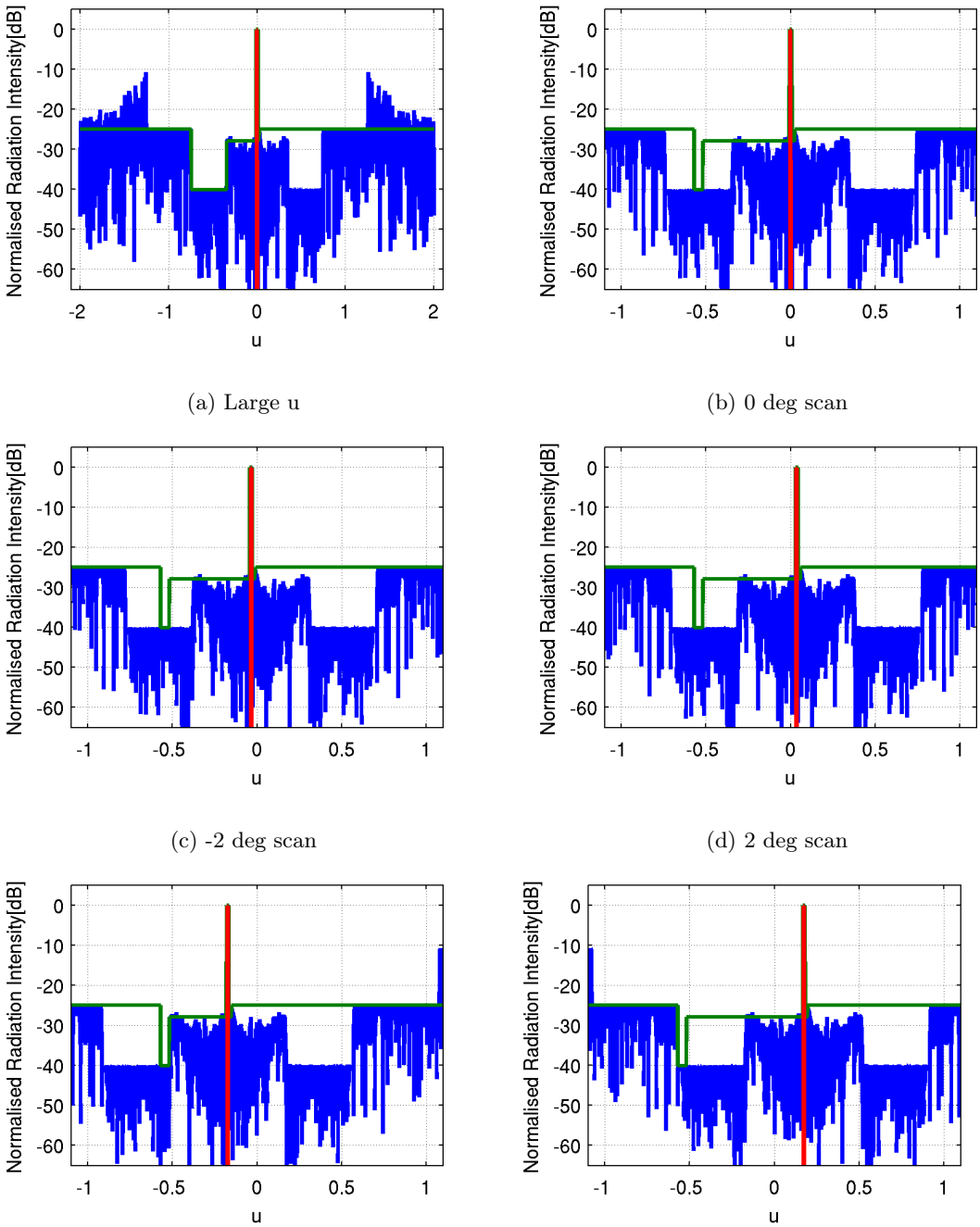

(a) Large u

(b) 0 deg scan

(c) -2 deg scan

(d) 2 deg scan

(e) -10 deg scan

(f) 10 deg scan

Figure 6.21: Results of the fourth step of the proposed density tapering method with N = 288 and using a larger domain for u: some characteristic scan angles

In summary various options for the density tapering method were presented. It should be noted that a fill factor of at least 90 percent (N = 288) with respect to the benchmark antenna was required in order to obtain acceptable results. Besides that the extension of the u-domain provided an easy way for beam scanning at the cost of a smaller interelement spacing in the center of the array lattice and an increased convergence time. In the next section the density tapering method will be applied to the benchmark antenna and its variations.

6.3 Array Lattice Concepts based on Density Tapering

In Section 5.1 a number of variations of the benchmark antenna were introduced. Each of these antenna concepts employed a synthesis method that sought to do one of two things. Either this method aimed to reduce the number of controls or it sought to reduce the grating effects in the azimuth cut. A taylor taper was employed over the rows of these array concepts in order to make sure the elevation cut remained below the mask specifications. In this section a new set of array lattice concepts will be considered that replace these taylor tapers by the second density taper obtained in Section 6.2. This taper was summarized in Figure 6.15, Figure 6.16 and Figure 6.21.

6.3.1 Discussion of the Array Lattices

Two examples of such concepts are depicted in Figure 6.22a and Figure 6.22b. These figures indicate how these array lattices have been generated. For each array lattice concept an array lattice with 288 rows was generated. These rows were then spaced according to the density taper. Thus, the interrow spacing corresponds to the spacings depicted in Figure 6.16a.

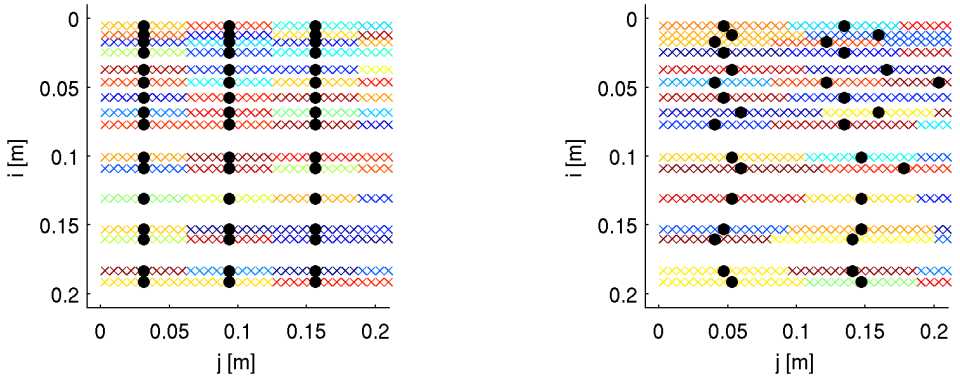

(a) Benchmark Array Lattice

(b) Linear Arrays Array Lattice

Figure 6.22: Close-up of the top-left corner of two density-tapered array lattices.

In Section 2.2 three guidelines were discussed that should help to make sure that the resulting antennas are industrially feasible. The nature of density tapering dictates that the electronics cannot follow a regular grid. Therefore, the first requirement is not met. The second guideline stating that not more than four building blocks can be used has been followed. The final guideline

depends on whether rows can be considered tiles. Following the discussion in Section 5.1 this guideline has not been violated nor honored.

6.3.2 Principle Plane Cuts

The elevation cuts of the density tapered variations of the benchmark antenna and its derivatives equal the radiation pattern depicted in Figure 6.16b. This is can be understood using the projection slice theorem. This theorem states that the one-dimensional fourier transform of a projection of a function onto a line yields the same result as taking the corresponding central slice of the two-dimensional fourier transform of that function. In operator terms, if $\mathcal{F}_1$ and $\mathcal{F}_2$ are the one-dimensional and two-dimensional fourier transforms, $\mathcal{P}_{1,\phi}$ is the projection operator and $\mathcal{S}_{1,\phi}$ is the central slice operator, then $\mathcal{F}_1\mathcal{P}_{1,\phi} = \mathcal{S}_{1,\phi}\mathcal{F}_2$. Since all array lattice concepts share the same projection onto the vertical axis ($\phi = \pi/2$), they must also share the same elevation cut.

It should also be noted that the application of the density taper does not affect the projection onto the horizontal axis ($\phi = 0$). Therefore the azimuth cuts of the density tapered antennas remain unchanged with respect to the taylor-tapered antennas. Hence, their azimuth cuts can be found in Figure 4.3, Figure 5.2, Figure 5.8a, Figure 5.8b, Figure 5.8c and Figure 5.8d.

6.3.3 Two-Dimensional Radiation Patterns

From the principal plane cuts the azimuth cuts show more grating lobes than the elevation cuts. Furthermore, the shape of the elevation cuts remain constant when the beam is scanned along the elevation plane. This is different from the azimuth cuts, where the grating effects increase while the beam is being scanned. This is the effect of subarraying. In elevation beam scanning is achieved using the fourier shift theorem, which states that translation in the u-domain can be achieved by applying an incremental phase taper. This theorem can not be applied in azimuth since the radiating elements cannot be controlled individually. In fact, the larger the scan angle, the larger the error introduced at the edges of the subarrays. This leads to quantization lobes, which are a form of grating lobes.

To see how these observations extend in two dimensions, the two-dimensional radiation patterns of the linear arrays concept are plotted in Figure 6.23. Four scan configurations are considered: 0 deg scanning in azimuth, 0 deg scanning in elevation (Figure 6.23a), 2 deg scanning in azimuth, 0 deg scanning in elevation (Figure 6.23b), 0 deg scanning in azimuth, 10 deg scanning in elevation (Figure 6.23c) and 2 deg scanning in azimuth, 10 deg scanning in elevation (Figure 6.23d).

These figures show that these observations extend to the two-dimensional radiation patterns. As long as the beam is only scanned in elevation the pattern is translated. However as soon as the beam is scanned in azimuth the quantization effects become apparent. These quantization effects depend only on the azimuth scan angle.

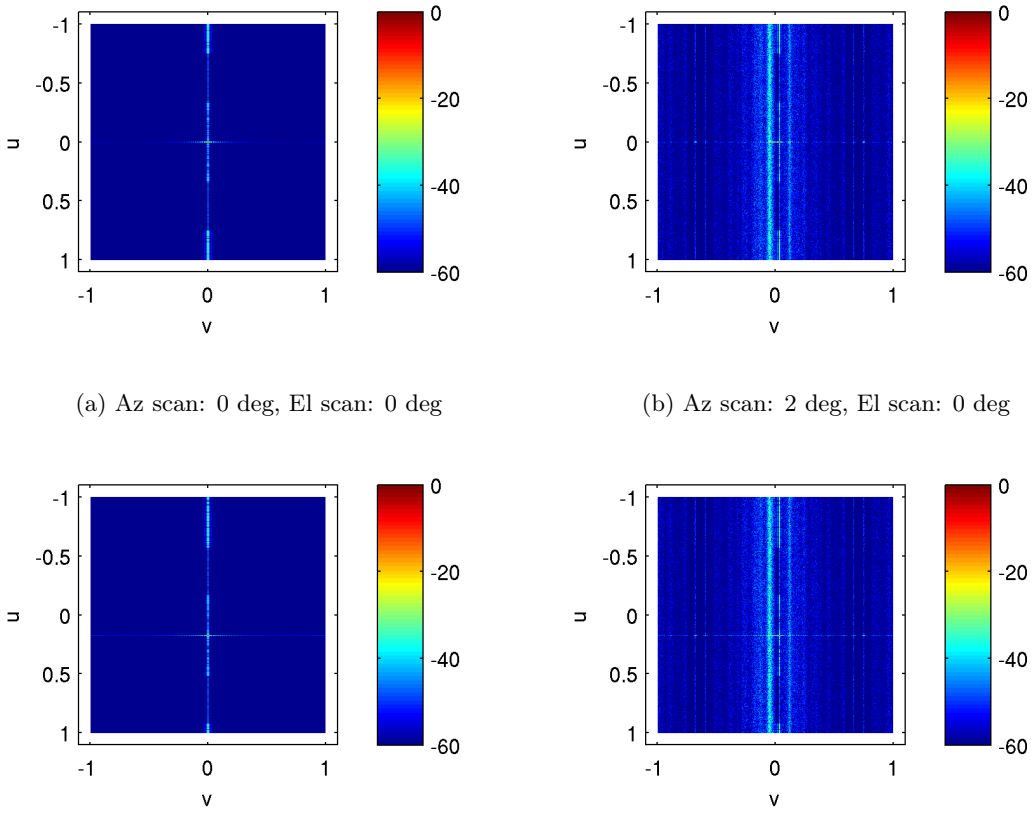

(a) Az scan: 0 deg, El scan: 0 deg

(b) Az scan: 2 deg, El scan: 0 deg

(c) Az scan: 0 deg, El scan: 10 deg

(d) Az scan: 2 deg, El scan: 10 deg

Figure 6.23: Illustration of scanning in two dimensions using the density-tapered linear arrays array lattice concept.

Similar effects can be observed for the other array lattice concepts. Their respective radiation patterns for a scan angle of 2 deg in azimuth are depicted in Figure 6.24. No elevation scan has been applied.

Two different array lattice concepts will be proposed for further study. Figure 6.24 indicates that staggering does not drastically improve two-dimensional radiation patterns. Therefore the density-tapered benchmark array lattice concept and the density-tapered variable-length linear arrays array lattice concept seem to be the most promising concepts.

The next chapter provides a short summary and the conclusions of this thesis.

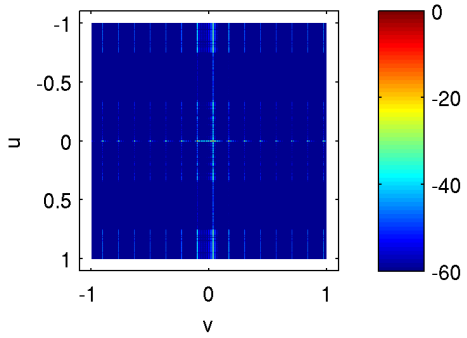

(a) Benchmark

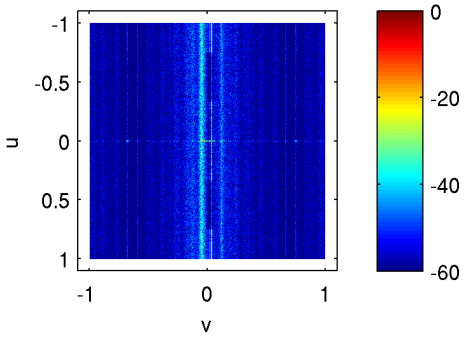

(b) Linear Arrays

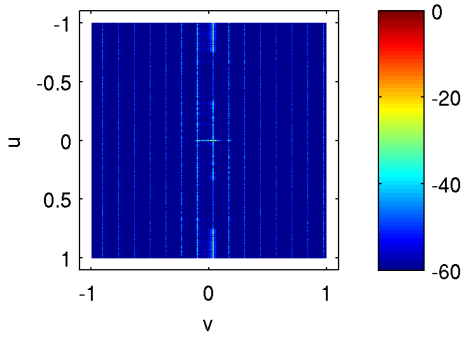

(c) Staggered Benchmark (5)

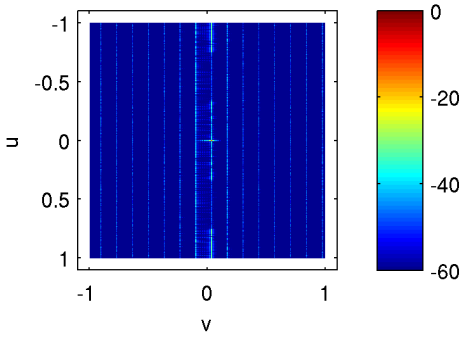

(d) Staggered Benchmark (10)

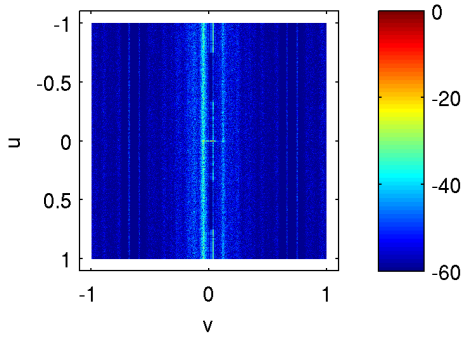

(e) Staggered Linear Arrays (5)

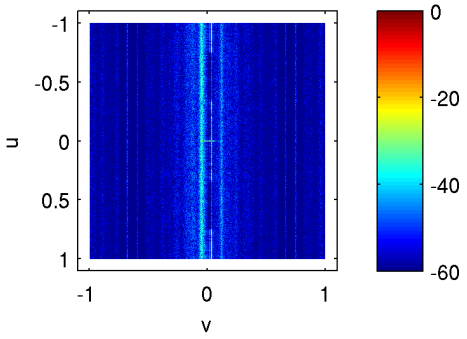

(f) Staggered Linear Arrays (10)

Figure 6.24: Two-dimensional radiation patterns of density tapered antennas scanned to 2 deg in azimuth. No elevation scanning has been applied.

Chapter 7

Conclusion

In the previous three chapters the complete extend of the work done for this research was presented. This chapter concludes this thesis and is organised as follows. First, in Section 7.1, a summary of the previous chapters will be provided. This summary leads to the final conclusions as presented in Section 7.2. The final two sections of this chapter elaborate on the limitations of the present work (Section 7.3) and on oppertunities for further research (Section 7.4).

7.1 Summary

The focus of this thesis, as detailed in Chapter 1, is the synthesis of a Ka-band sparse phased array antenna for spaceborne SAR applications. In this chapter also the research question has been formulated, which was supported by four subquestions. The research question is repeated here.

Research Question *Is it possible to design a sparse phased array antenna geometry that can be used in a Ka-band spaceborne SAR and is more cost-efficient than a comparable state of the art regular phased array antenna?*

1. *What are the characteristics of currently operating earth observation instruments?*
2. *What are the most important drivers in the requirement analysis?*
3. *Which design guidelines should be considered?*
4. *What is the range of acceptable sparsity levels?*

In order to answer the research question it should be possible to evaluate synthesized designs against the current state-of-the-art technology. To that end a benchmark antenna has been synthesized using conventional methods. This antenna uses linear subarrays in the azimuth dimension and a rather large spacing between its radiating elements in both dimensions, so it

introduces two initial levels of sparsity. Based only on the interelement spacing, the benchmark array lattice achieves a fillfactor in radiating elements of 0.4. The fillfactor in controls, which takes the use of subarrays into account, is 0.04.

Research activities related to the problem defined in Chapter 2 have been summarized in Chapter 3. In this chapter it is stated that, to the best of our knowledge, no previous work has been published that provides a complete solution for the problem at hand. That is, a method that solves the Ka-band sparse phased array lattice synthesis problem with respect to the desired amount of radiated power, the desired beamshape, the desired fillfactor, the desired array lattice shape and the desired level of industrial feasibility has yet to emerge. Because of this the philosophies behind existing synthesis methods need to be considered. Should a method prove useful, it should be adapted and combined with other useful methods such that a new method can be constructed that is capable of solving the previously mentioned synthesis problem.

To this end array lattice synthesis methods based on two different approaches have been considered. The first approach treated the two dimensions independently while the second approach sought to find a full twodimensional solution. The benchmark array lattice is an example of an array lattice that has been synthesized using a synthesis method from the first approach. An array lattice based on two-dimensional subarrays such as was considered in [21] is an example of an array lattice that has been synthesized using a synthesis method from the second approach.

For the first approach the concept of variable-length linear subarrays has been proposed. This concept utilized larger linear subarrays than the benchmark array lattice, which resulted in a lower fillfactor in controls. Larger subarrays resulted in higher quantization lobes, which in turn were suppressed due to the introduced irregularity. Methods to enhance the irregularity in phase center positions has been proposed in the form of staggering. It was seen that the application of staggering resulted in lower quantization lobes. In particular the first grating lobe has been reduced substantially. Analysis of the autocorrelation function of the array lattices confirmed that this was indeed due to the enhanced irregularity. Finally it has been noted that although these array lattices were synthesized using stochastic algorithms, the resulting radiation patterns did not show much variation because their statistical properties were identical.

The most promising set of linear subarray lengths was found to be $[13, 15, 17, 19]$. Each linear subarray length occurred with equal probability, so the average linear subarray length was 16. Hence, the fillfactor in controls with respect to a half wavelength spaced array lattice of comparable dimensions was 0.025.

Along the other dimension the concept of density tapering has been investigated. This concept allowed to synthesize a particular radiation pattern while maintaining the same excitation amplitude for all radiating elements. Only the excitation phases and the positions of the radiating elements were allowed to change. It was not without a cost: the use of density tapering was computational expensive and resulted in a completely irregular array lattice. In the end the use of density tapering allowed to reduce the number of rows in an array lattice from 320 to 288, which resulted in a fillfactor in controls of 0.0225. With respect to the benchmark array lattice, which obtained a fillfactor in controls of 0.04, this is a reduction factor of 0.56.

For the second approach an attempt has been made to extend the work of [21]. The rationale behind this concept was similar to the rationale behind the variable-length linear subarrays array lattice concept, but now extended to two dimensions. Quantization lobes introduced by a relatively large average phasecenter spacing can be suppressed by sufficient irregularity between phase center positions. However, generating completely filled array lattices that possess enough irregularity using only a limited number of building blocks is hard. In fact, in [30] it was proven that the problem of deciding whether a given set of polyominoes is capable of tiling an infinite plane is algorithmically undecidable.

7.2 Conclusions

From the summary in the previous section it should be clear that introducing sparsity to reduce costs is not a holy grail. A level of sparsity may be introduced without sacrificing total radiated power by means of subarrays, but at the cost of the introduction of quantization lobes. These grating effects can be reduced by introducing irregularity. This can be done by means of variable-size subarrays, as was attempted by the variable-length linear subarrays array lattice concept presented in Section 5.1 and by the use of polyominoes shown in Section 5.3. Both techniques share two appealing properties. The first is that the radiating elements maintain a regular grid, while the phasecenters do not. Apart from that both techniques use only a limited number of different subarrays in their synthesis process. Both properties are desirable from the industrial feasibility point of view, as has been detailed in Section 2.2. However, by the nature of both techniques, there is limited control over the resulting radiation pattern.

Another way to introduce irregularity was attempted by the density taper technique shown in Section 6.2. This technique does allow full control over the resulting radiation pattern at the cost of an irregular array lattice. From an industrial feasibility perspective this is not desirable. This has been an important tradeoff throughout the entire thesis. Control over the radiation pattern versus cost and industrial feasibility.

Finally the conclusion of this thesis will now be presented. It is in general not possible to synthesize a sparse array lattice that complies with the specifications listed in Section 2.1 and at the same time honors the design guidelines as listed in Section 2.2. However, the choice of introducing sparsity, if considered carefully, can still be beneficial. The costs of increased complexity should be traded against the desired level of control over the radiation pattern as well as the costs of reduced industrial feasibility.

For the problem defined in Chapter 2 the variable-length linear subarrays array lattice concept seems to be the most promising option. The application of staggering to the rows of the final array lattice is not necessary since sufficient performance is already achieved. Whether or not the application of a density taper is preferred over a taylor taper depends on whether the cost of a completely irregular lattice can be justified by the decrease in fillfactor and by the decrease in taper loss. A tradeoff between the most promising array lattice concepts can be found in Table 7.1.

Table 7.1: Tradeoff between the most promising sparse array lattice concepts. These are the (staggered) benchmark array lattice concept (BM) and the (staggered) variable-length linear subarrays array lattice concept (LA). For the LA concept following set of subarray lengths has been used: $[13, 15, 17, 19]$. Finally, the increase in gain (ΔGain) and the fillfactor (ΔFillfactor) are defined with respect to the benchmark array lattice.

Name	ΔGain	ΔFillfactor	Q_1
BM (-28 dB TT)	0 dB	1.000	-9 dB
BM (90% DT)	2.6 dB	0.900	-9 dB
LA (-28 dB TT)	0 dB	0.625	-13 dB
LA (90% DT)	2.6 dB	0.560	-13 dB
SBM (-28 dB TT)	0 dB	1.000	-38 dB
SBM (90% DT)	2.6 dB	0.900	-38 dB
SLA (-28 dB TT)	0 dB	0.625	-21 dB
SLA (90% DT)	2.6 dB	0.560	-21 dB

7.3 Limitations

The generation of the proposed array lattices is simple, as was dictated by the design philosophy in Section 4.2. Despite these appealing aspects the proposed methods do have their limitations. This section addresses the most important ones.

Array Factor The first limitation of the proposed synthesis method is that it is not generally possible to synthesize subarray constellations that radiate according to a desired radiation pattern. For a specified set of building blocks the array factors will be similar. This is especially true for large arrays, where the ensemble behavior dominates. In contrast, the density taper method does allow for this. Considering the boundary conditions for this research as described in Chapter 2, this is not a problem, but it is a limitation. Finding a solution to this limitation is suggested as further research.

High Power Amplifiers The second limitation is related to the different sizes of the subarrays. It was stated in Chapter 2 that a reduction in controls does not lead to a reduction in total radiated power, but this statement has some implications. First, it is assumed that the high power amplifiers are capable of delivering the requested amount of power. On top of that, it is assumed that the high power amplifiers are capable of doing so at peak efficiency. To date and for Ka-band radar, both assumptions are not true. It is however expected that this technology will become available within a couple of years.

Sparsity The third limitation bounds the amount of sparsity that can be allowed by the density taper method. Increasing the average interelement spacing in elevation above a certain value prevents the final optimization step of the density taper routine from reaching convergence. This limitation and corresponding trade-offs have been discussed in Chapter 6.

Industrial Feasibility The fourth limitation illuminates the concept of industrial feasibility. In Section 2.2 a number of guidelines have been presented that should ensure that the resulting array lattice concepts are industrial feasible. However, these design guidelines have not always been honored, or have been honored in a less desirable form.

Second order effects The final limitation is that the described methods only take first order effects into account. The choice of radiating element, their corresponding element pattern, mutual coupling and the effects of the discretization of the excitation signals are not taken into account in the proposed method. Incorporating second order effects will be suggested as further research in the next section.

7.4 Further research

Every research is fundamentally limited by resources and therefore not all relevant areas can be addressed. It might however be beneficial to investigate these excluded but relevant topics in a follow-up study. This section identifies some of the topics that fell outside the scope of this thesis.

A group of topics that could be beneficial to explore even further are the lattice synthesis concepts investigated in this thesis. Further in-depth investigation of these concepts could enhance their applicability. For instance, the variable-length linear subarrays array lattice concepts generate array lattices by using a simple stochastic synthesis method. This simplicity is appealing for large arrays from a computational point of view, but limits the synthesis power of the method. The applicability of these techniques could be enhanced if a more complex generation scheme could synthesize a desired array factor. An approach that is typically employed in the literature to such an end could be to use the rows of the variable-length linear subarrays array lattice as genes for a genetic algorithm.

A couple of general topics also deserve further investigation. The first such topic is the influence of mutual coupling. Mutual coupling will likely have an effect on both the total radiated power and on the shape of the radiation pattern. Furthermore, in a real antenna the excitation phases will be discrete. This will also have an effect on the radiation pattern. The last general topic worth mentioning is the influence of different radiating elements and the corresponding element patterns. The choice of radiating element can possibly improve the antenna gain and the sidelobe levels far away from the main beam, thus suppressing potential grating effects.

Appendix A

Synthetic Aperture Radar

In the previous section the research context and research objectives have been stated. In this section the basic operation of a SAR will be introduced. To that end, first the Side Looking Aperture Radar (SLAR) will be introduced, because a lot of the properties of a SAR system can be identified already in this less complex system. Then, a simplyfied view of the geometry will be given. At the end of this section, some of the most important parameters that define the basic performance of the SAR will be explained.

It is assumed that the reader is familiar with the basic operating principles of a radar system. If not, [6] and [7] are excellent introductory texts on this subject. In fact, most of the theory that is presented here is derived from these two sources[1].

A.1 What is Synthetic Aperture Radar?

Conventional SLAR systems suffer from the fact that their azimuth resolution depends on the width of the platform. In order to illuminate a spot of a given size a certain beamwidth is required. The requirements on this beamwidth tighten if the distance to the platform increases. This in turn leads to unrealistic requirements on the width of the antenna aperture, especially for spaceborne instruments.

As its name implies, a Synthetic Aperture Radar combines several radar measurements from various locations along the track of the platform in order to synthesize a virtual antenna. This virtual antenna can have a much larger azimuthal dimension than the width of the original antenna. Hence, the problem sketched in the previous paragraph can be solved this way.

[1] Ch. 9 from [6] and Ch. 2 and 9 from [7], to be precise.

A.2 Basic operation of a SLAR

One of the earliest and most simple forms of airborne radar systems is the Side Looking Aperture Radar (SLAR). The basic configuration of a SLAR system is depicted in two figures. Figure A.1 depicts the environment from above. The platform, which can be some form of aircraft or a satelite, moves along the track, which is indicated at the top of the figure. The radar images the swath, indicated by the gray area at the bottom of the figure. Notice that at any given time only the slice directly to the side of the platform is being imaged. This is comparable to the estimation the angle of approach of a target in a conventional rotating radar.

The other figure, Figure A.2, depicts the environment from behind. Notice that, as opposed to the alongtrack dimension, the radar illuminates the whole width of the swath. This is comparable with the estimation of the range of a target in a conventional rotating radar.

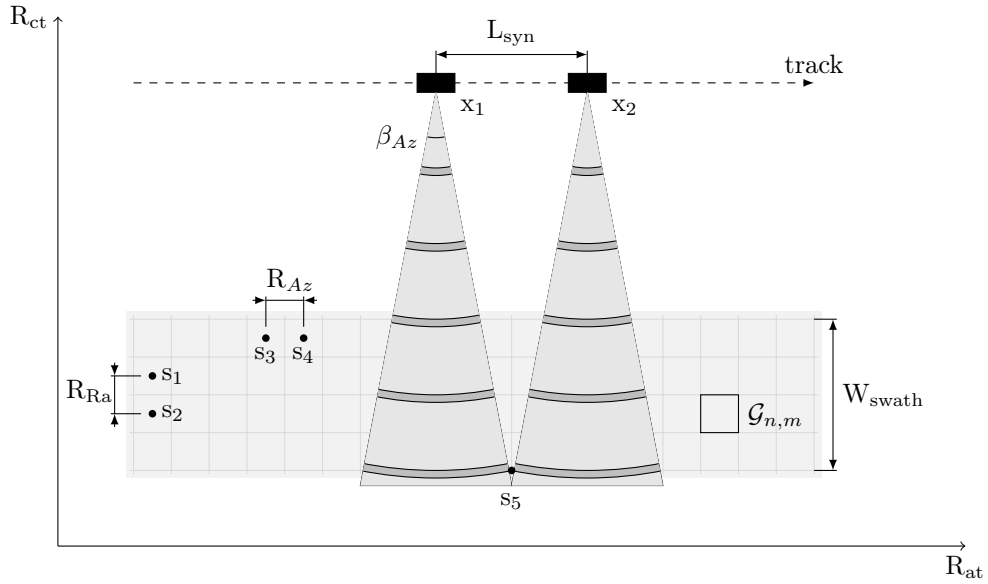

Figure A.1: Top view of the S(L)AR environment.

A.3 The Synthetic Aperture

In a phased array antenna system, electromagnetic waves incident to the antenna aperture are measured at different positions. These measurements are then coherently combined in such a way that only waves incident from certain directions persist, while waves from all other directions are suppressed. Although this happens concurrently in a regular phased array antenna, this is not necessary. If the measurement data, both amplitude and phase, are somehow stored, then this process of coherent addition can be performed at a later stage. Considering this, it is also possible to use one antenna to do a single reading, move it to the next position and repeat this process until all measurement data are obtained from all element positions, provided that, of course, the incidence fields remain constant during the measurement sequence. This is the idea behind a SAR.

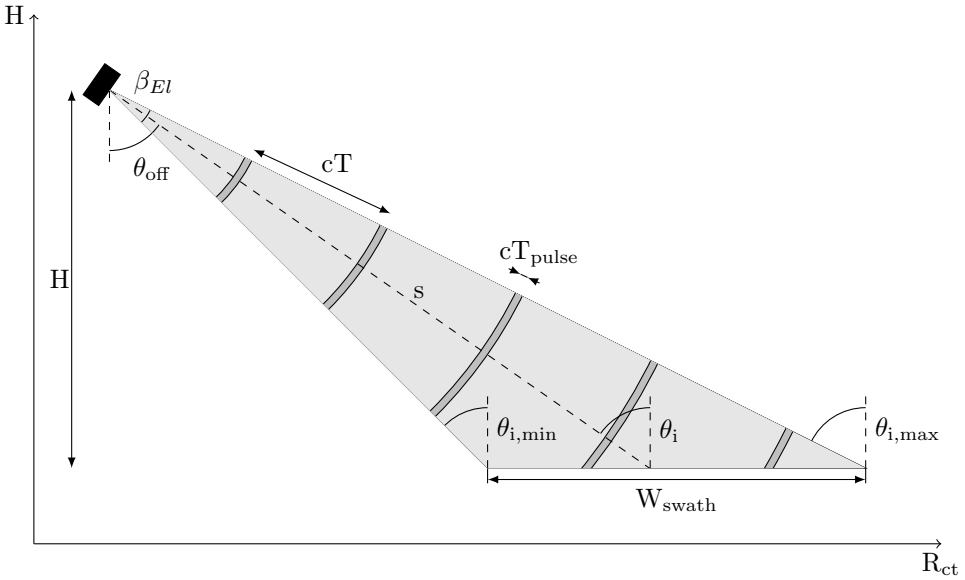

Figure A.2: Rear view of the S(L)AR environment.

The imaging of a particular scatterer starts as soon as it enters the radarbeam. Likewise, it ends as soon as it leaves the radarbeam. This is made more clear in Figure A.1: scatterer s_5 enters the radarbeam as soon as the platform passes position x_1 and leaves the radarbeam as soon as the platform passes position x_2. Thus, this part of the track can be thought of as a very large phased array antenna and is therefore called the synthetic aperture.

It should also be noted that, for SAR processing, the radar measurements need to be coherent. That is, along with the amplitude reading, definite phase information needs to be available. Also, the incident fields need to be constant. Under those conditions, the usual phased array antenna processing can be used to synthesize large antenna apertures.

The prime advantage of SAR over SLAR is the fact that the azimuthal resolution, R_{Az} is independent of H. Also, the azimuthal resolution improves as the antenna width decreases.

A.4 Important Characteristics

The performance of a radar system is defined according to a number of characteristics. In this section several of these characteristics will be discussed, as well as the driving parameters that determine the performance related to these characteristics. All discussed parameters, except for the antenna height and antenna width, can be found in Figure A.1 and in Figure A.2.

A.4.1 Resolution

Resolution is defined as the minimum distance between two pointscatterers such that they can be detected as such. We discriminate two different types of resolution.

The first type is the resolution in the cross-track direction, also known as the range resolution (R_{Ra}). In Figure A.1, the range resolution is the minimum distance between the scatterers s_1 and s_2 such that they can still be separated after detection by the SAR. This value is given by Equation A.1, where c is the speed of the radiation, τ is the pulse length and θ_i is the incidence angle as depicted in Figure A.2.

$$\Delta R_{Ra} = \frac{c\tau}{2 \sin \theta_i} \tag{A.1}$$

The second type is the resolution in the along-track direction, also known as the azimuthal resolution (R_{Az}). In Figure A.1, the azimuthal resolution is the minimum distance between the scatterers s_3 and s_4 such that they can still be separated after detection by the SAR. This value is given by Equation A.2, where s is the slant range, β_{Az} is the azimuthal beamwidth, H is the platform height, λ is the wavelength of the radiation, L is the antenna length and θ_i is the incidence angle as depicted in Figure A.2.

It should be noted that, when SAR processing is considered, the R_{Az} improves as the antenna gets smaller. This is because the synthesized aperture gets bigger as the beamwidth of the original antenna increases, and so does the synthesized aperture (see Figure A.1).

$$\Delta R_{Az} = s\beta_{Az} = \frac{sH\lambda}{L \cos \theta_i} = \frac{L}{2} \tag{A.2}$$

Equation A.1 and Equation A.2 show the relation between the resolution in either direction and the beamwidth in that same direction. The relation between the beamwidth and the antenna dimensions are given by the diffraction limits. The relations are given in equations A.3 and A.4 for elevation and azimuth direction, respectively.

$$\beta_{El} = \frac{\lambda}{W} \tag{A.3}$$

$$\beta_{Az} = \frac{\lambda}{L} \tag{A.4}$$

A.4.2 Accuracy

Accuracy is defined as the amount of certainty in a radar measurement. It was not at all treated in connection with SAR processing in the consulted texts so far, so additional research needs to be done here.

A.4.3 Ambiguity

Two targets are ambiguous to the radar if their location and velocity are different and their radar measurements are equal. There are several types of ambiguity: targets can be ambiguous in range, in doppler or, when SAR is considered, in a different way.

$$R_{\text{unambiguous}} = \frac{c}{2 \cdot PRF} \tag{A.5}$$

Doppler ambiguity originates from the situation where the induced dopplershift by a target is greater than the pulse repetition frequency, which puts a lower limit on the PRF. Other forms of ambiguity exist where objects are translated to other image locations because of their speed relative to the radar. Since the prescribed usecase for the SAR in this document is Radar Remote Sensing, only stationary (or very slow moving) targets are considered, such that these types of ambiguity fall outside the scope of this document. A few of these phenomena can be viewed as various types of distorsion typical to S(L)AR image processing and are briefly discussed in the next section.

A.4.4 Noise

Noise optimization in SAR image formation poses some unusual challenges due to the non-normal behavior of some of the noise sources.

The dominant source of noise in SAR images is speckle noise. Speckle noise originates from the fact that terrain mostly behaves like clutter, which can be modelled by an exponential distribution. By averaging neighbouring pixels, this noise sources start to behave like a chi-squared distribution with 2M degrees of freedom. M is the number of pixels that is used in the averaging process, referred to as the number of looks. The mean of this distribution equals the real radar cross-section and the noise power decreases as more pixels are averaged.

If there is too much noise to allow reliable detection the signal to noise ratio must be increased. This can be done in several ways. Increasing the pulse width (also known as the integration time), the pulse repetition frequency and the antenna gains are examples of ways how to do this.

A.4.5 Image distortion

There are several types of distortion present in SAR images. Some of the distortions are due to the geometry of the radar setup, like slant range distortion, layover or shadowing. These type of distortions need to be corrected for. Other types of distortion, like displacement due to range ambiguities or distortion due to undersampling of the synthetic aperture, can, to a certain extend, be taken care of by design.

A.4.5.1 Geometry-induced distortion

One type of distortion is distortion induced by the geometry. One example of such a type of distortion is slant range distortion. Reflections from scatterers in the swath that are close to the radar experience a smaller difference in slant range than those that are further away (see Figure A.2). Because of this, areas close to the radar get compressed while areas further away get stretched, resulting in image distortion with respect to the cross-track direction. Similar effects

occur if there are significant height differences in the terrain. Due to the platform altitude, mountain peaks are closer to the radar than the valleys below. Hence, the peaks are "pulled" towards the radar. This type distortion is known as layover. Finally, large objects, such as mountains, might cause pieces of the terrain to be blocked from the view of the radar. This type of distortion is called shadowing.

A.4.5.2 Motion-induced distortion

A second type of distortion is induced by the motion of the target. This type of distortion can be seen as a form of ambiguity It translates a difference in direction and velocity to a shift in the along-track direction according to Equation A.6. In this equation Δx_{at} is the shift that occurs in the along-track direction, Δx_{ct} is the difference between the position of the platform and the position of the scatterer in the cross-track direction, ϕ is the angle between the velocity vectors of the radar and the target, u is the magnitude of the velocity of the scatterer and v is the magnitude of the velocity of the platform.

$$\Delta x_{at} = \frac{\Delta x_{ct} u \sin\phi}{v - u\cos\phi} \tag{A.6}$$

Another type of distortion that is induced by motion of the target is blur. If the velocity of the target varies significantly during the coherence time of the SAR, blurring occurs. This is similar to the effect observed in photography, when the object moves too much during the time that the shutter is open. There is a slight difference though, since with SAR image processing it is the velocity that should be kept constant, while with original photography it is the position that should be maintained.

The final two phenomena that deserve recognition are range-walk and azimuthal defocussing. The condition for range-walk to occur is given in Equation A.7. In this equation u is the magnitude of the velocity of the target, phi is the angle between the velocity of the platform and the velocity of the target, R_{Ra} is the range resolution, R_{Az} is the azimuthal resolution, v is the magnitude of the velocity of the platform, s is the slant range and λ is the wavelength. Azimuthal defocussing occurs when the rate of change of the dopplershift in the reflection significantly differs from the rate of change expected from a stationary target.

$$|u\sin\phi| > \frac{2R_{Ra}R_{Az}v}{s\lambda} \tag{A.7}$$

A.4.5.3 PRF induced distortions

The final type of distortions are distortions that are in some way related to the pulse repetition frequency. It was already shown in Equation A.5 that the unambiguous range depends on the PRF, and thus distortions originating from this principle fall in this category. Instead of Equation A.5, the range ambiguity can also be written in terms of the angles $\theta_{i,min}$ and $\theta_{i,max}$, as in Equation A.8.

$$\frac{1}{\mathrm{PRF}} > \frac{2\mathrm{H}}{c}\left[\frac{1}{\cos\theta_{\mathrm{i,max}}} - \frac{1}{\cos\theta_{\mathrm{i,min}}}\right] \tag{A.8}$$

Apart from the range ambiguities, the PRF also determines the sampling interval of the synthetic aperture. According to the Shannon-Whittaker sampling theorem, Equation A.9 should be satisfied or spatial aliasing will occur. In this equation PRF is the pulse repetition frequency, v is the magnitude of the velocity of the platform and L is the length of the antenna. This is equivalent to the condition $\Delta\mathrm{x} < \mathrm{R_{Az}}$.

$$PRF \geq \frac{2\mathrm{v}}{\mathrm{L}} \tag{A.9}$$

Inequalities A.8 and A.9 can be combined to a final inequality from which the PRF has been eliminated. This leads to inequality A.10.

$$\frac{1}{\mathrm{R_{Az}}}\left[\frac{1}{\cos\theta_{\mathrm{i,max}}} - \frac{1}{\cos\theta_{\mathrm{i,min}}}\right] < \frac{\mathrm{c}}{2\mathrm{Hv}} \tag{A.10}$$

Bibliography

[1] T. Wahl, A. Skoelv, and J. H. S. Andersen. Practical use of ERS-1 SAR Images in Pollution Monitoring. In *Geoscience and Remote Sensing Symposium, 1994. IGARSS '94. Surface and Atmospheric Remote Sensing: Technologies, Data Analysis and Interpretation., International*, volume 4, pages 1954–1956, Augustus 1994.

[2] H. Ohkura, T. Jitsufuchi, T. Matsumoto, and Y. Fujinawa. Application of SAR Data to Monitoring of Earthquake Disaster. *Advances in Space Research*, 19:1429–1436, May 1997.

[3] S. Hasselmann, C. Brüning, K. Hasselmann, and P. Heimbach. An Improved Algorithm for the Retrieval of Ocean Wave Spectra from Synthetic Aperture Radar Image Spectra. *Journal of Geophysical Research: Oceans*, 101(C7):16615–16629, 1996.

[4] M. Neumann, L. Ferro-Famil, and A. Reigber. Estimation of Forest Structure, Ground, and Canopy Layer Characteristics From Multibaseline Polarimetric Interferometric SAR Data. *IEEE Trans. Geosci. Remote Sens.*, 48(3):1086–1104, March 2010.

[5] K. Ouchi. Recent Trend and Advance of Synthetic Aperture Radar with Selected Topics. *Remote Sensing*, 5:716–807, Feb 2013.

[6] Willian Gareth Rees. *Physical Principles of Remote Sensing.* Cambridge University Press, 2nd edition, 2001.

[7] Simon Kingsley and Shaun Quegan. *Understanding Radar Systems.* McGraw-Hill International (UK) Ltd, 1st edition, 1992.

[8] ESTEC. Innovative sar based on sparse direct radiating array antenna. Technical report, TNO and Thales Alenia, 2013.

[9] ESTEC. Sar based on sparse direct radiating array antenna - clarifications to negotiation points. Technical report, TNO and Thales Alenia, 2013.

[10] Ovidio Mario Bucci, Michele D'Urso, Tommaso Isernia, Piero Angeletti, and Giovanni Toso. Deterministic Synthesis of Uniform Amplitude Sparse Arrays via New Density Taper Techniques. *IEEE Trans. Antennas Propag.*, 58(6):1949–1958, June 2010.

[11] G. Caille, Y. Cailloce, C. Guiraud, D. Auroux, T. Touya, and M. Masmousdi. Large Multibeam Array Antennas with Reduced Number of Active Chains. *2nd European Conference on Antennas and Propagation*, pages 1–9, November 2007.

[12] Randy L. Haupt. Antenna Design with a Mixed Integer Genetic Algorithm. *IEEE Trans. Antennas Propag.*, 55(3):577–582, March 2007.

[13] Will P. M. N. Keizer. Synthesis of Thinned Planar Circular and Square Arrays using Density Tapering. *IEEE Trans. Antennas Propag.*, 62(4):1555–1563, June 2013.

[14] B. P. Kumar and G. R. Branner. Generalized Analytical Technique for the Synthesis of Unequally Spaced Arrays with Linear, Planar, Cylindrical or Spherical Geometry. *IEEE Trans. Antennas Propag.*, 53(2):621–634, February 2005.

[15] Christian Luison, Alberto Landini, Piero Angeletti, Giovanni Toso, Paolo Valle, Pasquale Capece, Stefano Selleri, and Giuseppe Pelosi. Aperiodic Arrays for Spaceborne SAR Applications. *IEEE Trans. Antennas Propag.*, 60(5):2285–2294, March 2012.

[16] W.-B. Wang, Q. Feng, and D. Liu. Synthesis of Thinned Linear and Planar Antenna Arrays Using Binary PSO Algorithm. *Progress In Electromagnetics Research*, 127:371–387, 2012.

[17] Joshua S. Petko and Douglas H. Werner. The Evolution of Optimal Linear Polyfractal Arrays Using Genetic Algorithms. *IEEE Trans. Antennas Propag.*, 53(11):3604–3615, November 2005.

[18] Joshua S. Petko and Douglas H. Werner. The Pareto Optimization of Ultrawideband Polyfractal Arrays. *IEEE Trans. Antennas Propag.*, 56(1):97–107, January 2008.

[19] Federico Viani, Giacomo Oliveri, and Andrea Massa. Compressive Sensing Pattern Matching Techniques for Synthesizing Planar Sparse Arrays. *IEEE Trans. Antennas Propag.*, 61(9): 4577–4587, June 2013.

[20] Robert J. Mailloux. *Electronically Scanned Arrays.* Morgan Claypool Publishers, 2nd edition, Januari 2007.

[21] Robert J. Mailloux, S.G. Santarelli, T.M. Roberts, and D. Luu. Irregular Polyomino-Shaped Subarrays for Space-Based Active Arrays. *International Journal of Antennas and Propagation*, 2009:1–9, Januari 2009.

[22] R. Tang. Survey of Time-Delay Beam Steering Techniques. *Phased Array Antennas: Proceedings of the 1970 Phased Array Antenna Symposium*, pages 254–260, 1972.

[23] Robert J. Mailloux. Subarray Technology for Large Scanning Arrays. *2nd European Conference on Antennas and Propagation*, pages 1–6, November 2007.

[24] Kiersten C. Kerby and Jennifer T. Bernhard. Sidelobe Level and Wideband Behavior of Arrays of Random Subarrays. *IEEE Trans. Antennas Propag.*, 54(8):2253–2262, Augustus 2006.

[25] V. Pierro, V. Galdi, G. Castaldi, I.M. Pinto, and L.B. Felsen. Radiation Properties of Planar Antenna Arrays Based on Certain Categories of Aperiodic Tilings. *IEEE Trans. Antennas Propag.*, 53(2):635–644, February 2005.

[26] Sebastiaan Jacobs. Summary of antenna parameters. Technical report, TNO, 2014.

[27] W. L. Doyle. *On Approximating Linear Array Factors.* RAND Corporation, 1st edition, 1963.

[28] A. S. Nemirovsky and D. B. Yudin. *Problem Complexity and Method Efficiency in Optimization.* John Wiley & Sons Ltd, 1st edition, April 1983.

[29] G. C. Rhoads. Planar Tilings by Polyominoes, Polyhexes and Polyamond. *Journal of Computational and Applied Mathematics*, 174(2):329–353, February 2005.

[30] Salomon. W. Golomb. Tiling with Sets of Polyominoes. *Journal of Combinational Theory*, 9(1):60–71, July 1970.

[31] G. Toso, P. Rocca, and R. J. Mailloux. GA-Based Optimization of Irregular Subarray Layouts for Wideband Phased Arrays Design. *Antennas and Wireless Propagation Letters, IEEE*, 14:131–134, 2015.

[32] D. Knuth. Dancing Links. *Millenial Perspectives in Computer Science*, pages 187–214, November 2000.

[33] Pietro S. Oliveto, Jun He, and Xin Yao. Time Complexity of Evolutionary Algorithms for Combinatorial Optimization: A Decade of Results. *IJAC*, 4(3):281–293, July 2007.

[34] R. Vescovo. Reconfigurability and Beam Scanning With Phase-Only Control for Antenna Arrays. *IEEE Trans. Antennas Propag.*, 56(6):1555–1565, June 2008.

[35] Monson H. Hayes. *Statistical Digital Signal Processing and Modeling.* John Wiley & Sons Ltd, 1st edition, 1996.

[36] J. Horstmann, P. Vachon, S. Lehner, and D. Hoja. SAR Measurements of Ocean Wind and Wave Fields in Hurricanes. In *Geoscience and Remote Sensing Symposium, 2003. IGARSS '03. Proceedings. 2003 IEEE International*, volume 1, pages 230–232, July 2003.